UNIVERSITÀ DEL PIEMONTE ORIENTALE

Scuola di Medicina
Dipartimento di Medicina Traslazionale

Corso di Dottorato di Ricerca in Medical Sciences and Biotechnologies
ciclo XXXIII

Growth arrest specific 6 - Feasible marker for septic patients and potential architect in the improvement of sepsis-induced organ damage in mice

SSD (Settore Scientifico Disciplinare) MED/09

Coordinatrice

Professoressa Marisa Gariglio

Tutor

Professor Gian Carlo Avanzi

Dottoranda

Livia Salmi

“All we have to decide is what to do with the time that is given us.”

INDEX

INTRODUCTION

In 2020 the entire world learned the meaning of 'a large-scale infection' and its horrible consequences. History is surrounded by epidemic and pandemic infections which have reduced repeatedly population and, even though infectious diseases constituted the most serious health issue in the world until the beginning of the 20th century, when chronic degenerative diseases began to dominate this scenario in developed countries, they are still a *drama* nowadays.

Infection is the term that describes the entrance and development of an infectious agent in a human or animal body and *infectious disease* is defined as an illness caused by a specific infectious agent or its toxic product that results from transmission of that agent or its products from an infected person, animal, or reservoir to a susceptible host, either directly or indirectly (Barreto et al., 2006).

Mammalian immune system is generally able to recognize infective agents through complex mechanisms mediated by both innate and adaptive immunity. Summarily, the innate immunity recognizes molecular patterns associated with entire classes of pathogens (PAMPs) and molecular patterns associated with cell damage and distress (DAMPs) through an assortment of cellular pattern recognition receptors (PRRs). Instead, system of adaptive immunity develops target-specific recognition and attack molecules aimed at specific and unique molecular signals of individual pathogens.

Taking together these two types of immunity the host organism can trigger a panoply of effector mechanisms aiming to delay, damage, expel, contain, or destroy infective agents. However, outside the academic definitions' reality is complex, and sepsis sets within this framework.

Sepsis was not clinically defined until the early '90s when a group of opinion leaders released the first consensus definition of sepsis (Bone et al., 1992). Herein, *systemic inflammatory response syndrome* (SIRS) has been defined and infection-associated SIRS was named sepsis. Within sepsis definition the increasing severities, including organ disfunction, were designated *severe sepsis* and *septic shock* when refractory hypotension also occurs.

Since SIRS diagnosis was based on non-specific criteria (such as body temperature, heart rate, respiratory rate and white blood cell count) distinguishing between non-infections SIRS and sepsis was not immediate. Therefore, approximately ten years later, in 2001, a second important conference occurred aiming at revisiting the definition of sepsis based on newly discovered biomarkers (Levy et al., 2018). However, after a considerable debate, the participants determined that the use of biomarkers for sepsis diagnosis was still premature and, therefore, only the expansion of the list of signs and symptoms of sepsis was introduced. Eventually, in 2016, the last revision was released according to the third international consensus definition for sepsis and septic shock (Sepsis-3) (Singer et al., 2016). For two years, from 2014 to 2015, a task force of 19 expert members was convened by Society of Critical Care Medicine and the European Society of Intensive Care Medicine to elucidate Sepsis based on the overview, which includes change in organ function, morphology, cell biology, biochemistry, immunology and circulation. The task force agreed to defined sepsis as life-threatening organ dysfunction caused by a dysregulated host response to infection, and the term 'severe sepsis' has been removed.

Epidemiology and Etiology

Sepsis is the most common cause of hospital deaths in United States and costs more than 24 billion dollars annually (Paoli et al., 2018), even if the majority of cases of sepsis and related deaths are estimated to occur in low and middle-income countries (**Figure 1**). However, accurate quantification of global sepsis incidence and mortality remains an impressive challenge nowadays. Recently, Rudd and colleagues developed a multinational individual-level data to produce global sepsis estimation. The authors highlighted an important change in sepsis incidence from early '90s to 2017: globally, there were an estimated 60.2 million cases of sepsis in 1990 compared to 48.9 million cases in 2017, resulting in a 18.8% decrease in cases. Regarding sepsis-related mortality, in 2017 there were an estimated 11 million deaths worldwide, which represented 19.7% of death that year. Among them, 1.8 million (16.4%) were attributable to lower respiratory infections, which has remained the leading cause of sepsis-related death from 1990. In fact, lower respiratory infections, diarrhoeal diseases and neonatal disorders has remained respectively the first, second and third cause of sepsis-related death during time. Instead, other well-known infective diseases as HIV, malaria and tuberculosis, which were a great burden in the past, have become more manageable, giving way to chronic diseases, such as cirrhosis and chronic obstructive pulmonary disease (CODP).

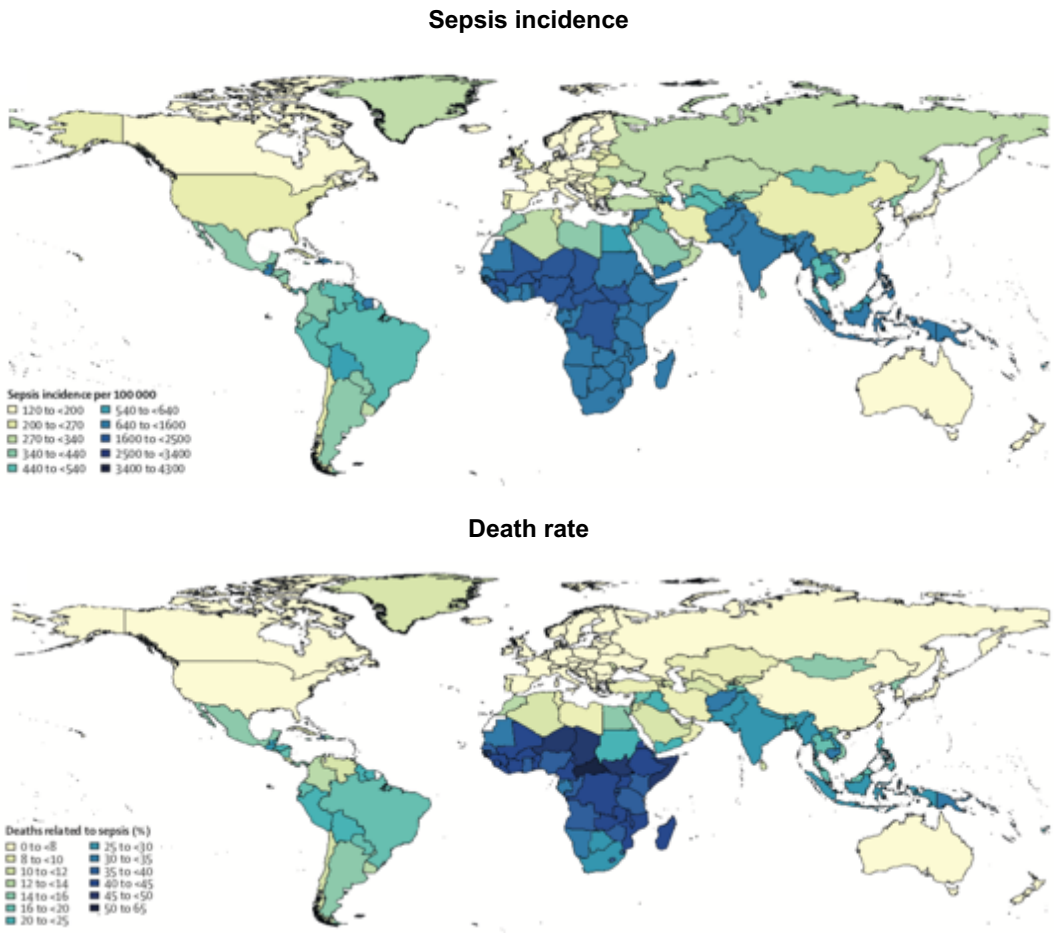

Figure 1. Global epidemiology. Sepsis incidence per 100 000 population for both sexes and percentage of all deaths related to sepsis in 2017. Modified from (Rudd et al., 2020).

As mentioned above, low/middle-income countries theoretically count the larger number of sepsis-related deaths; however, this is only an estimation since there is not a 'gold standard' diagnostic test for sepsis and definitions vary widely across areas. Indeed, according to Sepsis-3 guidelines is reported the clinical prompt 'Quick Sequential (Sepsis-related) Organ Failure Assessment (qSOFA) score' which has been only retrospectively evaluated in multiple datasets from low/middle-income countries, but not prospectively yet (referred to 2018). In addition, some clinical scoring of both qSOFA score and other Sepsis-3 criteria may be impractical to use at the bedside in low-resource settings. Furthermore, several sepsis variables in low-resource settings, such as differences in populations at risk, infecting pathogens, and clinical circumstances, suggest that sepsis care in high-resource settings may not be effective in low-resource settings (Rudd et al., 2018). Lastly, the available data in literature suggest that an estimate 90% of worldwide deaths from chest infections occur in low-resource settings and

about 70% of the 9 million deaths due to chest infections in neonates are associated with sepsis, remarkably most of these cases happening in Asia and Africa (Cecconi et al., 2018).

Regarding Italy, a recent published study has analyzed all the conditions mentioned in the death certificates to estimate the nationwide burden of sepsis-related mortality in this country (Grande et al., 2019). The retrospective study collected data from 2003 to 2015 by the Italian National Cause of Death Register, managed by the Italian National Institute of Statistics (ISTAT). This analysis revealed that the number of death certificates reporting sepsis increased from 18.939 in 2003 to 49.010 in 2015 (from 3 to 8% of total deaths). Moreover, another multicenter study which analyzed patients enrolled in intensive care unit (ICU) from 2008 and 2017 demonstrated that the 47%, among the 'healthcare associated infection', has led to sepsis (Agodi et al., 2018). As expected, the case fatality rate increased with the severity of sepsis, however the increase of sepsis-related death reported above (time 2003 – 2015) could be also related to the aging of the population, strictly connected with multi-chronicity, repeated hospitalization, malnutrition and age-related immune-senescence (Grande et al., 2019).

If the epidemiology is profoundly complicated and potentially underestimated, the etiology is a bit better known although sepsis can originate from virtually any infecting organism. In fact, clinical manifestations are very wide and varies substantially among geographical areas. Simplifying this concept, sepsis can originate and be defined as community-acquired sepsis or hospital-acquired sepsis. A recent review specified that about 80% of hospital-treated sepsis cases arise in the community and the most common site of infection leading to sepsis is the lung (64 %), followed by the abdomen (20 %), bloodstream (15 %), and renal and genitourinary tracts (14 %) (Cecconi et al., 2018).

Giving concrete importance to all these data, which highlighted how much sepsis is associated with unacceptably high mortality, the World Health Assembly and World Health Organization (WHO) made sepsis a global health priority in 2017 (Reinhart et al., 2017).

Diagnosis, Prognosis and Therapy

As written above, in 2016 'Sepsis' definitions has been changed because several limitations were present in the previous criteria, including the poor specificity attributable to SIRS definition.

One of the most important milestones was that sepsis condition was no longer considered to be only an inflammatory syndrome, although in practice pro and anti-inflammatory pathways are involved in the dysregulated response. Thus, the new diagnostic criteria are more focused on revealing organ dysfunction than on identifying signs of inflammation and, as an indirect consequence, also the classification has been changed: the previous categories of sepsis, severe sepsis, and septic shock have now converted to infection, sepsis, and septic shock (Cecconi et al., 2018).

Importantly, for diagnosis have been introduced feasible tools aimed to stratify the risk and to determine the SOFA score (**Table 1**). Thus, sepsis is now defined and diagnosed as the presence of an infection combined with an acute change in SOFA score of 2 points or more.

The Sepsis-3 definitions also introduced a new diagnostic tool aimed to the early identification of patients with infections who are likely to have either a prolonged stay in ICU or who are at a high risk of death: the quik-SOFA (qSOFA). However, this qSOFA score was found to be marginally superior to the original SIRS criteria in predicting this high-risk category of patients. In fact, this system should not be used to rule out patients as being at high risk, as it is likely to be more specific, but not more sensitive, than the old SIRS criteria (Seymour et al., 2016). Notwithstanding, qSOFA is very fast and easily measurable at the patient's bedside. Briefly, patients are considered with high risk if they meet at least two of the criteria, as follows: alteration in mental status, systolic blood pressure less than 100 mmHg, or a respiratory rate of more than 22 breaths per minute.

A separate consideration regards septic shock which is described, by Sepsis-3 definitions, as a clinically defined subset of sepsis cases, wherein, despite adequate fluid resuscitation, patients have hypotension requiring vasopressors to maintain a mean arterial blood pressure above 65 mmHg and have elevated serum lactate concentrations(>2 mmol/L) (Seymour et al., 2016).

However, some criticisms have been made regarding septic shock recognition. In fact, septic shock is associated with presence of hypotension, but this valuation is insufficient, since in most of patients the onset of hypotension is preceded by tissue hypoperfusion (Lee et al., 2016). Hypotension often does not appear, or appears late, whereas tissue perfusion may be severely compromised (Lokhandwala et al., 2015).

	SOFA score 0	SOFA score 1	SOFA score 2	SOFA score 3	SOFA score 4
Respiratory system PaO_2/FiO_2 (kPa)	≥ 53.3	≥ 53.3	< 40	< 26.7	< 13.3
Coagulation system Platelets (× 10^3/μL)	≥ 150	< 150	< 100	< 50	< 20
Hepatic system: Bilirubin (μmol/L)	< 20	20 – 32	33 – 101	102 – 204	> 204
Cardiovascular system	MAP > 70 mmHg	MAP < 70 mmHg	Dopamine < 5 μg/kg per min, or dobutamine administered	Dopamine 5.1 - 15 μg/kg per min, or epinephrine or norepinephrine ≤ 0.1 μg/kg per min administered	Dopamine > 15 μg/kg per min, or epinephrine or norepinephrine > 0.1 μg/kg per min administered
Central nervous system Glasgow Coma Scale	15	13 – 14	10 – 12	6 – 9	< 6
Renal system Creatinine (μmol/L) Urine output (mL/day)	< 110 -	111 – 170 -	171 – 299 -	300 – 440 < 500	> 440 < 200

Table 1. Description of sequential organ failure assessment (SOFA) scoring system. SOFA system includes respiratory, coagulation, hepatic, cardiovascular central nervous and renal systems. Table modified from (Seymour et al., 2016).

Another important aspect, least mentioned, is the prognosis of septic surviving patients. Data from a recent meta-analysis revealed that one in five sepsis survivors are re-hospitalized within 30 days from discharge from hospital even though this re-hospitalized risk is comparable with non-sepsis acute medical patients (Shankar-Hari et al., 2020). However, another important study demonstrated that the dysregulated host immune response activated during sepsis may persist up to 1 year. Additionally, individuals with persistent biomarkers of inflammation and immunosuppression, which represent two-thirds of patients who survived a hospitalization for sepsis, had a higher risk of readmission and death due to cardiovascular disease and cancer compared with those with normal circulating biomarkers (Yende et al., 2019).

Mortality is strictly related to therapy and its effectiveness. An important study, published in 2017, demonstrated the association between time to treatment and outcome among patients with sepsis or septic shock treated in the emergency department. Authors ruled that a longer time to completion of a 3-hour regarding the administration of broad-spectrum antibiotics are associated with higher risk-adjusted in-hospital mortality for patients with sepsis (Seymour et al., 2017).

In support, Rhee and colleagues' findings revealed that an inadequate therapy was associated with a 20% to 40% higher odds of death depending on whether all cultures or only blood cultures were analyzed (Rhee et al., 2020).

Currently, patients with suspected sepsis are treated with broad spectrum antibiotics and crystalloid within 3 hours to the ICU admission. For the first hours patients are defined as "patients with suspected sepsis" because current clinical standard of practice for bacterial identification is age-old technology, which often take 48h plus delays. Even though the delay in first antibiotic administration is associated with increase in the risk of mortality, as mentioned above, it is essential consider that the use of broad-spectrum antibiotics could cause several collateral damages. Indeed, antibiotic administration may cause bacteria in the bowel and other sites to become resistant. Additionally, long courses of antibiotics often have no benefit and can predispose to overgrowth of resistant flora over normal resident commensal flora (Perner et al., 2016). In conjunction with antibiotic administration, it is foreseen the administration of crystalloids or resuscitation fluids. However, there is evidence that fluid resuscitation used, and the cumulative dose administered over the course of the ICU admission may independently affect patient outcomes. Thus, resuscitation fluids should be used with the same caution and care as any other potentially toxic intravenous drug (Boyd et al., 2011).

As a "next-step" of septic shock management is the administration of vasopressors which should occur within the first 6 hours. Norepinephrine is the current recommended first line vasopressor in septic shock, to which vasopressin may be added (Dellinger et al., 2013). However, also vasopressor administration should be managed with caution since it can produce inappropriate effects including organ dysfunction, specifically cardiac-related. Lastly, sepsis and septic shock can lead to anemia due to hemorrhages, sepsis-induced coagulopathy and/or impaired erythropoiesis for which blood transfusion remains the most effective treatment (Perner et al., 2016).

Physiopathology

Sepsis is a highly complex and lethal syndrome with interconnected pathways and sepsis-related death cannot be considered only infection-dependent. The immune response against infection induces severe tissue, organ and microcirculatory dysfunctions thus leading to a profound global damage, collectively known as multi-organ failure (MOF) or multi-organ distress syndrome (MODS). Each organ injury contributes substantially to the patient's risk of death with a complex crosstalk among the whole system.

Precisely, because sepsis is not organ/tissue specific, different targets can be involved and disruption and failure usually occur both at cellular and macroscopical levels. Dysregulation and homeostasis disruption can occur in one or more organs thus, to make the description easier, the macro-system involved will be listed even though it is important to take in consideration all the interconnections among them.

Vascular dysfunction – at microvascular and capillary levels the permeability is increased, implicating leak with a reduction of effective vascular volume and the impairment of systemic perfusion. This condition is exacerbate by the failure of the vascular smooth muscle to contract with neurohormonal stimuli, resulting in systemic arterial and venous vasodilatation and a global hypoperfusion and hypotension (Burgdorff et al., 2018).
Although the mechanisms are not well understood, inflammation-induced endothelial dysfunction seems to be associated with an overexpression of an inducible nitric oxide synthase (iNOS). The subsequent excessive production of nitric oxide (NO) directly induces vascular smooth muscle cells relaxation and hyperpolarization, preventing their response to vasoconstrictors and thus perpetuating hypotension. Moreover, NO exacerbates mitochondrial dysfunction diminishing global cellular oxygen consumption (Bloch et al., 2016; Caraballo and Jaimes, 2019).

Cardiac dysfunction – after fluids resuscitation or vasopressors administration, venous return increases and patients initiate a phase characterized by high cardiac output and low systemic vascular resistance. Additionally, this phenomenon is often accompanied by a depressed myocardial function also due by the action of cytokines, such as interleukin-1β (IL-1β) and interleukin-6 (IL-6), able to decrease cardiomyocyte contractility. Furthermore, sepsis is associated with incidental clinical cardiac events like acute heart failure, life-threatening arrhythmias, myocardial infarction, and non-ischemic myocardial injury (Caraballo and Jaimes, 2019).

Lungs – sepsis is the most common cause of acute respiratory distress syndrome (ARDS), which is an acute inflammatory lung injury, associated with increased pulmonary vascular permeability, increased lung weight, and loss of aerated lung tissue (Bellani et al., 2016). Increased vascular permeability leads to leaking of liquids and proteins across the lung endothelium, generating edema in the lung interstitium. Subsequently, the edematous fluid move into the alveoli, often facilitated by injury to the naturally tight barrier properties of the

alveolar epithelium. Exudate edematous fluid containing proteins, neutrophils and red blood cells (resulting in their accumulation into the alveolar space) is the hallmark of ARDS. This process is also permitted by damage and alterations of endothelial cells that can be caused by pathogens and their toxins, and in particular by the host-response against these pathogens. Pro-inflammatory signaling molecules, such as tumor necrosis factor (TNF), interleukin (IL)-1β, angiopoietin 2 (Ang2) or vascular endothelial growth factor (VEGF), generated by alveolar macrophages, circulating leukocytes and platelets foster and exacerbate ARDS-related damage (Matthay et al., 2019).

The 40% of septic patients develop ARDS and among them roughly 40% die of ARDS-related complication. In addition, it has long been found that patients with sepsis-related ARDS have higher 60-day mortality rate than those which develop ARDS due to any other reason (Sheu et al., 2010).

Kidneys – sepsis is the most common contributing factor for acute kidney injury (AKI) in critical patients. An increase of serum creatinine is a hallmark of AKI, although serum creatinine is also limited for diagnosis by the absence of baseline value in many patients. The incidence of AKI in septic patients is around 50% and it is associated with worse prognosis and delay in recognizing renal injury leads to increased risk of poor outcomes. Patients with sepsis-associated AKI have roughly 60% higher risk of in-hospital mortality compared to septic patients without AKI and, moreover, sepsis-associated AKI increase of one-third the risk of mortality rate compared to patients with non-sepsis associated AKI (Caraballo and Jaimes, 2019). It has been observed that early antibiotic administration improves the outcome in sepsis and its delay results as independent predictor factor for the development of sepsis-associated AKI. Sepsis-mediated kidney hypoperfusion can cause ischemic injury and can contribute to AKI development; additionally, acute tubular necrosis has been described in around 20% of patients with sepsis-associated AKI.

However, glomerular perfusion pressure and relative intrarenal shunting appear to be the primary aberration occurring early during sepsis simultaneously with altered vascular permeability, excess of fluid extravasation, and renal tissue edema. Furthermore, cellular debris, including leukocytes, platelets, and coagulation activation, further contribute to endothelial disruption and occlusion (Poston and Koyner, 2019).

Liver – almost half of septic patients develop concomitant hepatic dysfunction, which has been associated with 28-day mortality (Caraballo and Jaimes, 2019). Although liver is not the first

organ correlated to sepsis-associated MOF leading to patients' death, it significantly participates and orchestrates a large part of responses against sepsis thanks also to its unique anatomical location. Specifically, the majority of mechanisms related to immune surveillance or bacterial clearance by the liver take place within the hepatic sinusoid compartment. Hepatic sinusoid structures are lined by endothelial cells (named liver sinusoidal endothelial cells – LSEC) and Kupffer cells. Multifunctional hepatic stellate cells and various immune active cells are localized within the space of Disse between the sinusoid and the adjacent hepatocytes. Flow within the sinusoids can be compromised by physical or chemical agents, pressure blockage in their lumina as well as obstructive processes within the space of Disse (Brunt et al., 2014).
It is important to highlight that the liver-induced immunogenic response represents a double-edged sword contributing to both clearance of microbial products and organ damage due to an overwhelming systemic inflammatory response, In fact, it is possible recognize different types of response and if they are not well balanced and meticulously controlled the impact of this non-homeostatic status will mirror the overall systemic condition. The pro-inflammatory response, featuring inflammatory cytokines as IL-6 and IL-1 cytokines from Kupffer cells, monocytes and other macrophages, triggers the production and release of acute-phase proteins by hepatocytes. On the other hand, hepatic response against sepsis involves also the activation of anti-inflammatory pathways and the over production of cytokines such as IL-10 and TGFβ, with the suppression of $CD4^+$ and $CD8^+$ T-cell responses by secreting iNOS and by inducing regulatory T cells (Strnad et al., 2017). One consequence of the sepsis-related unbalanced homeostasis is the hypoxic hepatitis, which occurs with an incidence around 10%, and it is associated with an in-hospital mortality of ~50% (Fuhrmann et al., 2009; Kramer et al., 2007). It is triggered by inadequate oxygen concentration that leads to reduced O_2 delivery to or consumption by the liver. This damage is manifested by increasing of serum aspartate aminotransferase (AST) and alanine aminotransferase (ALT) levels which can be measured a few hours after the initiation of hepatic damage and are usually accompanied by elevated lactate dehydrogenase (LDH) activity. Lastly, after initial hypoxic liver damage, one-third of patients develop cholestatic hepatic dysfunction, which is a common complication in patients with sepsis and results either from impaired bile formation at the hepatocellular level, or from defective bile flow at the level of small or large bile ducts without, necessarily, a biliary obstruction (Bhogal and Sanyal, 2013).

Central Nervous System – sepsis-associated encephalopathy is frequently encountered in critical patients in intensive care units, and in up to 70% of patients with severe systemic

infection. However, mortality in patients with sepsis-associated encephalopathy occurs almost always due to MOF rather than neurological complications (Gofton and Young, 2012). Sepsis-associated encephalopathy is likely to be largely due to inflammatory mediators as cytokines; in severe cases brain dysfunction and even structural lesions can be diverse, including ischemic lesions, encephalopathy due to failure of other organs and/or hematological disorders (such as disseminated intravascular coagulation – DIC). In fact, the marked inflammatory response, characteristic of sepsis condition, contributes to microcirculatory failure and disruption of the blood-brain barrier, allowing inflammatory mediators and neurotoxins diffusion into the brain tissue. Importantly, the increased NO diffuses through the intact blood-brain barrier, causing oxidative stress and, as a consequence, neuronal dysfunction and cell apoptosis (Sweis et al., 2016).

Coagulation system – coagulopathy is a common and important complication in patients with sepsis and contributes to the development of organ dysfunction. Among patients with sepsis and septic shock, more than half develop thrombocytopenia and the same amount is diagnosed for disseminated intravascular coagulation (DIC) (Caraballo and Jaimes, 2019). It is well known that activated endothelium becomes prothrombotic in sepsis conditions, leading to the formation of microvascular thrombosis. Furthermore, other cells (i.e. monocytes/macrophages, neutrophils and lymphocytes) and mediators (coagulation factors) participate in this critical complication. Tissue factor (TF) expressed on macrophages and monocytes play a central role in clot formation, additionally TF together with activated neutrophils and DAMPs released by surrounding cells exert a potent prothrombotic effect.
Also, vascular endothelial cells release NO, which normally has antithrombotic effects in physiological condition, whereas they promote prothrombotic effects under septic conditions by expressing TF and releasing von Willebrand factor, thus generating a vicious circle. Derangement of the coagulation/fibrinolytic/endothelium system is a hallmark of DIC (Iba et al., 2020).

Metabolism – sepsis pathogenesis is strongly influenced by profound changes in metabolic homeostasis. Importantly, one recurrent feature in sepsis is a clear problem of mitochondrial respiration; this feature was demonstrated also in patients by Brealey and colleagues, who observed that skeletal muscle biopsies showed a significant decrease of ATP/ADP ratio in non-survivor compared to survivor septic patients (Brealey et al., 2002). In addition, proteomic and metabolic screen on plasma of sepsis patients identified glucose metabolism and fatty acid

beta-oxidation pathways as being significantly different between sepsis survivors and non-survivors. Moreover, the metabolomes and proteomes of surviving patients with mild sepsis did not differ from survivors with severe sepsis or septic shock (Langley et al., 2013). At clinical level, hyperglycemia is very often observed and only occasionally hypoglycemia occurs in septic patients (Van Wyngene et al., 2018). A clear increase in lactate is usually directly related to poor outcome, besides signs of poor fatty acid oxidation and amino acid catabolism. The increased concentration of circulant lactate in sepsis is likely the result of increased glycolysis activity. In fact, in sepsis conditions, glycolysis appears to be perfectly ongoing and pyruvate is abundantly generated in the cytoplasm of cells. However, pyruvate transformation into acetyl-CoA and CO_2, after its crossing into mitochondria, is heavily compromised in sepsis and Krebs cycle cannot be triggered. Furthermore, mitochondria display physical damage: dysfunction of mitochondria in sepsis has been described as being a direct result of NO, CO, and reactive oxygen species (ROS), whereby mitochondrial DNA is damaged as well as proteins of the electron transport chain. In addition to being damaged and less active as a consequence, the electron transport chain is less abundant in cells in some of its complexes: specifically complex I, II and IV (Hüttemann et al., 2012). Taking these considerations together, it is possible to state that sepsis leads to cytopathic hypoxia. In fact, oxygen levels in tissues during sepsis are rather normal but there is a reduced capacity of the tissues to utilize O_2 from the blood. During this condition cells perform a hypoxic response characterized by transcriptional increase and activation of hypoxia-inducible factor α (HIF1-α), which is responsible to induce transcription of other genes coding for proteins that are involved in glycolysis and most importantly lactate dehydrogenase (LDH). LDH is the enzyme that converts pyruvate into lactate; as mentioned above high plasma levels of lactate is a typical biomarker of bad prognosis in sepsis, correlating with disease severity, morbidity, and mortality (Nichol et al., 2010; Rishu et al., 2013; Van Wyngene et al., 2018).

Lastly, depending on cell type and state, mitochondria are the major source of ROS and among them superoxide radicals ($O_2^{\bullet-}$) and hydrogen peroxide (H_2O_2) are important. ROS are acting either via intracellular signaling cascades, or via induction of oxidative stress, damaging intracellular structures. Rather than low ATP levels (due to mitochondrial dysfunction), ROS significantly contribute to cellular, tissue and ultimately organ damage (Kozlov et al., 2017).

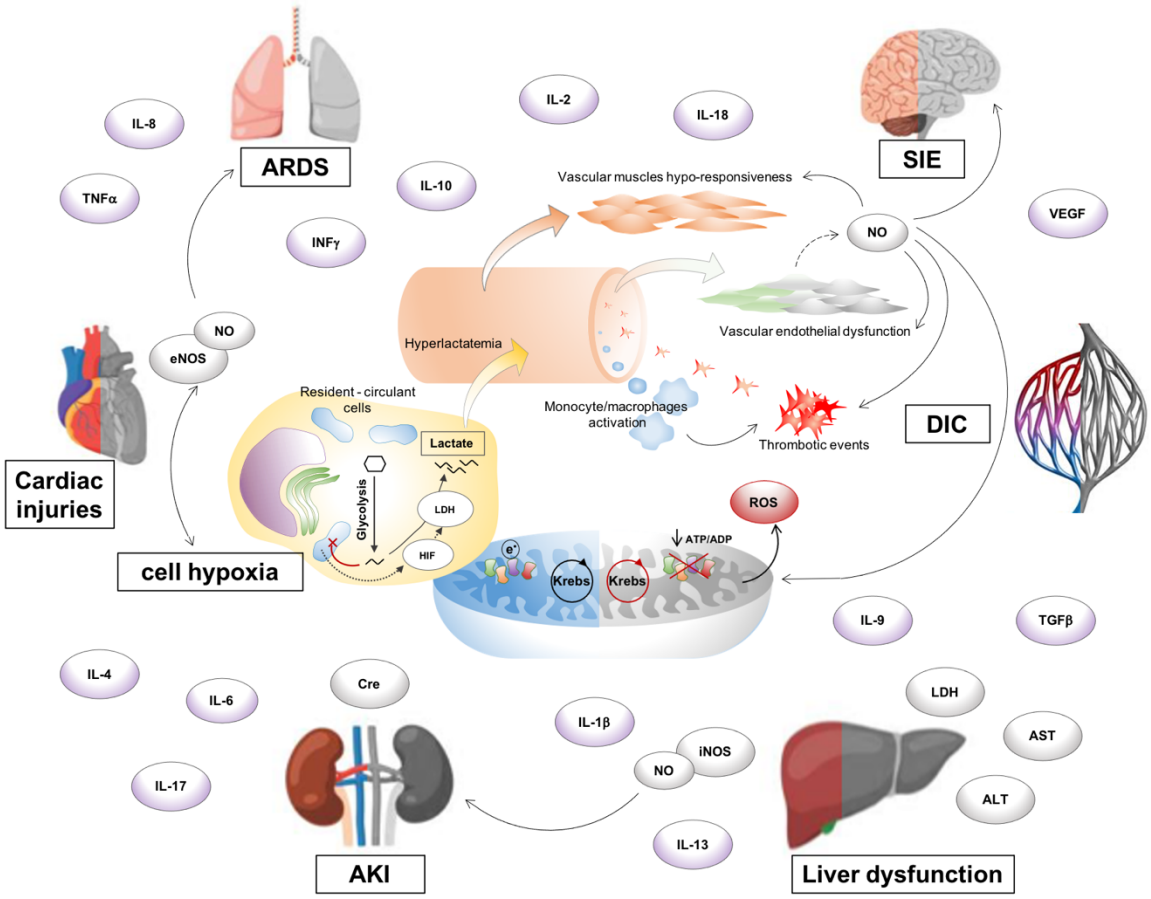

Figure 2. Confusing? This is MOF. Multi-organ failure (MOF) or multi-organ distress syndrome (MODS) is the development of potentially reversible physiologic derangement involving two or more organ systems not involved in the disorder and arising in the wake of a potentially life-threatening physiologic insult. MOF is characterized by disruption at molecular > cellular > tissue and vascular levels until organ(s) involvement. Moreover, it is the crosstalk among immune system cells and tissue resident cells, with the contribution of both innate and adaptive immunity. At molecular and cellular levels there are evidence of a reduced O_2 consumption, although there is not a hypoxia general condition: Krebs cycle and electron transport chain are substantially impaired and reactive oxygen species (ROS) are the first consequence; the cellular-hypoxia state stimulate the stabilization of hypoxia-inducible factor (HIF) which in turn induce lactate dehydrogenases (LDH) upregulation. With Krebs cycle impairment, glycolysis is highly active, and the over production of pyruvate is readily metabolized in lactate by LDH enzyme. Lactate is then secreted in the bloodstream leading to systemic hyperlactatemia. At vascular level, serious disruptive mechanisms occur; starting from vascular muscle cells which, due to cell membrane repolarization, no longer respond to neuromuscular stimuli and lose their contractile ability causing general vasoplegia. Furthermore, vascular endothelial cells have an important role in MOF due to overproduction of nitric oxide (NO), able to cross cell membrane and diffuse in all surrounding tissues/organs, including brain. Remaining at vascular levels, circulant immune cells and platelets, together with an impaired coagulation system, trigger uncontrolled mechanisms leading to clot formation and thrombotic events generating the disseminated intravascular coagulation (DIC) phenomena. DIC is tangibly dangerous in organs as liver, kidney and brain; in the latter, DIC and NO diffusion cooperate developing sepsis-induce encephalopathy (SIE). The overproduction of NO is directly depending by endothelial nitric oxide synthases (eNOS) and inducible nitric oxide synthases (iNOS) overexpression: eNOS and iNOS are expressed by several cells of all organs, particularly when they are damaged. Liver damaged is superficially identifiable by increasing in the blood concentration of aspartate aminotransferase (AST) and alanine aminotransferase (ALT); as well as acute kidney injury (AKI) is identified

through creatinine (Cre) increase. Other important causes of MOF are acute respiratory distress syndrome (ARDS), in which pulmonary function are largely compromised, and acute cardiac events such as acute heart failure and non-ischemic myocardial injury. All these confused but strictly linked events are orchestrated by molecules (i.e. NO, ROS) and importantly by a cytokines storm, which includes a plethora of cytokine mediators expressed and secreted in an uncontrolled way (i.e. interleukin – IL – 1β, 2, 4, 6, 8, 9, 10, 13, 17 and 18, vascular endothelial growth factor – VEGF –, interferon – INF – γ, tumor necrosis factor – TNF – α and transforming growth factor – TGF – β)

Animal models

To date an animal model of sepsis is unfortunately essential to mimic the pathophysiology in humans and better understand and clarify the pathophysiological mechanisms of sepsis. The idea that a perfect murine model of sepsis exists is untenable, owing to the complex and heterogenous nature of the condition, but a variety of good options for modeling exist depending on the focus of the research. Among them: I) Lipopolysaccharide Injection, II) Bacteria and Fibrin Clot Implantation, III) Colon Ascendens Stent Peritonitis, IV) Cecal Ligation and Puncture and the more recent, V) Cecal Slurry Injection (Lewis et al., 2016). For many years the most used model was Cecal Ligation and Puncture (CLP) model, while the first three listed were used only occasionally. CLP involves the ligation of the distal caecum to the ileocecal valve followed by the perforation of the caecum by needle to allow fecal contents leakage into peritoneum. Theoretically the severity of the disease can be controlled by the needle puncture size, by the number of punctures and the length of ligated cecum. However, there are contradictory data on this, and the size/number of punctures may not dictate the severity of the disease (Kingsley and Bhat, 2016). Additionally, CLP is affected by many variables. In fact, the severity of CLP-induced sepsis is highly dependent on the degree of infection, which can be influenced by volume, rapidity and duration of cecal content released into the abdomen, and by bacterial flora present in the cecum. For these reasons with the same procedure, it is impossible to compare animals with different body size, under different diet regimens and different gastrointestinal conditions. Moreover, the fact that it is a surgical invasive procedure turns out to be difficult work on animals with particular pathophysiological conditions, such as deficient wound-healing capability or higher sensitivity to surgery (Kingsley and Bhat, 2016). Recently the Cecal Slurry Injection (CSI) model has taken wide use, partially replacing CLP model. CSI model of sepsis is based upon intraperitoneal injection of cecal contents from a donor rodent that has been standardized in quantity and suspended in fluid. This technique seems more consistent than CLP because of the ability to standardize the bacterial inoculum, which is not possible in CLP. Moreover, mice subjected to CSI do not undergo to the surgical tissue trauma and ischemic tissue generated by standard CLP method (Lewis et al., 2016).

Biomarkers

Over the last decade, there has been great interest in finding out biomarkers for several applications, including diagnosis of infection, prognostication, and therapeutic guidance, in patients with sepsis. Many potential sepsis biomarkers have been proposed, procalcitonin (PCT) and C-reactive protein (CRP) being the most frequently studied. In 2017, Kim et al. demonstrated a possible prognostic utility of procalcitonin (PCT), presepsin (sCD14-subtypes), soluble suppression of tumorigenicity 2 (sST2), and Gal-3 in sepsis (Kim et al., 2017a). However, authors suggested that a multi-marker approach could be beneficial for an optimized management of patients with sepsis. The idea of a multi-marker approach has been recently reclaimed by Mearelli et al. in a multicenter prospective study comprising a large cohort of patients. They developed and validated a high-performing, reproducible, and cost-effective algorithm to assist physicians of the emergency department in distinguishing sepsis/septic shock from noninfectious systemic inflammatory response syndrome (SIRS) (Mearelli et al., 2018). Nowadays, it is becoming evident that the use of biomarkers in clinical procedures can be helpful and essential for a correct diagnosis, to discriminate noninfectious SIRS, sepsis, and septic shock patients, and to estimate the prognosis. An interesting potential biomarker disposable for sepsis status is high mobility group box 1 (HMGB1), a nuclear protein emerged as a key inflammatory mediator that is released during infection and cellular insult by activated immune cells and necrotic tissue and functioning as a DAMP. Clinical and preclinical studies have implicated HMGB1 as a mediator of sepsis pathogenesis and mortality (Diener et al., 2013).

Interestingly, in a recent publication it has been demonstrated that the administration of anti-HMGB1 polyclonal antibody to a murine model of severe sepsis alters the pattern of cytokine signaling to a more favorable profile, improves survival, and protects against the development of post-septic immunosuppression (Stevens et al., 2017).

Another protein strictly related to HMGB1 is osteopontin (OPN). Today it is well know that HMGB1 is an important OPN's downstream mediator and their crosstalk orchestrates several responses, at least in the liver (Borthwick and Mann, 2016). OPN and inflammation/infection relationship has long been known and OPN is still studied in several pathologies. Already in the late 90s it was established that OPN gene expression in human pulmonary macrophages increases after infection with virulent *Mycobacterium bovis* (Nau et al., 1997), progressively other authors studied and investigated the role of OPN in SIRS/sepsis condition. Serum OPN

concentrations were found higher in patients with sepsis compared to patients with SIRS (Vaschetto et al., 2008). In 2015 it was observed that the use of anti-OPN polyclonal antibody to a CLP-murine model of sepsis can have beneficial aspects, protecting against acute lung injury (Hirano et al., 2015). Eventually, OPN expression was found increased in cardiomyocytes of pediatric subjects with sepsis or pneumonia (Irion et al., 2018).

Among possible biomarkers growth arrest specific 6 (Gas6) need to be cited and it is also one object of interest of this thesis. Gas6 is a protein normally secreted in the bloodstream and in physiological conditions its plasma concentration in adult human is averagely 18 ng/mL (Balogh et al., 2005). Circulant Gas6 is known for long time, but the biological role of Gas6 is not completely understood yet. However, Gas6 expression and its concentration in the bloodstream and in different compartments were found to change in several pathological conditions, both chronic and acute such as hepatic fibrosis, cirrhosis and hepatocellular carcinoma, chronic kidney diseases, systemic lupus erythematosus as well as acute dyspnea (Salmi et al., 2019). Several studies were performed investigating Gas6 levels also in SIRS and sepsis: Borgel et al. and Gibot et al. were among the first studies to depict the correlation between Gas6 and sepsis condition in 2006 and 2007 respectively (Borgel et al., 2006; Gibot et al., 2007), and few years later Ekman et al. confirmed that Gas6 levels are increased during sepsis, finding a correlation between Gas6 and the degree of organ damage (Ekman et al., 2010a). More recently, plasma levels of Gas6 in septic patients were found higher in sepsis-induced ALI and the authors suggested the direct involvement of endothelial compartment (Yeh et al., 2017).

Gas6 and TAM receptors

Gas6, together with Protein S (Pros1), is the most studied TAM's ligand. They are members of the vitamin K-dependent protein family, containing one Gla domain in which the glutamate residues are post-translationally modified to form gamma-carboxyglutamate through a vitamin K-dependent carboxylation and this latter is required to confer to these proteins their activities. Additionally, a peculiar domain that lends uniqueness to these proteins, compared to other vitamin K-dependent ones, is the sex-hormone-binding globulin (SHBG)-like domain. Although it shares only 30% sequence identity with SHBG and its lacking in enzymatic activity (Saposnik et al., 2003). Importantly, despite Gas6 and Pros1 sharing structural homology, their functions to date-known are dissimilar: Gas6 is limited to binding TAM receptors, while Pros1

circulates in the bloodstream in two forms, one linked to C4b-binding protein and implicated in coagulation processes (60%) and the other free circulating, potentially able to bind TAM receptors (40%) (Dahlbäck, 2007).
Gas6 interacts with TAM through its SHBG-like domain, positioned at the C-terminus of its sequence, activating downstream signaling pathways (stated below). Furthermore, Gas6 'Gla domain' is able to bind phosphatidylserine (PtdSer) exposed by dying cells and through the SHBG-like domain binds the Ig-like domain of TAM receptors, thus Gas6 is able to work as a bridge between apoptotic cells and the TAM expressing effector cells (Salmi et al., 2019) (**Figure 3**).

TAM receptors belong to tyrosine kinase receptor family and include Tyro 3 (T), Axl (A) and Mer (M). They share structural similarity, notably two Ig-like domains, two fibronectin type III domains, a hydrophobic transmembrane domain, and a tyrosine kinase domain.
TAM were discovered and cloned by several groups in the 90s (Rothlin et al., 2015). In the first years from their discovery, their role in the maintenance of homeostatic balance through the regulation of the phagocytosis of apoptotic bodies (efferocytosis) has been demonstrated (Scott et al., 2001). Gradually, their role in the innate inflammatory response and in the regulation of cell proliferation and apoptosis was elucidated, leading to growing interest. In fact, a deficiency in TAM expression is related to autoimmune diseases (Rothlin et al., 2015) and, oppositely, their overexpression or aberrant activation is associated with the development and progression of cancer (Wu et al., 2018). In this context, the complex network of TAM functions has been clarified in recent years, as it seems more linked to the environmental context, or "milieu," rather than to the expressing cell/tissue, such as neurodegenerative diseases (Pierce and Keating, 2014), autoimmune diseases, and cancer (Wium et al., 2018). TAM activation, which occurs through tyrosine cross-phosphorylation, is normally mediated by the binding with their ligands, Gas6 and Pros1 as written above. Precisely, Gas6 is able to bind and activate all TAM receptors, while Pros1 can only bind Mer and Tyro3, without interacting with Axl. In 2014, Lew et al. published a detailed paper showing that Gas6 is capable of binding and activating all TAM, but the most powerful effect was observed following Axl activation. Moreover, authors showed that the PtdSer-binding Gla domain present on Gas6, PtdSer itself, and Ca^{++} are all essential to achieve a full receptor activation, but none of them is involved in receptor binding (Lew et al., 2014). Interestingly, Gas6-TAM receptor binding is not able to determine the receptor activation per se; so all the conditions described above need to be fulfilled in order to trigger the numerous signal transduction

pathways, such as phosphoinositide 3-kinase (PI3K)/Akt, mitogen-activated protein kinase (MAP kinase), nuclear factor-light-chain-enhancer of activated B cells (NF-κB), signal transducer and activator of transcription protein (STAT), phospholipase C (PLC), growth factor receptor-bound protein 2 (Grb2), Ras, extracellular-signal-regulated kinase (ERK), MLKL phosphorylation and others (Alciato et al., 2010; Lemke, 2013; Najafov et al., 2019). Eventually, Rothlin et al. demonstrated that TAM signaling triggers the expression of the suppressor of cytokine signaling proteins, SOCS1 and SOCS3. In fact, in dendritic cells from mice knockout for all three TAM receptors (TAM triple knockout; TAM TKO), the induction of SOCS1 was substantially impaired (Akalu et al., 2017; Rothlin et al., 2007). All these mentioned tangled pathways have crucial role in both physiological and pathological conditions and recently therapies targeting Gas6 and TAM receptors have been hypothesized (Wu et al., 2017, 2018) (**Figure 3**).

Despite their structural homology, following activation TAM receptor signaling is shut down in different ways: the signal desensitization that occurs through the shedding of the ectodomain by proteolytic cleavage was reported for Mer and Axl, but not for Tyro3 (Miller et al., 2017; Thorp et al., 2011) (**Figure 3**). Between the TAM-common-fibronectin type III domains and the transmembrane domain, the proline residue Pro485 present in the Mer sequence makes it susceptible to cleavage by the metalloproteinase ADAM17, a disintegrin and metalloproteinase domain 17, also known as tumor necrosis factor-alpha converting enzyme (TACE). Although the examination of the cleavage site sequence of several substrates shed by ADAM17 indicates that the distance between ADAM17 and its target is more important than the specific sequence in ectodomain shedding, the site-directed mutagenesis of the Pro485 cleavage site results in Mer resistance to proteolysis (Thorp et al., 2011).
Importantly, the PPRs activation by lipopolysaccharide (LPS) or polycytidylic acid (Poly:C) in macrophages results in the induction of cleavage of Mer extracellular domain. Furthermore, LPS-induced Mer/Axl shedding is dependent on ADAM17, as it is abrogated in ADAM17 gene knockdown macrophages. Sather et al. have shown that the shedding of the Mer ectodomain results in the inactivation of the receptor and in additional neutralization of TAM ligands, which are sequestered by the released soluble form of the receptor ectodomain (Sather et al., 2007). In 2010, Ekman et al. demonstrated that Gas6 is trapped by soluble Axl (sAxl) due to the higher affinity of Gas6 for Axl in comparison to Mer (Ekman et al., 2010b). Indeed, Gas6 binds Axl with a dissociation constant in the subnanomolar range, whereas its affinity for Mer is at least 10-fold lower (Nagata et al., 1996). Conversely, a previous study published by Sather

et al. demonstrated that both sAxl and sMer are able to inhibit the Gas6 activity and that the inactive sMer/Gas6-complex leads to a defective macrophage-mediated engulfment of apoptotic cells (Sather et al., 2007).

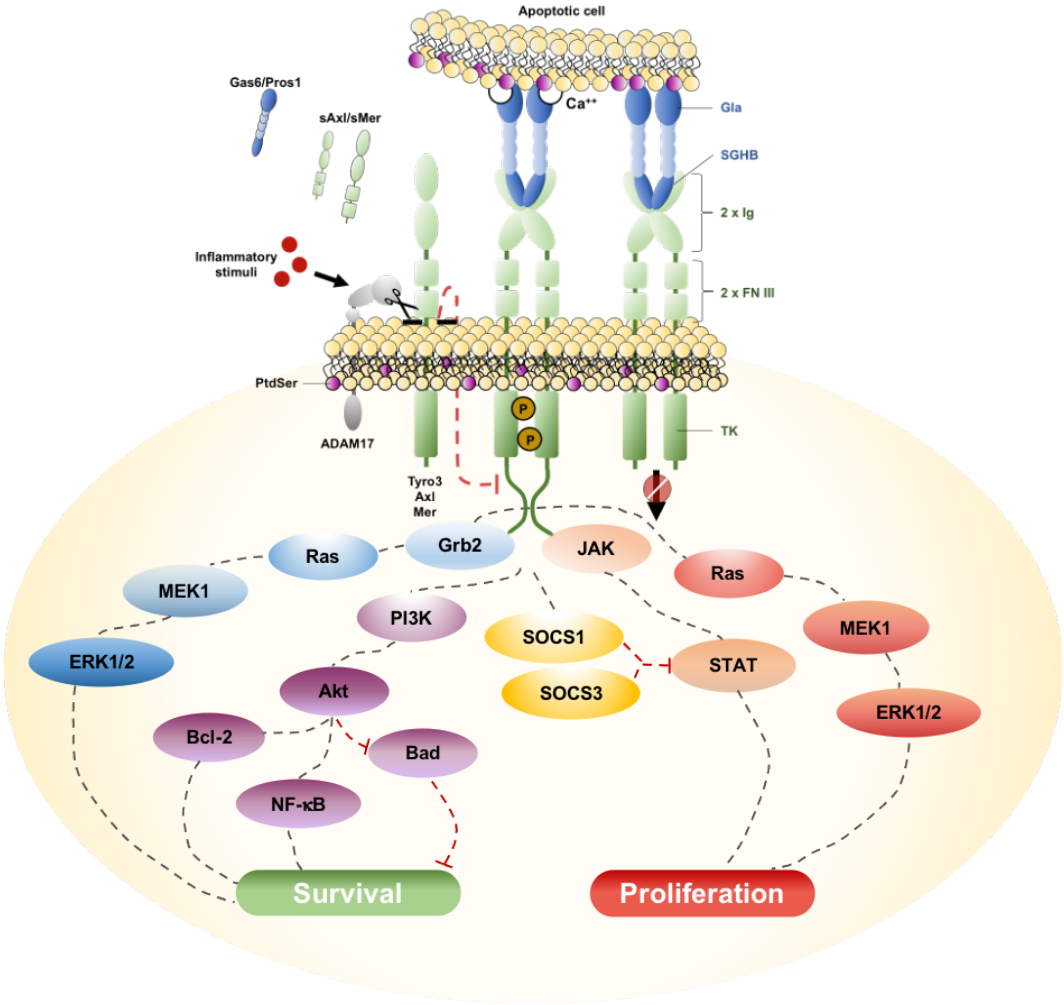

Figure 3. Gas6/TAM structures, posttranslational regulation and downstream pathways. Schematic representation of TAM receptors and their ligands (Gas6 and Pros1) with downstream pathways. All TAM receptors share structural domains, i.e., the tyrosine kinase (TK) domain, the transmembrane domain, two fibronectin type III domains (FN III), and two Ig-like domains (Ig) from the C-terminal to the N-terminal (right). The TAM ligands Gas6 and Pros1 share a sex hormone-binding globulin (SHBG) domain and a gamma-carboxyglutamic acid-rich (Gla) domain (right). The Gla domain binds phosphatidylserine (PtdSer) exposed in the outer side of the apoptotic cell plasma-membrane, while the SHBG domain interacts with TAM receptor Ig-like domains on the surface of TAM-expressing cells, thus acting as "bridge" proteins (right). The binding itself does not result in receptor activation that occurs through receptor transphosphorylation and in a Ca^{++}-dependent fashion (center). For Mer and Axl, the signal transduction is shut down by proteolytic cleavage of the receptor ectodomain (shedding), which is mediated by the transmembrane disintegrin and metalloproteinase (ADAM) 17. Shedding can be induced by inflammatory stimuli (e.g., lipopolysaccharide) leading to the extracellular domain release of the receptor and generating a soluble Axl (sAxl) and soluble Mer (sMer) forms able to interact with and sequester the ligands Gas6 and Pros1 (left).

Gas6 binds to TAM and thereby exerts its biological effects, including the promotion of survival and proliferation; several pathways are involved and in the schematic representation are divided by the endpoint. Furthermore, the Grb2 → Ras → MEK1 → ERK1/2 pathway is shown in blue and red when is activated by Mer and Axl, respectively. Molecular mediator list: Grb2 = growth factor receptor-bound protein 2, Ras = Ras superfamily, MEK1 = mitogen-activated protein kinase kinase, ERK1/2 = extracellular signal-regulated kinases, PI3K = phosphoinositide 3-kinases, Akt = protein kinase B, Bcl-2 = B-cell lymphoma 2, BAD = Bcl-2-associated death, NF-κB = nuclear factor-light-chain-enhancer of activated B cells, SOCS = suppressor of cytokine signaling, JAK = Janus kinase, STAT = signal transducer and activator of transcription.

In the end, despite their deep resemblance, TAM receptors are expressed by different cell types and tissues (**Table 2**): Tyro3 is generally localized in the nervous system, whereas Mer and Axl have been found in different tissues and they are frequently co-expressed by the same cells (Rothlin et al., 2015). This co-expression can be either equivalent in some cells, such as Kupffer cells in the liver and red pulp macrophages in the spleen, or unbalanced in others, such as for $CD68^+$ tingible macrophages, which are primarily Mer^+, and $CD11c^+$ white pulp dendritic cells (DCs), which are mostly Axl^+ (Zagórska et al., 2014). Regarding Gas6, its expression has been described in $CD11b^+F4/80^+$ bone marrow macrophages (Zahuczky et al., 2011), in microglia (Butovsky et al., 2014), in apoptotic thymocytes (Wallet et al., 2008), in Sertoli cells (Lu et al., 1999), in peritoneal macrophages (Deng et al., 2012) and in $CD11c^+$ DCs (Loges et al., 2010). Moreover, Gas6 is particularly expressed by endothelial cells, platelets, and leukocytes (Avanzi et al., 1997; Manfioletti et al., 1993).

	Tyro3	Axl	Mer
Brain	• Microglial cells [1] • Astrocytes [1]	• Microglial cells [1] • Astrocytes [1]	• Microglial cells [1] • Astrocytes [1]
Heart			• Cardiomyocytes [2]
Breast			• Mammary epithelial cells [3]
Lung		• Macrophages CD11b^{low} CD11c^{high} [4]	• *Alveolar macrophages* [5]
Liver	• *Kupffer cells* [6]	• *Kupffer cells* [6] • *HSC (quiescent/activated)* [6] • *LSEC* [6] • Hepatocytes [6]	• *Kupffer cells* [6] • *HSC (activated)* [6] • *LSEC* [6]
Spleen		• DCs CD11c^{high} [7]	• Macrophages F4/80^{high} B220^{-} CD11c^{+} MHCII^{+} red pulp [8] • Macrophages F4/80^{+} CD68^{+} (tangible body) [8]
Kidney	• *Podocytes* [9]		• *Podocytes* [9]
Testis	• Sertoli cells [10]	•Sertoli cells [10]	• Sertoli cells [10] • Leidyg cells [10]
Peritoneum		• Macrophages [11]	• Macrophages [11]
Blood/ BM-derived	• *Platelets* [12] • Monocytes [13] • Mon-der macrophages^{low} [13] • NK cells [14] • DCs CD11c^{+} [15]	• *Platelets* [12] • Monocytes [13] • Mon-der macrophages^{low} [13] • NK cells [14] • DCs CD11c^{+} [15]	• *Platelets* [12] • Monocytes [13] • Mon-der macrophages^{high} [13] • NK cells [14] • DCs CD11c^{+} [15] • DCs CD11b^{+} B220^{+} [16] • NKT cells [17] • *Lymphocytes CD8^{+} memory* [18]

Table 2. Expression of TAM receptors in different organs/tissues. Italic shows TAM expression located in human cells; all the others were found in murine cells. BM derived = bone marrow derived, HSC = hepatic stellate cells, LSEC = liver sinusoidal endothelial cells, Mon-der macrophages = monocyte-derived macrophages, DCs = dendritic cells; NK = natural killer, NKT = natural killer T. Table modified from Salmi et al. (Salmi et al., 2019) List of references: [1] (Ji et al., 2014), [2] (Wan et al., 2013), [3] (Sandahl et al., 2010), [4] (Fujimori et al., 2015), [5] (Kazeros et al., 2008), [6] (Mukherjee et al., 2016), [7] (Subramanian et al., 2014), [8] (Shao et al., 2009), [9] (Zhong et al., 2018), [10] (Wang et al., 2005), [11] (Deng et al., 2012), [12] (Gould et al., 2005), [13] (Malawista et al., 2016), [14] (Paolino et al., 2014), [15] (Seitz et al., 2007), [16] (Wallet et al., 2008), [17] (Behrens et al., 2003), [18] (Peeters et al., 2019).

AIM

Our group published in 2019 a review focusing on TAM-Gas6 axis and sepsis (Salmi et al., 2019). In this review we highlighted, speculated and hypothesize the use of Gas6 as a biomarker in the complex pathophysiology of sepsis, since several data seem to suggest a role of Gas6 as a useful biomarker for discriminating between noninfectious SIRS, sepsis, and septic shock. This data could suggest that Gas6 is physiologically released in response to insult. Furthermore, Gas6 came out as an early predictor of organ damage. Our hypothesis was that the organism triggers a Gas6-mediated response against sepsis-related insult and consequently Gas6 administration could be envisaged as a therapeutic reinforcement to the current treatment in sepsis (**Figure 4**). To test this hypothesis we pursued the following aims:

- Aim 1: to investigate Gas6 diagnostic and prognostic potential. We analyzed Gas6 plasma levels in different SIRS and septic patient's cohorts and we tried to investigate its potential from both diagnostic and prognostic point of view along with other potentially useful biomarkers.
- Aim 2: to determine the biological role of the Gas6/TAM axis in a mouse model of sepsis following broad-spectrum antibiotic administration. We investigated whether the administration of full-length murine Gas6 protein combined with standard antibiotic therapy would ameliorate the widespread organ damage observed in septic mice.

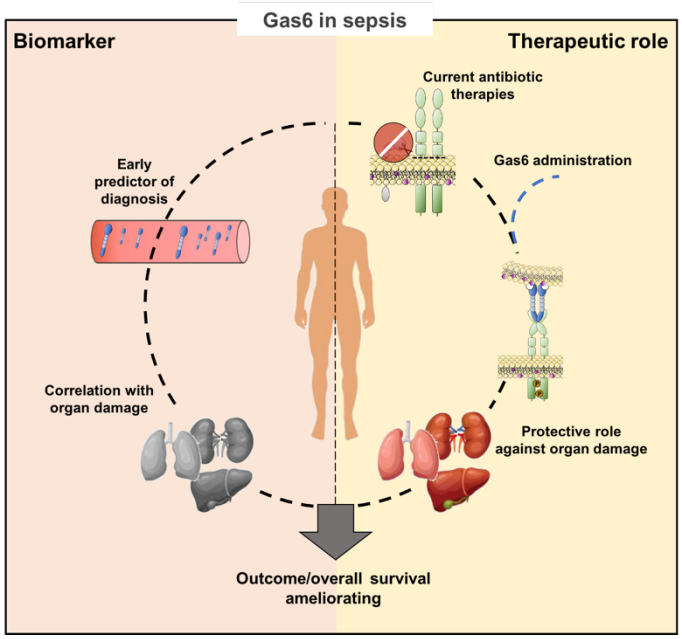

Figure 4. Gas6 potential role in septic status. Modified from Salmi et al. (Salmi et al., 2019). The high levels of Gas6 released in the bloodstream during sepsis seem to be aimed at counterbalancing sepsis dysfunctions; however, because inflammatory stimuli downregulate TAM receptors, the Gas6 over release is ineffective. Current therapy for sepsis is aimed at decreasing inflammatory stimuli. Gas6 administration after current therapy could operate on activated TAM receptors and protect the organs from sepsis-induced damage. The combination of a correct early diagnosis and the additional protective effects mediated by Gas6 could ameliorate the outcome/overall survival of patients.

MATERIAL and METHODS

Patients

Need-Speed Trial

Need-Speed Trial is an observational multicentre study, in which consecutive patients older than 18 years has been admitted to the emergency departments (ED) of five centres (Novara, Rome, Trieste, Turin and Brescia) between March 2013 and March 2015. Patients were enrolled within 24 h from admission if they met two or more criteria of systemic inflammatory response syndrome (SIRS) (Levy et al., 2018). Exclusion criteria were age < 18 years, pregnancy proven or suspected, witnessed aspiration, blood collection for biomarkers done 24 hours after ED admission, and refusal to give informed consent. The study was approved by the local ethical committee of each centre involved and was conducted in conformity to the principles of the Declaration of Helsinki. Patients were included prospectively. Mortality was evaluated at 7 and 30 days from enrolment through telephone follow-up calls at 30 days, indicating whether the patient was alive or dead and the possible death date.

Raise Aim Study

This single-centre, prospective, observational, pilot study was performed in the ED of the "Maggiore della Carità" University Hospital in Novara (Italy) from October 2016 to March 2018. Patients presenting to the ED with suspected sepsis according to the Sepsis-3 criteria (suspected infection and quick SOFA ≥ 2) were consecutively enrolled (T0). Exclusion criteria were pregnancy, age < 18 years and lack of a signed informed consent. The study was conducted according to the guidelines of the local ethical committee in conformity to the principles of the Declaration of Helsinki and was prospectively registered at the Australian New Zealand Trials Registry (ACTRN12617000429358). Patients were then clinically re-evaluated after 24 and 48 h and at 7 days or at discharge. A telephone follow-up was performed at 30 days in order to assess mortality. At 24 hours a second blood draw was performed for biomarkers studies (T1). At the end of the study period, two expert emergency physicians evaluated the clinical record of each patient in order to assess the final diagnosis according to the Sepsis-3 criteria. Therefore, patients were firstly divided in two groups depending on whether the suspected sepsis detected at ED admission was later confirmed ("sepsis") or ruled out ("non-sepsis"). Then, septic patients were further divided in two groups ("sepsis" and "septic shock") in order to perform additional analyses.

Blood processing

Blood was collected through 5 mL vacuum tubes, with and without anticoagulant (EDTA), and maintained at 4°C until the processing. Blood samples were centrifuge at 3000 rpm for 10 minutes at room temperature (RT) plasma and serum were aliquoted separately and stored -80°C.

Biomarkers analysis - Need Speed Trial

Blood samples for biomarkers analysis were obtained within 24 hours from ED admission and centrifuged in the local laboratory facility of each Unit. The plasma aliquots were then stored at -80°C in the different units and sent to the main Unit of Investigation (Laboratory of Emergency Medicine, Department of Translational Medicine, Università del Piemonte Orientale, Novara, Italy) for biomarkers plasmatic levels determination.

Gas6 was measured with a sandwich ELISA developed and validated in our laboratory (Alciato et al., 2008). Briefly, a 96-well plate was coated overnight with anti-Gas6 capture antibody (goat polyclonal affinity purified IgG, catalog number AF885, R&D Systems, MN, USA). Plasma samples were diluted 1:100, then human Gas6 was detected by a secondary biotinylated antibody (goat polyclonal IgG antigen affinity purified, human Gas6 biotinylated antibody, catalog number BAF885, R&D Systems), streptavidin–peroxidase conjugate (Sigma-Aldrich, MO, USA) and TMB (3,3',5,5'-tetramethylbenzidine). The reaction was blocked with sulfuric acid 2 N and absorbance determined by spectrophotometer (VICTOR Multilabel Plate Reader, PerkinElmer®) at 450 nm.

Biomarkers analysis - Raised Aim Study

Blood samples for biomarkers analysis were obtained within 24 hours from ED admission, aliquoted and stored at -80°C. Gas6 was measured with a sandwich ELISA developed and validated in our laboratory (Alciato et al., 2008) as described above. Osteopontin (OPN) plasma levels were quantified using a commercially available ELISA kit (enzyme-linked immunosorbent assay; R&D system codes DY1433 and DY007) according to the manufacturer's protocol. The optimal sample dilution was set at 1:1000. Lastly, HMGB1 plasma levels were quantified using a commercially available ELISA kit (IBL INTERNATIONAL, TECAN, system code ST51011) according to the manufacturer's

protocol. Finally, absorbances were determined by spectrophotometer (VICTOR Multilabel Plate Reader, PerkinElmer®) at 450 nm.

Statistical analysis

Statistical analysis was performed with the MedCalc® software v12.5.0 (MedCalc software, Ostend, Belgium). The normality of data distribution was assessed through the Kolmogorov-Smirnov normality test. Data are expressed as median [interquartile range] for continuous variables and as absolute numbers (percentages) for categorical variables. Comparison between groups was performed through the Mann-Whitney U test for continuous variables and through the Chi-square test for categorical variables.

A multiple regression analysis was performed to identify independent predictors of OPN concentration. Statistical significance was set at two-tailed $p < 0.05$.

In-vivo Studies

Bacteria Mix Preparation

One male C57Bl/6 male mouse was sacrificed. Cecum intestine portion was removed to collect fecal material and stored in 1.5 mL tube. Fecal material (FM) was resuspended in sterile phosphate buffered saline (PBS) at the concentration of 100 mg/mL. Then, FM was squeezed with sterile loop to release bacteria and centrifuged at 500 rpm for 1 minute room temperature (RT). Supernatant was collected and cultured in Luria broth (LB) medium for approximately 6 hours in orbiting incubator at 37°C and 200 rpm. Bacteria quantification was performed by measuring the absorbance of bacterial growth with a spectrophotometer (Eppendorf) at 595 nm (OD_{595} 1 = 10^9 bacteria) and aliquots of 10^9 bacteria/500 µL LB containing 20% glycerol (Sigma-Aldrich, St. Louis, Missouri, US, code G9012) were stored in -80°C.

Mouse Model of Bacteria-Induced Sepsis

All animal studies were approved by the Animal Care and Use Committee of the Università del Piemonte Orientale (Novara, Italy), number 702/2020-PR. Male C57Bl/6 mice (N. 29) were used with weight ranging from 30 to 36 grams and age from 13 to 26 weeks. Weight and age were used to match the different treatment groups. The eight treatment groups are shown in **Table 11** of Results section. Bacteria aliquots of cecal slurry stored at -80°C (as described above) were thawed at RT, cultured in LB medium for 30 min at 37°C and 200 rpm, washed once and resuspended in PBS. Sepsis was induced by intraperitoneal injection of 10^8 bacteria,

while mice injected with sterile PBS served as control group. After ~16 hours, 200 mg/kg ampicillin (Sigma Aldrich, St. Louis, Missouri, US, code 171257) were administered by tail vein (TV) injection as previously reported by Majhi et al. [23], while the control group received the same volume of PBS. Seven hours after ampicillin injection, 5 µg of recombinant murine Gas6 (full-length protein; R&D systems, Minneapolis, Minnesota, US) and the same amount of PBS in control groups were TV injected in each mouse. **Figure 5** shows a schematic representation of the treatment timeline. Mice were daily monitored and fed with wet food to maintain hydration, and cages were warmed using heating pads to avoid hypothermia. Approximately 40 hours after sepsis induction, mice were deeply anesthetized (isoflurane 1.5-2% O2), blood samples collected by intracardiac puncture and organs harvested for subsequent analysis. Due to difficulties in evaluating clinical parameter in mice, such as blood pressure, pale skin etc., a vitality score was set up and mice were evaluated in a double-blinded fashion. Each mouse was monitored and evaluated according to the following scoring system: 0 = dead mouse; 1 = living mouse, motionless with closed eyes, white ears and tachypneic; 2 = living mouse, slow movements, opened eyes, pink ears and normopneic; and 3 = living mouse, normal movements and normal behaviours.

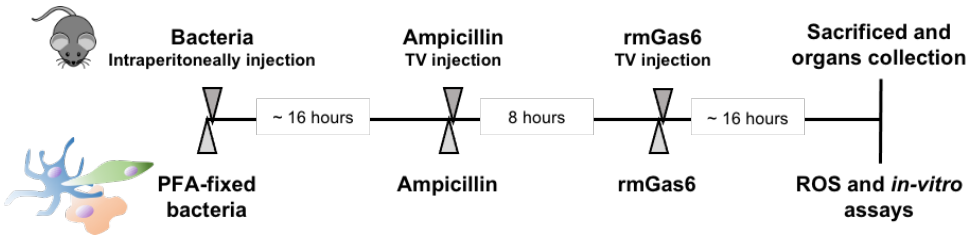

Figure 5. Timeline of treatments of *in-vivo* and *in-vitro* studies.

Blood and Organ Storage

Blood was collected using a 25G needle and 1mL syringe and maintained in sterile 1.5 mL tube with 3.4% sodium citrate anticoagulant (1/10 of total volume), in ice until the processing. Blood samples were centrifuge at 3000 rpm for 10 minutes at RT. Finally, plasma and buffy coat were aliquoted separately and stored -80°C.

Liver, spleen, kidneys and lungs were harvested from each mouse. All the organs underwent morphological analysis followed by anatomical sectioning and preservation for subsequent RNA analysis (-80°C) histochemical and morphological analysis (formalin-fixed paraffin-

embedded) and immunofluorescence (directly frozen in in Killik inclusion medium; Bio-Optica, Milano, Italy, code 05-9801).

Biochemical Analysis

Alanine transaminase (ALT) and lactate dehydrogenase (LDH) levels in plasma samples were determined using commercially available kits (ALT-GPT LR, code E380340130, and LDH LR code E4000230; Gesan, Campobello di Mazara, Italy).

RNA Extraction and Gene Expression Analysis

Organ samples (50 - 80 mg) were homogenized, and total RNA was extracted from each sample using TRIzol™ (Thermo Scientific, code 15596026), according to the manufacturer's instruction. RNA (1 - 3 µg) was retrotranscribed into cDNA with Applied Biosystems™ High-Capacity cDNA Reverse Transcription Kit (Thermo Scientific, code 4368814). Gene expression analysis was performed using primers for Sybr Green assay or TaqMan Probes (**Table 3**) and relative expression of candidate genes are relative to β-actin, which was use as housekeeping gene.

Gene	Alias	Forward Primer	Reverse Primer
ACTB	β-actin	5'-TGCCTGACGGCCAGGTCAT-3'	5'-ATCTCCTTCTGCATCCTGTCGG-3'
IL1B	Interleukin-1β	5'-GCTGTCCTGATGAGAGCATCC-3'	5'-CATGAGTCACAGAGGATGGGCTC-3'
IL6	Interleukin-6	5'-GCTGGTGACAACCACGGCCTTC-3'	5'-TTCTGCAAGTGCATCATCGTTGTTC-3'
IL10	Interleukin-10	5'-AGCCTTATCGGAAATGATCCAGT-3'	5'-GGCCTTGTAGACACCTTGGT-3'
TGFB1	TGF-β	5'-CTCCCGTGGCTTCTAGTGC-3'	5'-GCCTTAGTTTGGACAGGATCTG-3'
NOS2	iNOS	5'-CCCCGCTACTACTCCATCAG-3'	5'-CCACTGACACTTCGCACAAA-3'
MERTK	Mer	5'-CTCTGGAGTGGAGGCACTG-3'	5'-ATCTTCCAGTCTGGGGTGGT-3'
AXL	Axl	5'-GAACTTGCCAGGCTCCTACTCT-3'	5'-GGAGTTGACACAGGTCTGCTCA-3'
Gene	**Alias**	**TaqMan™ probe**	**GeneBank®**
ACTB	β-actin	Mm00607939_s1	AK07935.1
TNF	TNF-α	Mm00443258_m1	AK153319.1

Table 3. Primers sequences and TaqMan probes.

Histochemistry

Formalin-fixed paraffin-embedded organs were processed for morphological (haematoxylin and eosin – H&E – staining and Periodic acid-Schiff – PAS – staining) and

immunohistochemical (myeloperoxidase - MPO) staining. For MPO staining, organs sections were incubated with anti-myeloperoxidase rabbit polyclonal antibody (Cell Marque™, Rocklin, California, US) diluted 1:200. Histological images were acquired using a Pannoramic MIDI II (3DHISTECHTM, Budapest, Hungary). Images were analyzed using QuPath software (open source digital pathology, University of Edinburgh, UK). With this method, we also evaluated the ischemic areas in the kidney section of each mouse.

Immunofluorescence

Six to 7 µm thick Killik-embedded mouse organs sections were fixed in 4% PFA for 5 min at RT and rinsed in PBS for 10 min. Samples were incubated for 30 minutes in PBS containing 0.1% Triton X-100 and 5% goat serum and finally incubated for 2 hours at RT with 1:200 dilutions of the following antibodies: Tyr691 phospho-Axl (pAxl) (rabbit polyclonal; Invitrogen, Carlsbad, California, US, PA5-39729, previously validated (Tutusaus et al., 2020a)) and Tyr681, Tyr749 phosphor-MerTK (pMer) (rabbit polyclonal; Abcam, Cambridge, UK, ab192649, previously validated (Kim et al., 2017b)). Hematopoietic cells were detected using a rat anti-mouse CD45 (clone IBL-5/25; Immunotools, Friesoythe, Germany) diluted 1:200, for 2 hours at RT. After washing in PBS containing 0.1% Tween-20, Alexa Fluor®488- or 546-conjugated goat anti-rabbit, anti-rat IgGs (1:500, Molecular Probes) were added for 1 hour. Nuclei were stained with 4′,6-diamidino-2-phenylindole (DAPI; Sigma Aldrich) or TO-PRO-3 (ThermoFisher Scientific). Images were acquired using fluorescence (Leica DM 2500) or confocal (Leica TCS SP2) microscope and analysed with ImageJ software (NIH and LOCI, University of Wisconsin, US).

In-vitro Studies

Cell Culture Models of Sepsis

Monocytic Raw264.7 (ATCC®, Manassas, Virginia, US - TIB-71™) cells were cultured in Dulbecco's Modified Eagle's Medium (DMEM) (Thermo Fisher Scientific, Waltham, Massachusetts, US) in the presence of 10% fetal bovine serum (FBS), 2 mM glutamine (Sigma Aldrich) and antibiotic solution (Sigma Aldrich). Immature dendritic JAWSII cells (ATCC® CRL-11904™) were maintained in Iscove's Modified Dulbecco's Medium (IMDM) (Thermo Fisher Scientific) in the presence of 20% FBS 4 mM glutamine, 1 mM sodium pyruvate and antibiotic solution (Sigma Aldrich). Pancreatic islet endothelial MS1 cells (MILE SVEN 1) (ATCC® CRL-2279™) were cultured in DMEM with 5% FBS and antibiotic solution.

Evaluation of Mitochondrial Activity

For cell treatment, bacteria were fixed with 3 volumes of PFA 4% in PBS for 3 hours at 37°C, washed twice, and resuspended in PBS to remove the excess of PFA before use. Raw264.7 cells ($30 \cdot 10^3$), JAWSII cells ($30 \cdot 10^3$) and MS1 cells ($20 \cdot 10^3$), cultured in antibiotic-free medium, were incubated for ~12 hours in the presence or absence of 10^7 PFA-fixed bacteria followed by 8 hours treatment with ampicillin (0.1 mg/mL) (Sigma Aldrich, St. Louis, Missouri, US, code 171257) and subsequent ~12 hours incubation with Gas6 (100 ng/mL) (full-length protein; R&D systems, Minneapolis, Minnesota, US). The timeline of the various treatments is shown in **Figure 5**.

Mitochondrial activity was assessed by MTT (3-[4,5-dimethylthiazol-2-yl]-2,5 di-phenyl tetrazolium bromide; Sigma-Aldrich) assay. Cells were incubated for 90 min in the presence of 0.5 mg/mL MTT followed by formazan solubilization in dimethyl sulfoxide (DMSO) (CARLO ERBA Reagents©, Cornaredo, Milano, Italy, code 445103). Since MTT assay does not discriminate proliferative effects, the quantification of mitochondrial activity was normalized to crystal violet (CV) (Sigma Aldrich, St. Louis, Missouri, US, code C0775) staining, performed in parallel. Briefly, after treatments, cells were fixed in a 10% glutaraldehyde (Sigma Aldrich, St. Louis, Missouri, US, code G6257) solution for 5 min at RT, washed twice in water and stained 15-20 min at RT with a CV solution (0.1% crystal violet + 20% methanol in water). Cells were washed extensively following staining, and CV was solubilized in 10% acetic acid in water. Both MTT and CV signals were measured at OD570nm using a Victor X microplate reader (PerkinElmer, Waltham, Massachusetts, US). Mitochondrial activity was calculated as MTT OD570nm/CV OD570nm ratio.

Quantification of Oxidative Stress and Lipid Staining

Raw264.7 ($90 \cdot 10^3$), JAWSII ($90 \cdot 10^3$) and MS1 cells ($70 \cdot 10^3$), plated on 15 mm round cover glasses, were incubated for ~12 hours in the presence or absence of $5 \cdot 10^7$ PFA-fixed bacteria following 8 hours treatment with ampicillin (0.1 mg/mL) (Sigma Aldrich) and subsequent ~12 hours incubation with Gas6 (100 ng/mL) (R&D systems). Relative changes in intracellular reactive oxygen species (ROS) were measured using the oxidation-sensitive fluorogenic dye CellROX® Green Reagent (Thermo Fisher Scientific), and nuclei were stained with Hoechst (Thermo Fisher Scientific), according to the manufacturer's instructions. In parallel to oxidative stress analysis, lipids were stained with BODIPY™ 493/503 (Thermo Fisher

Scientific) according to manufacturer's instructions. Dye-loaded cells were rinsed twice in Hank's balanced salt solution (HBSS) and mounted on glass slide using Mowiol (Sigma Aldrich). Images were acquired using a fluorescence microscope (Leica DM 2500 – Leica, Wetzlar, Germany) and analysed (integrated density) with ImageJ software (NIH and LOCI, University of Wisconsin, US). To minimize photoactivation artifacts, cells fields were imaged under identical fluorescent conditions, using identical software settings.

Statistical Analysis

Data are expressed as mean ± SD or median [IQR] as appropriate. Normality of data distribution was evaluated by Kolmogorov-Smirnov test. One-way ANOVA, two-way ANOVA and multiple t-test for independent samples were performed to analysed parametric data, while Kruskal-Wallis test was performed for non-parametric data, as appropriate. Gene expression analysis for cytokines (IL1B, IL6, IL10, TGFB1, TNF) was generated as follows: the mean differences of each gene were calculated by multiple t-test of relative expression (between P group and treatment conditions). The comparison among groups was then performed by ANOVA Tukey's multiple test. Statistical significance was set at a p-value < 0.05.

Statistical analysis was performed with Prism GraphPad software 6 (San Diego, California, US). Graphs were created using Prism GraphPad software 6.

RESULTS

Patients

Gas6 in SIRS Patients

Firstly, we analyzed a considerably numerous population with SIRS diagnosis. A total of 890 patients were enrolled through multi-center trial (Need Speed Trial) which included Brescia, Novara, Rome, Trieste and Turin. In this draft are included only general demographic variables and plasmatic Gas6 levels (**Table 4**): patients median age was 80 years [72 – 87] with a male prevalence of 54% (N. 477) and median BMI of 24.2 kg/m^2 [21.7 – 27.3]. Globally, circulating Gas6 levels were 31.1 ng/mL [23.2 – 43.5].

Variable	Patients (N. 890)
Age, years	80 [72 – 87]
Gender, M/F	477 (54) / 413 (46)
BMI, Kg/m^2	24.2 [21.7 – 27.3]
Gas6, ng/mL	31.1 [23.2 – 43.5]

Table 4. Demographic characteristic and Gas6 plasma levels. Continuous variables are represented by median and [interquartile range], while categoric variables are represented by number and (percentage). BMI = body mass index, Gas6 = growth arrest specific 6.

As reported more than ten years ago by Jiang and colleagues, plasma Gas6 levels in healthy subjects is ranging from 13 to 28 µg/L, with median of 16 µg/L (Jiang et al., 2009). In SIRS patients of our study was almost double, 31.1 ng/mL [23.2 – 43.5]. Thus, we investigated more deeply Gas6 circulating levels in survivors and non-survivors SIRS patients, analyzing mortality at 7 and 30 days (**Table 5**).

At 7 days from the admission in Emergency Department 9.7% (N. 87) of patients died and none of analyzed variable shown a significant difference between survivor and non-survivor, except age. Non-survivor patients showed a median age of 85 years [78 – 90] vs survivor patients whom were 80 years old [71 – 86], $p < 0.0001$. Instead, Gas6 circulating levels were similar: 31.0 ng/mL [23.2 – 43.2] in survivor, compared to 32.2 [23.1 – 47.1] ng/mL in non-survivor patients, $p = 0.336$. Similar results were observed for 30 days mortality, where 177 (19.8%) patients died: median age was significantly different, and surprisingly survivor were

averagely older than non-survivor subjects, with 89 years [71 – 86] vs 85 years [79 – 90] respectively ($p < 0.0001$). Gas6 plasma levels were nearly the same in the two groups, 31.3 ng/mL [23.3 – 43.4] and 30.5 [22.6 – 44.2] for survivor and non-survivor respectively, $p = 0.821$.

Variable	Alive at 7 days (N. 803)	Dead at 7 days (N. 87)	*p*-Value
Age, years	80 [71 – 86]	85 [78 – 90]	**<0.0001**
Gender, M/F	436 (54) / 367 (46)	41 (47) / 46 (53)	0.246
BMI, Kg/m^2	24.2 [21.7 – 27.3]	23.9 [21.3 – 27.3]	0.623
Gas6, ng/mL	31.0 [23.2 – 43.2]	32.2 [23.1 – 47.1]	0.336
Variable	**Alive at 30 days (N. 713)**	**Dead at 30 days (N. 177)**	***p*-Value**
Age, years	89 [71 – 86]	85 [78 – 90]	**<0.0001**
Gender, M/F	393 (55) / 320 (45)	84 (47) / 93 (53)	0.081
BMI, Kg/m^2	24.3 [21.9 – 27.4]	24.0 [20.9 – 26.4]	0.246
Gas6, ng/mL	31.3 [23.3 – 43.4]	30.5 [22.6 – 44.2]	0.821

Table 5. Demographic characteristic and Gas6 plasma levels between survivor and non-survivor patients. Mortality was analyzed at 7 days and 30 days after ED admission. Continuous variables are represented by median and [interquartile range], while categoric variables are represented by number and (percentage). BMI = body mass index, Gas6 = growth arrest specific 6.

Biomarkers in Septic Patients

OPN

SIRS is a non-specific condition related to infection and/or inflammation, and moreover it is an old definition which was replaced by Sepsis-3 criteria from 2016. However, the instant and specific sepsis diagnosis is still difficult to achieve, and new biomarkers could help to overcome this issue. Thus, a cohort of 101 patients with suspicious sepsis through Sepsis-3 criteria were enrolled in ED of "Maggiore della Carità" hospital (Novara). Among 101 patients, 92 (91%) were confirmed as septic patients, whereas 9 (9%) subjects were declared non-septic patients (**Table 6**). The overall cohort was characterized by a median age of 80 years [73 – 88], with a male prevalence (57 male subjects, 56%) and a median BMI of 24.8 kg/m^2 [22.0 – 27.5]. Circulating Osteopontin (OPN) was measured in this cohort as possible biomarker and the median plasma OPN was 204.6 ng/mL [112.5 – 376.8].

Then non-septic and septic patients were analyzed: no significant differences were found in demographic parameters (age, gender and BMI) between subjects with or without sepsis.

Instead, OPN was significantly higher in septic patients (225.2 ng/mL [138.2 – 387.8]) compared to patients without sepsis (91.3 ng/mL [63.9 – 105.4]), $p < 0.001$ (**Table 6**).

Variable	Patients (N. 101)	Non-sepsis (N. 9)	Sepsis (N. 92)	*p*-Value
Age, years	80 [73 – 88]	84 [64 – 90]	80 [73 – 88]	0.934
Gender, M/F	57 (56) / 44 (44)	7 (78) / 2 (22)	50 (54) / 42 (46)	0.317
BMI, Kg/m^2	24.8 [22.0 – 27.5]	28.9 [24.6 – 31.2]	24.2 [22.0 – 27.1]	0.071
OPN, ng/mL	204.6 [112.5 – 376.8]	91.3 [63.9 – 105.4]	225.2 [138.2 - 387.8]	**<0.001**

Table 6. Demographic characteristic and OPN plasma levels. Variables are shown for the whole cohort and compared by patients without sepsis (non-sepsis) and patients with sepsis. Continuous variables are represented by median and [interquartile range], while categoric variables are represented by number and (percentage). BMI = body mass index, OPN = osteopontin.

Successively, a logistic regression analysis including clinical variables together with OPN showed that OPN was an independent predictor of sepsis (OR = 1.020, 95% CI 1.002 to 1.039 with $p = 0.031$). Furthermore, the diagnostic performance of OPN was also evaluated through a ROC curve analysis: area under the curve (AUC) was 0.878 (95% CI 0.798 to 0.935) and a cut-off of 112.8 ng/mL showed an 80.4% sensitivity and an 88.9% specificity in detecting septic patients (Youden's index J = 0.693) (data not shown, published by Castello et al. (Castello et al., 2019)).

Since OPN determination have showed a significant diagnostic power, we investigated the OPN prognostic role in septic subgroup. Considering mortality at 30 days neither demographic characteristic, nor OPN levels were significantly different between alive (N. 58, 63.0%) and dead patients (N. 34, 36.0%) (**Table 7**).

Variable	Alive at 30 days (N. 58)	Dead at 30 days (N. 34)	*p*-Value
Age, years	80 [71 – 86]	84 [75 – 89]	0.175
Gender, M/F	33 (57) / 25 (43)	17 (50) / 17 (50)	0.671
BMI, Kg/m^2	25.0 [22.2 – 27.3]	24.1 [21.3 – 26.1]	0.283
OPN, ng/mL	216.8 [144.0 – 356.6]	231.3 [123.4 – 526.4]	0.482

Table 7. Demographic characteristic and OPN plasma levels between survivor and non-survivor patients. Mortality was analyzed at 30 days after ED admission. Continuous variables are represented by median and

[interquartile range], while categoric variables are represented by number and (percentage). BMI = body mass index, OPN = osteopontin.

HMGB1 and Gas6

An extended cohort, of same study described above, which included N. 117 patients demonstrated the similar trend of non-septic (10, 8.5%) and septic (107, 91.5%) patients (**Table 8**). In this analysis, time 1 (T1), performed 24 hours after enrollment time (T0), was also introduced. In this cohort BMI, in contrast to age and gender, was significantly higher in non-septic patients (29.2 kg/m^2 [25.7 – 31.3] compared to subjects with a confirmed sepsis diagnosis (24.2 kg/m^2 [22.0 – 26.6]), $p = 0.030$.

Both Gas6 and HMGB1 biomarkers were significantly higher in septic patients compared to subjects without sepsis and this trend was maintained not only at T0 but also after 24 hours (T1). The median value of plasma Gas6 at T0 was 53.7 ng/mL [24.7 – 83.6] in non-septic patients and 77.8 ng/mL [63.3 – 108.3] in septic patients ($p = 0.009$), therefore about double compared to SIRS patients (31.1 ng/mL [23.2 – 43.5]) (**Table 4**). At T1 Gas6 levels were 78.7 ng/mL [57.0 – 98.9] and 56.4 ng/mL [35.0 – 64.7] for patients with and without sepsis respectively, $p = 0.005$. Circulating levels of inflammatory molecule HMGB1 were also measured in this cohort: at T0 the median HMGB1 value was 1.9 ng/mL [1.3 – 3.8] in non-septic patients and 4.1 ng/mL [1.7 – 7.5] in septic subjects ($p = 0.021$), whereas 24 hours later median levels were 1.4 ng/mL [1.1 – 2.1] and 2.5 ng/mL [1.8 – 4.5] respectively, $p = 0.015$ (**Table 8**).

Variable	Patients (N. 117)	Non-sepsis (N. 10)	Sepsis (N. 107)	*p*-Value
Age, years	80 [73 – 88]	83 [65 – 90]	80 [73 – 88]	0.903
Gender, M/F	63 (54) / 54 (46)	7 (70) / 3 (30)	56 (52) / 51 (48)	0.460
BMI, Kg/m^2	24.4 [22.0 – 27.4]	29.2 [25.7 – 31.3]	24.2 [22.0 – 26.6]	**0.030**
Gas6 T0, ng/mL	77.0 [57.9 – 106.5]	53.7 [24.7 – 83.6]	77.8 [63.3 – 108.3]	**0.009**
Gas6 T1, ng/mL	75.3 [54.8 – 97.9]	56.4 [35.0 – 64.7]	78.7 [57.0 – 98.9]	**0.005**
HMGB1 T0, ng/mL	3.9 [1.6 – 7.1]	1.9 [1.3 – 3.8]	4.1 [1.7 - 7.5]	**0.021**
HMGB1 T1, ng/mL	2.4 [1.5 – 4.0]	1.4 [1.1 – 2.1]	2.5 [1.8 - 4.5]	**0.015**

Table 8. Demographic characteristic, Gas6 and HMGB1 plasma levels. Variables are shown for the whole cohort and compared by patients without sepsis (non-sepsis) and patients with sepsis. Gas6 and HMGB1 plasma concentrations were measured at ED admittance (T0) and 24 hour later (T1). Continuous variables are represented by median and [interquartile range], while categoric variables are represented by number and (percentage). BMI = body mass index, Gas6 = growth arrest specific 6, HMGB1 = high mobility group box 1.

Deepening, we then analyzed patients based on specific diagnosis: patients without sepsis (N. 10) as previously divided, patients with sepsis diagnosis (N. 77) and patients who developed septic shock (N. 30). Thus, 39% of septic patients worsened in septic shock condition (**Table 9**). Both HMGB1 and Gas6 plasma levels showed an increase based on the disease severity. In fact, median plasma levels of HMGB1 in septic shock patients were significantly higher compared to circulating levels in septic patients, 6.39 ng/mL [3.30 – 9.65] and 3.61 ng/mL [1.48 – 6.61] respectively ($p = 0.003$) (**Figure 6a**). The same trend was shown by Gas6: sepsis 75.58 ng/mL [55.13 – 98.97] vs septic shock 96.95 ng/mL [72.04 – 123.80], $p = 0.021$ (**Figure 6b**). Septic shock patients had significantly higher circulating Gas6 and HMGB1 levels compared to patients without sepsis (no sepsis) ($p = 0.0016$ and $p = 0.0019$, respectively). However, neither Gas6 nor HMGB1 were significantly different between septic patients and no sepsis patients (**Figure 1a and b**). We lastly performed ROC curve analysis to determine predictive value of diagnosis obtaining weak values for both biomarkers: HMGB1 AUC = 0.715 and Gas6 AUC = 0.746 (**Figure 1c and d**).

Variable	No sepsis (N. 10)	Sepsis (N. 77)	Septic shock (N. 30)
HMGB1 ng/mL	1.93 [1.14 – 3.81]	3.61 [1.48 – 6.61]	6.39 [3.30 – 9.65]
Gas6 ng/mL	53.68 [24.75 – 83.57]	75.58 [55.13 – 98.97]	96.95 [72.04 – 123.80]

Table 9. Biomarkers plasma levels divided by diagnosis. HMGB1 and Gas6 values are shown as median levels (ng/mL) and [range interquartile].

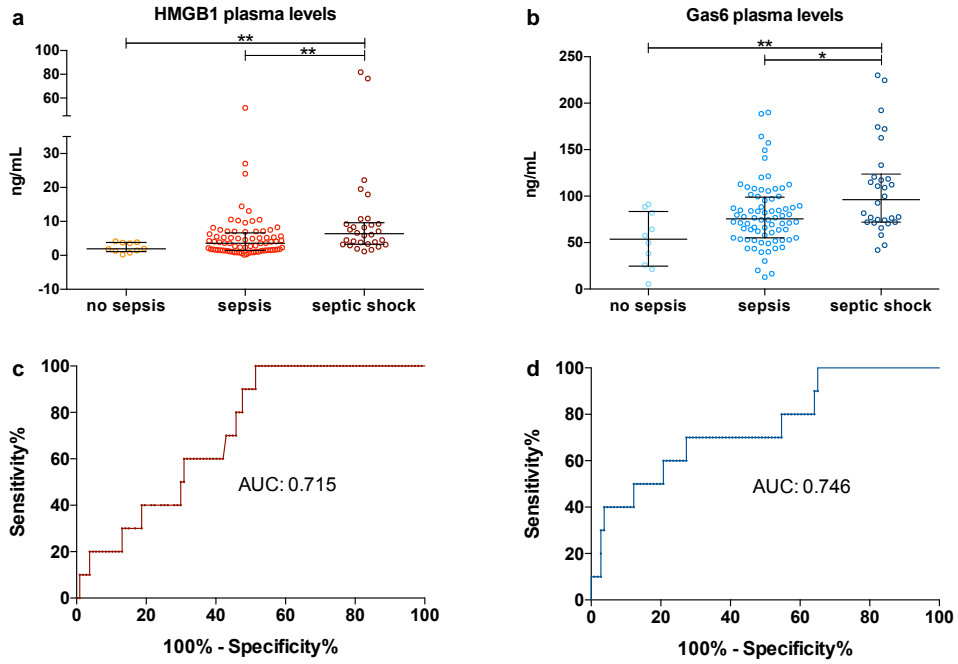

Figure 6. Biomarkers plasma levels divided by diagnosis and ROC curves. Plasma HMGB1 (a) and Gas6 (b) levels in patients without sepsis (no sepsis), with sepsis and with septic shock. Diagnostic performance of HMGB1 (c) and Gas6 (d) in discriminating non-septic from septic patients. Receiving Operating Characteristic (ROC) curve analysis with area under the curve (AUC) was performed and reported in the figures.

Analyzing mortality at 7 and 30 days, neither demographic variables nor Gas6 plasma levels demonstrated significant correlation with mortality. At 7 days the 24% (N. 28) of patients died, while mortality after one month (30 days) reached 35% (N. 41). Dissimilarly from Gas6 and OPN plasma levels, HMGB1 was significantly higher in non-survivors compared to survivor subjects both at T0 (6.6 ng/mL [2.9 – 9.3] vs 3.8 ng/mL [1.6 – 6.8]) and T1 (3.6 ng/mL [2.5 – 7.0] vs 2.4 ng/mL [1.7 – 3.9], $p = 0.017$) in the evaluated mortality in the first week (**Table 10**). The same trend was observed in the analysis of mortality at 30 days: dead subjects showed median plasma HMGB1 levels of 6.1 ng/mL [1.9 – 8.8] compared to alive subjects who had HMGB1 levels of 3.7 ng/mL [1.6 – 5.6], $p = 0.041$. Values of HMGB1 measured at T1 were 3.2 ng/mL [2.3 – 5.3] in dead subjects and 2.3 ng/mL [1.6 – 3.9] in alive patients, $p = 0.039$ (**Table 10**).

Variable	Alive at 7 days (N. 89)	Dead at 7 days (N. 28)	*p*-Value
Age, years	80 [71 – 87]	82 [75 – 88]	0.277
Gender, M/F	43 (54) / 37 (46)	13 (48) / 14 (52)	0.779
BMI, Kg/m^2	24.4 [22.2 – 27.2]	23.9 [21.1 – 25.8]	0.197
Gas6 T0, ng/mL	76.7 [57.6 – 99.7]	87.0 [65.3 – 120.5]	0.163
Gas6 T1, ng/mL	75.0 [52.4 – 95.6]	87.0 [65.7 – 114.5]	0.129
HMGB1 T0, ng/mL	3.8 [1.6 – 6.8]	6.6 [2.9 – 9.3]	**0.035**
HMGB1 T1, ng/mL	2.4 [1.7 – 3.9]	3.6 [2.5 – 7.0]	**0.017**
Variable	**Alive at 30 days (N. 76)**	**Dead at 30 days (N. 41)**	***p*-Value**
Age, years	80 [71 – 86]	82 [75 – 89]	0.200
Gender, M/F	36 (54) / 31 (46)	20 (50) / 20 (50)	0.779
BMI, Kg/m^2	24.8 [22.3 – 27.3]	23.9 [21.1 – 25.9]	0.101
Gas6 T0, ng/mL	77.1 [55.2 – 99.6]	76.7 [65.4 – 119.4]	0.189
Gas6 T1, ng/mL	75.3 [52.1 – 95.7]	84.7 [63.5 – 98.6]	0.216
HMGB1 T0, ng/mL	3.7 [1.6 – 5.6]	6.1 [1.9 – 8.8]	**0.041**
HMGB1 T1, ng/mL	2.3 [1.6 – 3.9]	3.2 [2.3 – 5.3]	**0.039**

Table 10. Demographic characteristic, Gas6 and HMGB1 plasma levels between survivor and non-survivor patients. Mortality was analyzed at 7 days and 30 days after ED admission. Gas6 and HMGB1 plasma concentrations were measured at ED admittance (T0) and 24 hour later (T1). Continuous variables are represented by median and [interquartile range], while categoric variables are represented by number and (percentage). BMI = body mass index, Gas6 = growth arrest specific 6, HMGB1 = high mobility group box 1.

In-vivo Experiments

Groups of Mice Divided for Treatments and Timeline Treatments

Animals were divided in eight groups of treatments: group P (N. 3 mice), A (N. 3), G (N. 3) and AG (N. 3) were control groups, whereas group B (N. 4), BA (N. 4), BG (N. 4) and BAG (N. 5) were septic mice treated differently with antibiotic standard therapy and/or growth arrest-specific 6 (Gas6). All mice were matched by their weight. 10^8 bacteria were intraperitoneally injected (control groups were treated with PBS); ampicillin was tail-vein injected as broad-spectrum antibiotic (200 mg/kg) and 5 µg of recombinant murine (rm) Gas6 was tail-vein injected (**Table 11**).

Group	Mice (N.)	Median weight (g)	Treatment(s)	Fecal bacteria	Ampicillin	rmGas6
P	3	33	PBS	-	-	-
A	3	33.5	ampicillin	-	8 hours	-
G	3	33	Gas6	-	-	~ 16 hours
AG	3	33	ampicillin, Gas6	-	8 hours	~ 16 hours
B	4	34	bacteria	~ 16 hours	-	-
BA	4	33	bacteria, ampicillin	~ 16 hours	8 hours	-
BG	4	33.5	bacteria, Gas6	~ 16 hours	-	~ 16 hours
BAG	5	33.5	bacteria, ampicillin, Gas6	~ 16 hours	8 hours	~ 16 hours

Table 11. Mice and treatment(s). Table represents group of treatments, mice number for each group and their median weight. Treatments and their schedule are reported for each group: 10^8 fecal bacteria were intraperitoneally injected, 200 mg/kg of ampicillin and 5 µg of recombinant murine (rm) Gas6 were tail vein injected.

Mice Vitality Evaluation

Since it is difficult to evaluate clinical parameter in mice, such as blood pressure, pale skin etc. a vitality score was set up. To avoid bias in monitoring the clinical parameters in septic mice, we devised a mouse vitality score (see Material and Methods, section Mouse Model of Bacteria-Induced Sepsis) that was used in a double-blind fashion. While healthy mice, such as mice injected with PBS (group P), and groups A, G and AG obtained a score of 3 (data not shown), mice injected with bacteria to induce sepsis (group B, N. 4) had a score of 0–1 with one mouse dead before 24 hours. Septic mice treated with broad spectrum antibiotic (group BA, N. 4), the current standard therapy for septic patients, obtained a score of 1–2, similar to that of septic mice treated with Gas6 (group BG, N. 4). Interestingly, 4 out of 5 septic mice receiving both antibiotic and Gas6 (group BAG, N. 5) obtained a mean score of 2.8 (±0.4), almost identical to that of healthy mice (3, dotted line) (**Figure 7**).

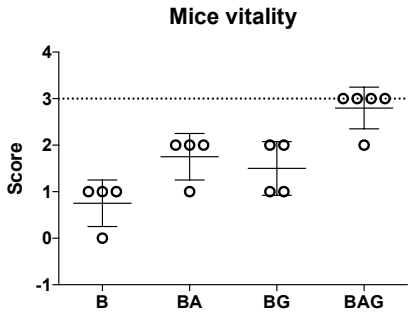

Figure 7. Mice vitality. Mice were classified according to the following vitality scheme. 0 = live mouse, motionless with closed eyes, white ears and tachypneic, 2 = live mouse, slow movements opened eyes, pink ears and normopneic; 3 = live mouse, normal movements/normal behaviors. The dotted line corresponds to the score (3) of control mice (P). Bars represent mean with standard deviation.

Mice Organs Evaluation

Lung

As septic patients frequently develop acute respiratory distress syndrome (ARDS) (Sevransky et al., 2009) and acute kidney injury (AKI) (Peerapornratana et al., 2019), we next evaluated lung (**Figure 8 and 9**) and kidney (**Figure 10, 11 and 12**) tissues by histological analysis of septic, treated septic and controls mice. Pulmonary histology was characterized by an increased number of nuclei in the alveolar space in septic mice, as highlighted by hematoxylin staining. However, we have noticed a decreased nuclei number in BA, BG and BAG mice compared to mice in B group. In particular, the alveolar space of BA mice and especially of BAG mice appeared morphologically similar to control P mice; this aspect was more remarkable at higher magnification (**Figure 8**). Moreover, we calculated number of nuclei for total pulmonary areas and we normalized values to the average of P mice. We found that BA and BAG mice showed a significant decreased of total cell number (% nuclei/μm^2) compared to not further treated septic mice (B): BA mice 115.0% (± 3.74) and BAG mice 112.9% (± 10.3) vs. B mice 140.7% (± 4.3), $p = 0.020$ and $p = 0.009$ respectively (**Figure 9**). On the other hand, healthy treated mice (A, G and AG) did not show morphological and histological differences compared to P mice (**Figure 8)** and nuclei count was just the same as P mice (dotted line) (**Figure 9**).

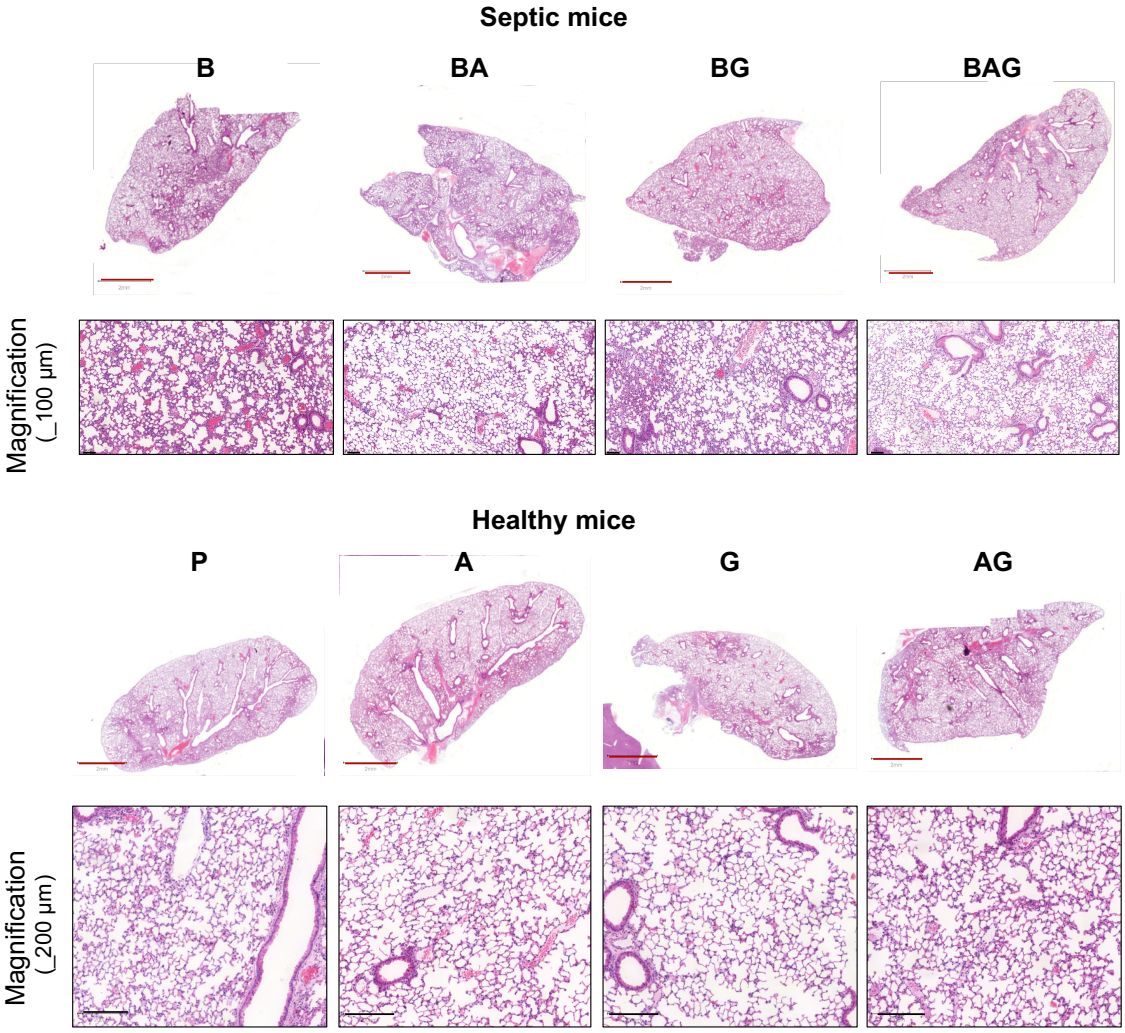

Figure 8. Lung histology and morphology. Hematoxylin and eosin (H&E) staining of representative lung section of septic mice (B), septic treated mice (BA, BG and BAG), healthy control mice (P) and healthy treated mice (A, G and AG). Upper panels shown whole lungs with red line = 2mm; lower panels shown magnification areas with black line = 100 µm for septic mice and = 200 µm for healthy mice.

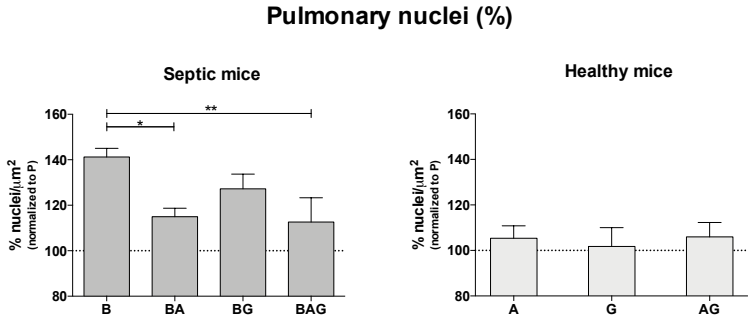

Figure 9. Pulmonary nuclei count. Histograms show the percentage (average ± SD) of infiltrating cells in the lungs of all septic (**a**) and healthy (**b**) mice. Values are calculated as a number of nuclei per area (µm2) normalized to P (control groups) average (%). Columns and bars represent means and standard deviation, respectively. * $p < 0.05$, ** $p < 0.01$.

Kidney

As mentioned above, renal injury is a common complication of sepsis status and therefore we also analyzed mice kidney morphology. In **Figure 10** are shown representative sections of whole kidneys and their magnifications**.** Septic kidneys from B mice showed an extended ischemic area with tubule edema. These ischemic areas with pale staining and unstructured glomeruli were also visible in the kidneys from BA mice, while septic mice additionally treated with Gas6 (BG) and the ones who received antibiotic plus Gas6 (BAG) showed a better histological outcome, similar to that observed in the kidneys of control mice (P) (**Figure 12**).

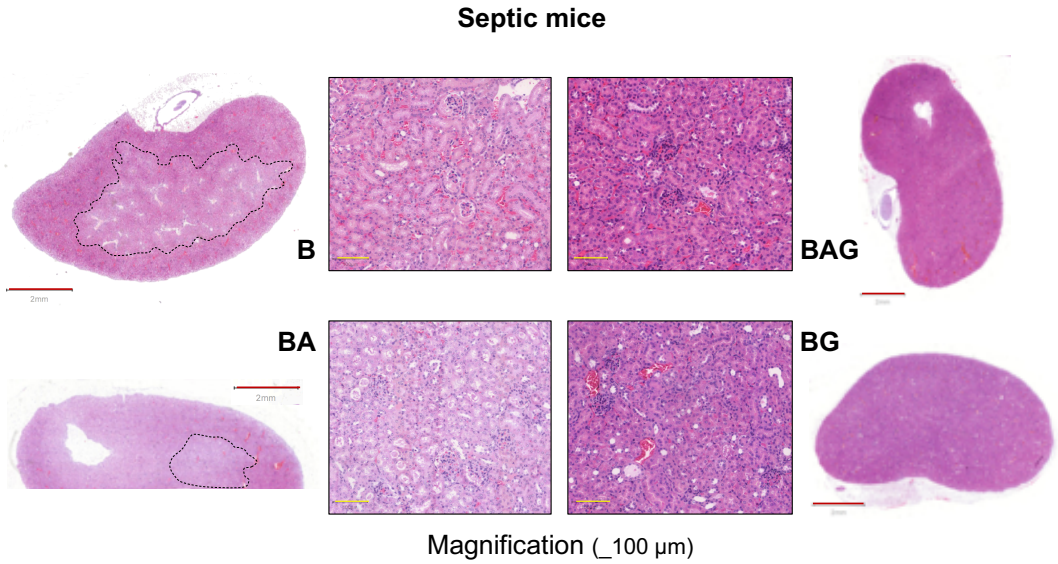

Figure 10. Kidney histology and morphology of septic mice. Hematoxylin and eosin (H&E) staining of representative renal section of septic mice (B), septic treated mice (BA, BG and BAG). Red line = 2mm; magnification areas with yellow line = 100 µm. The dotted lines show ischemic areas found in kidney sections from B and BA mice.

The histogram of **Figure 11** shows the percentage of ischemic kidney area if present: specifically, 3 mice out of 4 in group B, one mouse out of 4 in group BA and one mouse out of 5 in group BAG developed renal ischemia (no ischemic area was detected in septic mice treated with Gas6). Ischemic area was measured, reported to total area and finally calculated as percentage: as shown by the histogram, ischemic areas of BA and BAG mice were lower than 1% of total kidney.

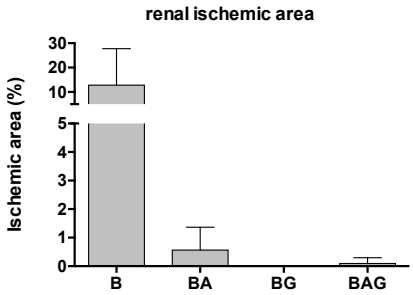

Figure 11. Renal ischemic areas in septic mice. The histogram represents the ischemic area (μm^2)/whole area (μm^2) as percentage (%). Columns and bars represent means and standard deviation, respectively.

We also evaluated renal features of healthy treated mice and we did not observe any morphological differences among healthy mice treated with ampicillin (A), Gas6 (G) or both (AG) compared to healthy control mice (P) (**Figure 12**).

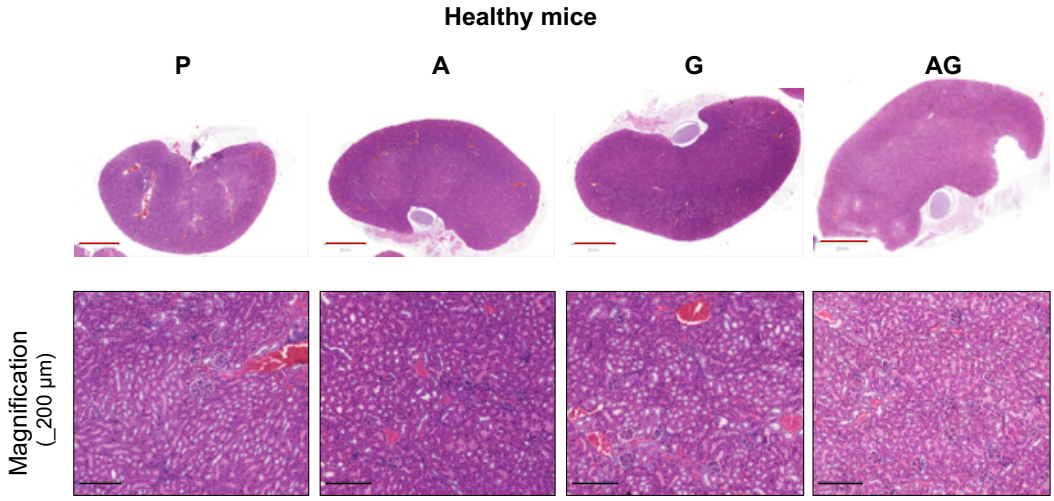

Figure 12. Kidney histology and morphology of healthy mice. Hematoxylin and eosin (H&E) staining of representative kidney section of healthy control mice (P), healthy treated mice (A, G and AG). Red line = 2mm; magnification areas with black line = 200 µm.

Infection, and not only silent-chronic infection but also the acute-severe one, can induce molecular pathway initiating and driving fibrosis. This could be a physiological process which can provide defense against infection. Therefore, we also performed kidney PAS staining for septic, septic-treated mice and healthy control mice (P) (**Figure 13**). Septic (B) and ampicillin-treated septic (BA) mice showed strong staining in their kidney sections, whereas PAS intensity decreases in BG mice and it became pale in BAG mice, resembling the healthy control (P) mice. Destructured glomeruli were present not only in untreated septic mice, but also in BA mice as indicate by black asterisk in **Figure 13**. In addition, general morphology degeneration

in septic mice and tubule cell swelling, with collapse structure, in ampicillin treated mice was observed (highlighted by black triangle, BA section). Furthermore, in BG and especially in BAG mice were clearly evident tubule and glomerular basement membranes and proximal convoluted tubule brush borders outlined by PAS staining (black arrows), which were nearly to totally absent in B and BA mice (yellow arrows).

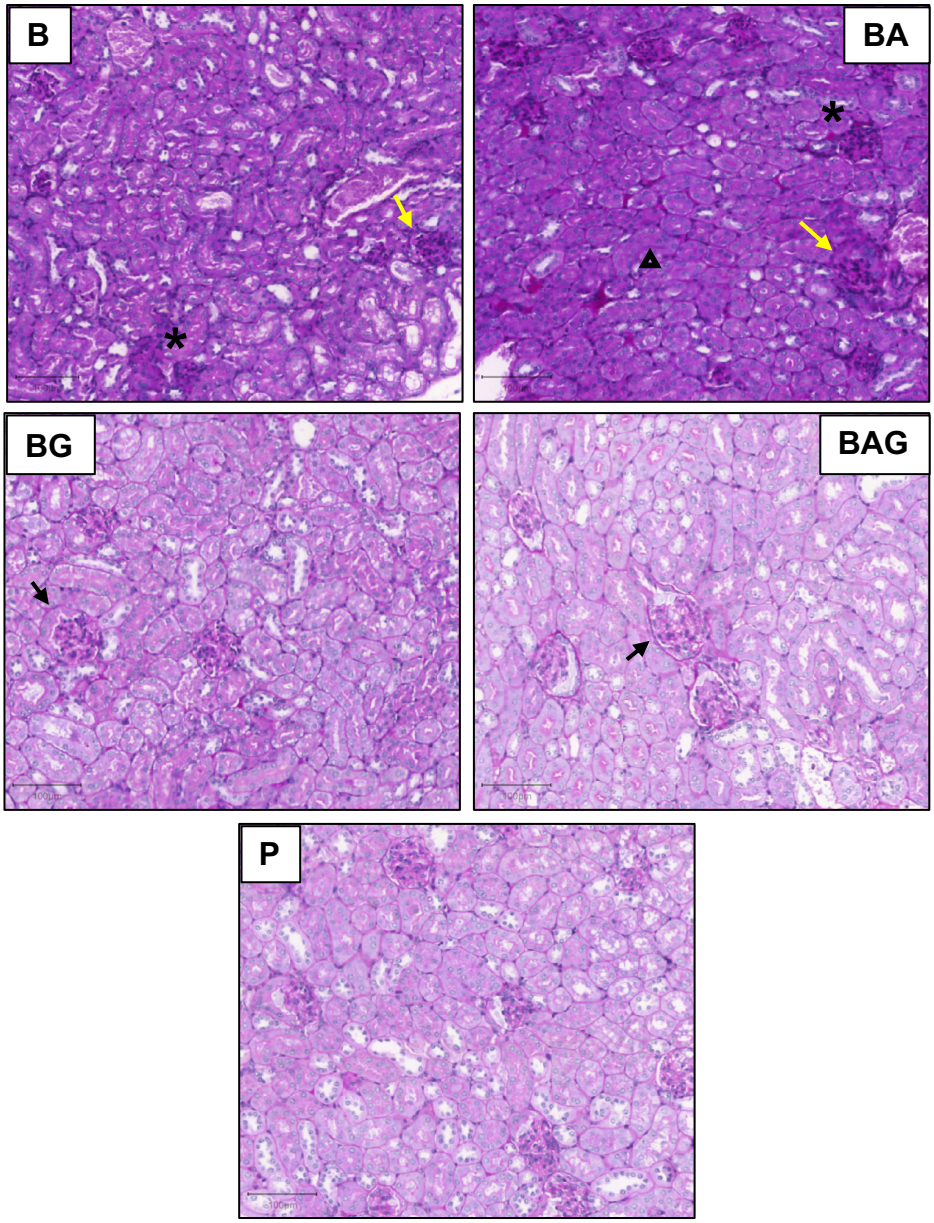

Figure 13. Periodic acid-Schiff (PAS) staining in renal tissue. Histology sections magnification (-) = 100 µm. Asterisk(s) highlights glomeruli, arrow(s) membranes and borders and triangle tubule edema.

Liver Morphology and Function

Although liver, conversely to lung and kidney, is not the first common organ compromised by sepsis-induced MOF, it is far from a bystander in sepsis given that it is a regulator of the inflammatory process and a target of host response.

Therefore, in general histology investigation we also analyzed liver through H&E staining and hepatic function by measuring plasma alanine aminotransferase (ALT) levels (**Figure 14**).

Regarding histology features, we did not find any marked difference among analyzed livers. In fact, septic livers were resembling healthy livers with only one exception: one septic mouse (from group B) which developed septic shock and died within 24 hours (mouse who obtained score equal to 0 in vitality score, **Figure 7**); this mouse developed moderate hepatic ischemia visible in the central panels of **Figure 14**. From a functional point of view, we measured plasma ALT level in each mouse observing exactly the same values among healthy mice, both untreated (P) and treated healthy mice (A, G, AG) (**Figure 14**, histogram). On the contrary, ALT plasma concentrations in septic mice (B, BA, BG, BAG) were rather higher than healthy mice, specifically plasma ALT mean of B mice was 167.0 U/L (± 288.9), including the outlier mouse which exhibits 600.3 U/L. Another mouse with high ALT levels was a septic mouse treated with Gas6 (BG), 319.2 U/L and averagely BG mice shown ALT levels equal to 117.7 U/L (± 139.4). Then, BA and BAG mice displayed plasma ALT concentration equal to 50.5 U/L (± 20.5) and 60.3 U/L (± 49.0), respectively. Despite being higher ALT levels in septic than in healthy mice, the differences were not significant ($p = 0.617$) (**Figure 14**, histogram).

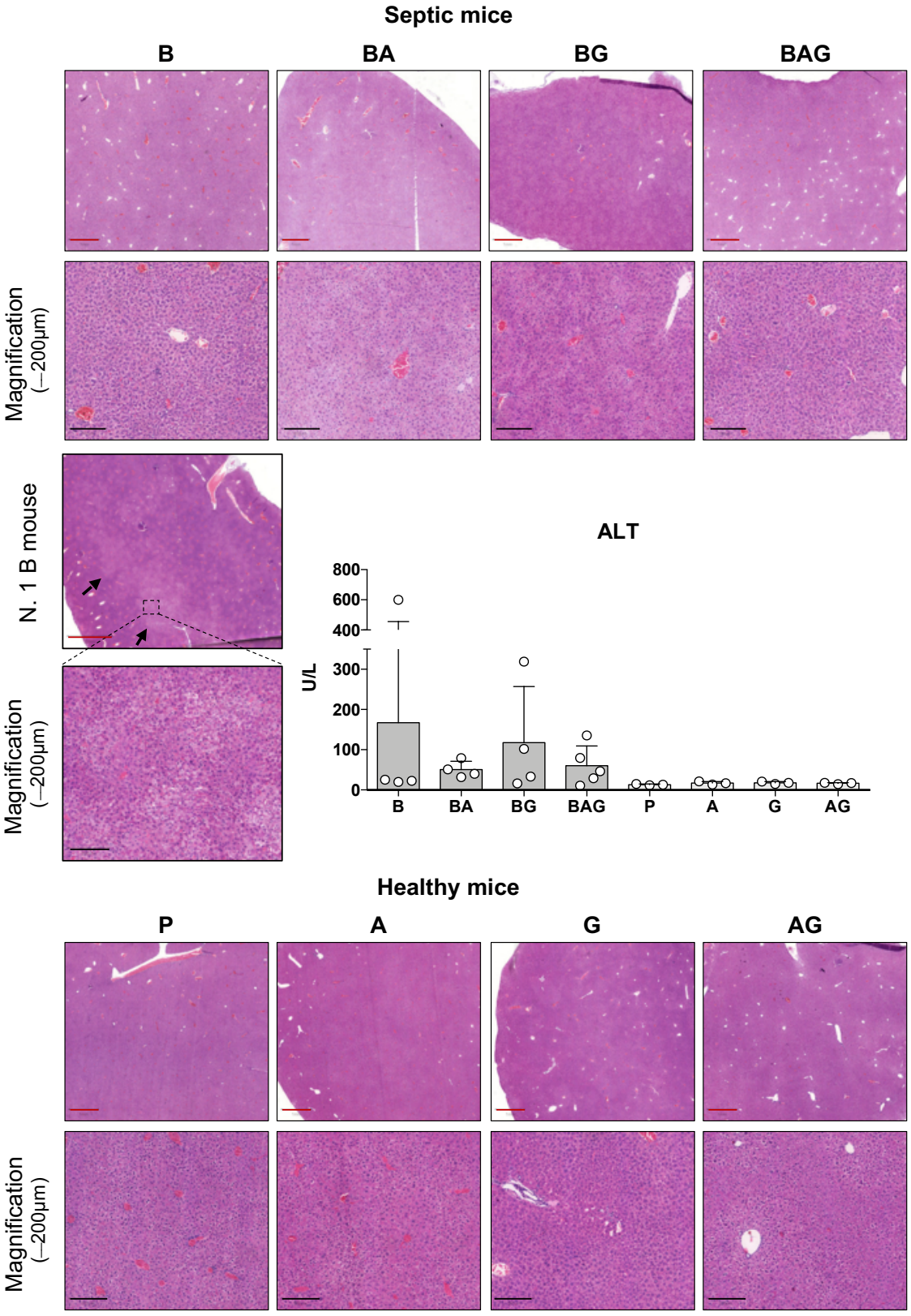

Figure 14. Liver histology and alanine aminotransferase (ALT) levels. Hematoxylin and eosin (H&E) staining of representative liver section of septic mice (B), septic treated mice (BA, BG and BAG), healthy control mice (P), healthy treated mice (A, G and AG). Red line = 2mm; magnification areas with black line = 200 µm. arrows highlight ischemic area found in one septic mouse. The histogram shows alanine aminotransferase (ALT) levels (U/L) for all mice group, columns and bars represent means and standard deviations, respectively.

In-Vivo Systemic Homeostasis

Cytokines Gene Expression

As sepsis-induced disruption of tissue homeostasis leads to aberrant regulation of both anti- and pro-inflammatory cytokines (CKs), we sought to determine the expression, by real time qPCR, of IL-1β, IL-6, IL-10, TGF-β1, and TNF-α, the main drivers of tissue inflammation.

In **Figure 15** are reported CKs relative expression, investigated in mice from B, BA, BG and BAG and divided by organ analyzed, specifically liver, kidney and lung. For the statistical analysis we included all groups of septic mice, but we were mainly focused on the comparison between standard therapy against sepsis (BA mice) and standard therapy plus Gas6 treated mice (BAG). Despite being differences between BA and BAG treated mice for some CKs in lung and kidney, they are not statistically significant. In fact, a common feature of lung and kidney is the significant and strong upregulation of CKs, both pro and anti-inflammatory, in septic (B) mice compared to septic treated mice (BA, BG and BAG). The only exception was found in kidney for TGF-β1, which was found downregulated in B mice compared not only to septic treated mice but also to healthy mice (dotted line). However, this result was not statistically significant. By analyzing hepatic CKs expression, we observed a significant downregulation of IL-1β, IL-10 and TGF-β1 in BAG mice compared to BA mice ($p = 0.009$, $p < 0.001$, $p = 0.006$, respectively). Generally, no significant differences were observed between BAG and BG mice.

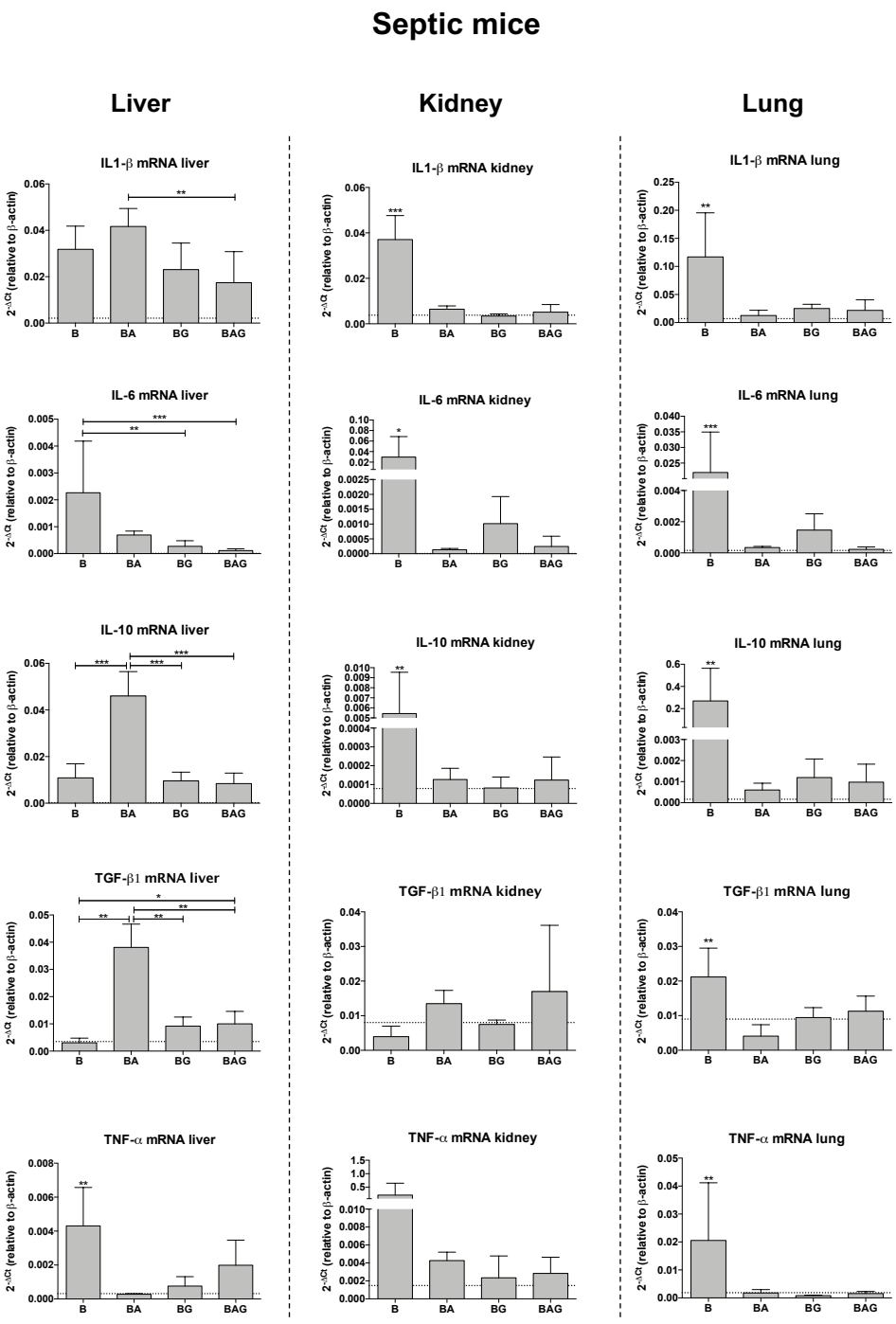

Figure 15. Relative cytokines expression (mRNA) in septic groups. mRNA (relative to β-actin) expression in all septic and septic-treated mice of pro- and anti-inflammatory cytokines (CKs), specifically IL-1β, IL-6, IL-10, TGF-β1, and TNF-α. CKs were investigated in liver, kidney and lung and shown in the left, central and right column respectively. Column and bars represent means and standard deviations; the dotted line corresponds to the mean value of healthy control (P) mice. * $p < 0.05$, ** $p < 0.01$, *** $p < 0.001$.

We additionally investigated the same pattern of CKs in healthy and healthy-treated mice and we found a slight significant effect of Gas6 in liver. In fact, Gas6 treated (G) mice shown higher levels of IL-1β and IL-10 compared to the other healthy treated (A and AG) and untreated (P)

mice ($p < 0.001$ and $p < 0.005$, respectively). No other differences were observed in kidney and lung (**Figure 16**).

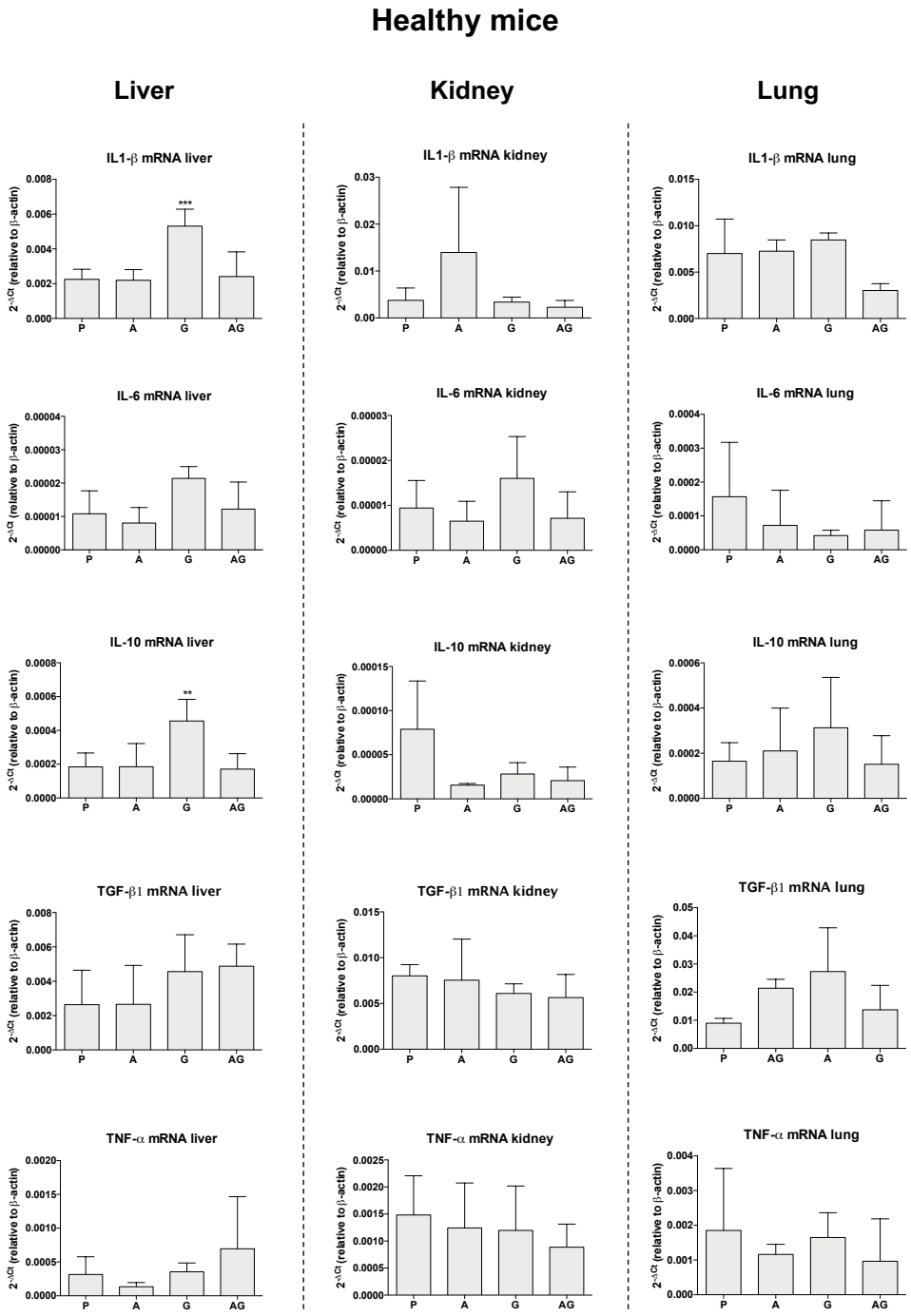

Figure 16. Relative cytokines expression (mRNA) in healthy groups. mRNA (relative to β-actin) expression in all healthy and healthy-treated mice of pro- and anti-inflammatory cytokines (CKs), specifically IL-1β, IL-6, IL-10, TGF-β1, and TNF-α. CKs were investigated in liver, kidney and lung and shown in the left, central and right column respectively. Column and bars represent means and standard deviations. ** $p < 0.01$, *** $p < 0.001$.

However, the analysis of these individual data and divided by organ is poorly informative if we consider a context of systemic homeostasis disruption, key feature of septic status.

To this end, CKs mRNA expression in kidneys, livers and lungs from B, BA, BG and BAG mice was compared to that of healthy control animals. **Figure 17** shows the difference distribution between the control P group (dotted line) and the various treatment groups (i.e., B, BA, BG and BAG) in terms of CK expression levels, which was calculated by pooling together the results obtained from all organs analyzed (i.e., liver, kidney and lung). Thus, the graph shows how far the distribution of every CKs is (in B, BA, BG and BAG mice) compared to the mean distribution of healthy (P) mice, from a systemic point of view. This analysis was performed to point out how much the CKs distribution of septic groups differ from the physiological one of P group. Therefore, according to the treatment group: B = 4.3 ± 3.2; BA = 2.4 ± 1.6; BG = 2.1 ± 1.9; BAG = 1.8 ± 0.8; mean difference ± SE.

The distribution of systemic CKs was significantly different between B and BAG mice (p = 0.037). In particular, B mice showed high variability in the expression of all CKs analyzed, which was associated with homeostasis disruption. In contrast, mice receiving antibiotic therapy (BA) or Gas6 (BG) showed a reduction in CKs expression variability. Finally, BAG mice displayed a statistically significant difference in CKs expression, with an overall improvement of systemic homeostasis, as judged by a more homogeneous CKs distribution similar to that of control mice (dotted line) (**Figure 17**).

Analyzing the distribution of systemic CKs in healthy mice we found that variation of the CKs distribution was paltry and non-significant in healthy mice treated with ampicillin (A), Gas6 (G) or both (AG). Hence, this variation could also be likely attributable to biological variability (**Figure 17**).

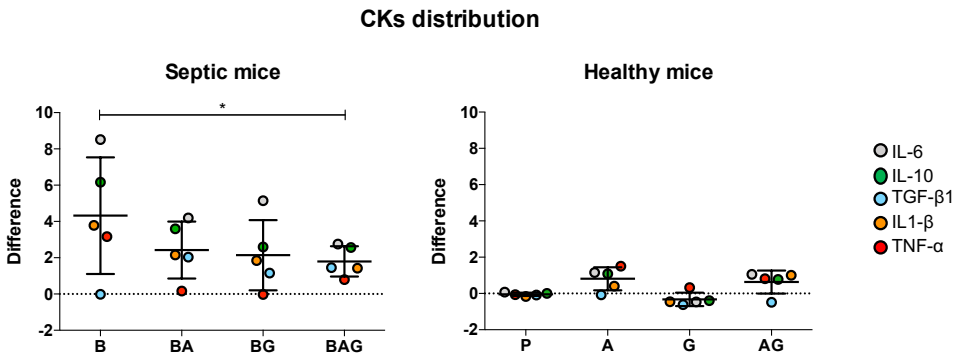

Figure 17. Systemic cytokines (CKs) distribution. Difference distribution between the control group (P, dotted line) and septic groups (i.e., B, BA, BG and BAG) of logarithmic cytokines mean (± SE) from all organs analyzed (i.e., liver, kidney and lung) (left panel). Same analysis of CKs distribution for healthy treated mice (A, G and

AG) is shown in right panel. The pro- and anti-inflammatory cytokines analyzed were IL1-β (orange dots), IL-6 (grey dots), IL-10 (green dots), TGF-β1 (blue dots) and TNF-α (red dots). * $p < 0.05$.

Lactate Dehydrogenase Levels

During sepsis and septic shock, organ damage and cell death increase the concentration of lactate dehydrogenase (LDH) in the bloodstream. Of note, a study published in 2018 has shown that LDH concentration is associated with 28-day mortality in patients with sepsis (Lu et al., 2018).

Plasma LDH levels were measured in both septic and healthy mice and surprisingly we recorded a considerable decrease in plasma LDH levels in septic mice treated with Gas6 alone (BG), and especially when was used in combination with ampicillin (BAG), compared to standard antibiotic therapy (BA). Consistent with an opposing role of Gas6 in sepsis-induced MOF, we found BAG mice with LDH average levels of 1115 U/L (± 1001) whereas BA mice showed mean value six-time greater (6572 U/L ± 605) ($p < 0.001$). Moreover, BA mice did not differ from B mice (6495 U/L ± 837) in plasma LDH concentration and although BAG mice had higher LDH levels compared to P mice (261 U/L ± 51) this difference was not statistically significant ($p = 0.858$). Among healthy treated mice no differences have been found (A = 287 ± 97, G = 382 ± 205, AG = 302 ± 71, $p = 0.674$) (**Figure 18**).

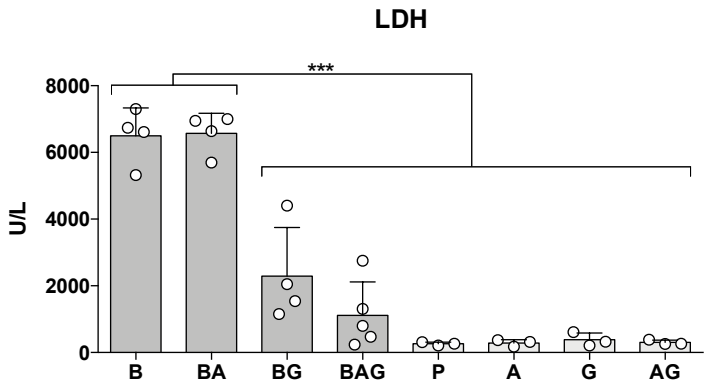

Figure 18. Plasma lactate dehydrogenases (LDH) levels. The histogram shows lactate dehydrogenase (LDH) levels (U/L) for all mice group. Columns and bars represent means and standard deviations, respectively. *** $p < 0.001$.

Reactive Oxygen Species and Myeloperoxidase

Since we observed plasma LDH concentration significantly lower in BAG mice, we analyzed another element which has a pivotal role in tissue metabolism, notably reactive oxygen species (ROS) production. ROS are involved in tissue homeostasis disruption in sepsis (Mantzarlis et

al., 2017). Moreover, overproduction of nitric oxide (NO) due to inducible NO synthase (iNOS) activity has been associated with harmful effects, such as general vasodilatation and vasoplegia (Prauchner, 2017). Thus, we next investigated iNOS expression in the kidneys, livers and lungs of both septic and healthy mice groups. As expected, septic mice from B group showed a significant upregulation of iNOS mRNA in all three organs compared to healthy untreated (P) mice (dotted line) (**Figure 19**, septic panels). By contrast, generally we found lower iNOS mRNA levels in septic mice treated with antibiotics and/or Gas6 compared to B mice. Interestingly, average iNOS levels were significantly downregulated in lungs of BAG vs. BA mice: 0.0012 ($2^{-\Delta ct}$) ± 0.0005 vs. 0.008 ($2^{-\Delta ct}$) ± 0.0046, $p = 0.014$, respectively. Instead, among healthy treated mice we found partly variability but not significant differences among groups (**Figure 19**, healthy panels).

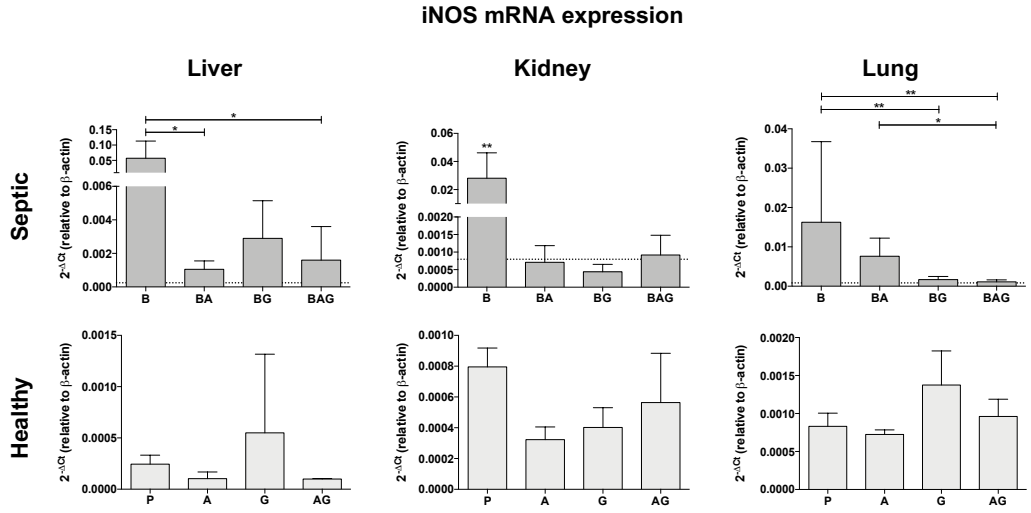

Figure 19. Inducible nitric oxide synthase (iNOS) mRNA expression in the kidney, liver and lung. iNOS mRNA (relative to β-actin) expression in both septic and healthy mice. Columns and bars represent means and standard deviations, respectively. Dotted line corresponds to the mean value of healthy control (P) mice. * $p < 0.05$, ** $p < 0.01$.

Then, since ROS formation and myeloperoxidase (MPO) expression are strictly related, we decide to evaluate MPO expression in sections tissue of all groups.

We detected overexpression of MPO in splenic red pulp from septic untreated (B) mice, while septic mice treated with antibiotic and/or Gas6 showed decreased MPO expression, with BAG mice resembling control animals in terms of MPO staining. We also quantified the intensity of DAB-MPO signal and the quantification of MPO, normalized by number of nuclei, was assessed as previously described (Crowe and Yue, 2019) for all septic groups. Quantification is shown in histogram and we found that the differences among septic groups were statistically

significant ($p < 0.001$). By contrast, we did not find differences among healthy untreated (P) and treated mice (A, G, AG) (**Figure 20**).

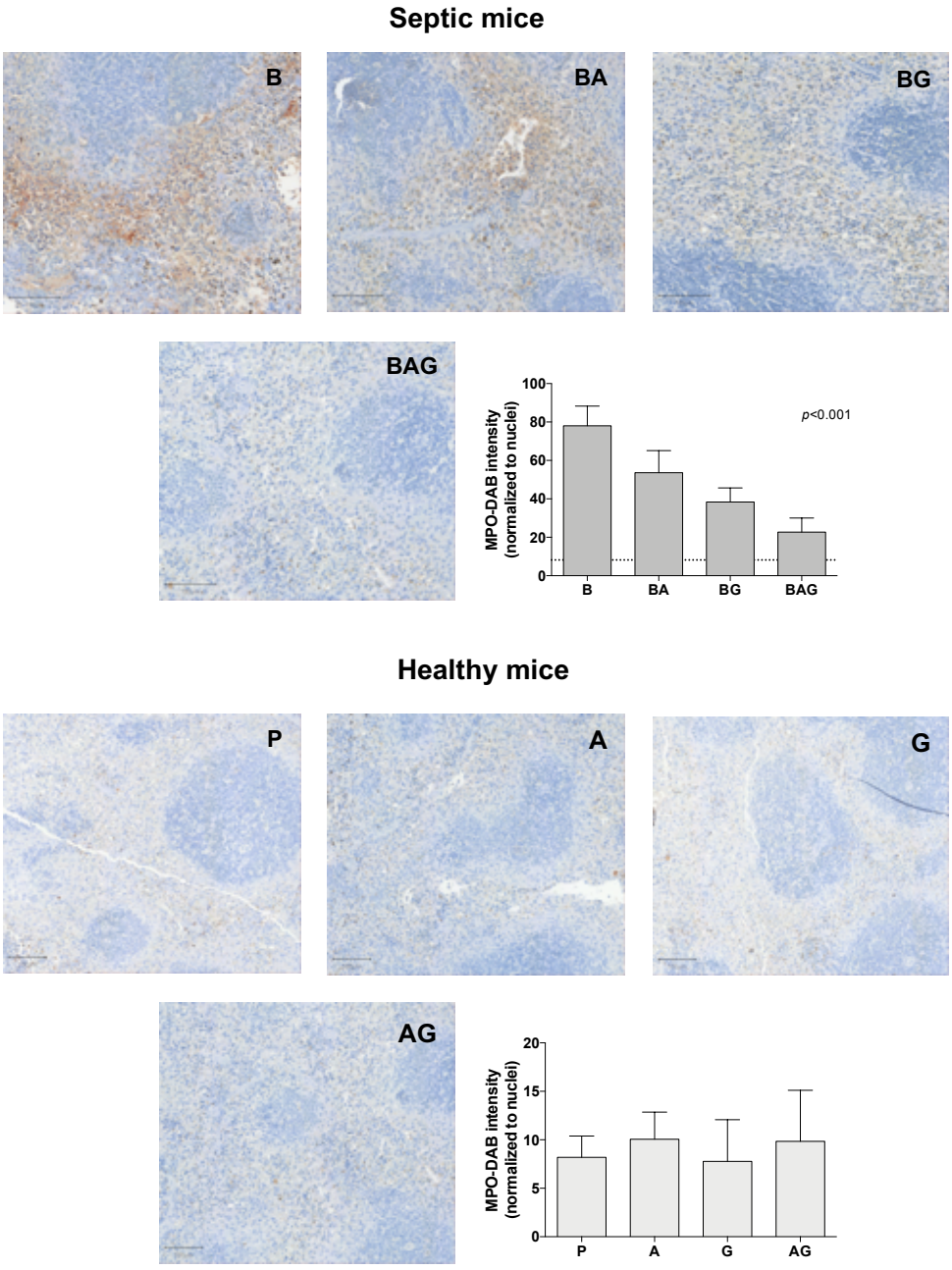

Figure 20. Splenic myeloperoxidase (MPO) expression. Representative images and quantification (as MPO intensity/number of nuclei, histograms) of myeloperoxidase staining (brown color) in spleen samples from all mice groups. Columns and bars represent means and standard deviations, respectively. Dotted line corresponds to the mean value of healthy control (P) mice.

In-Vitro Experiments

Reactive Oxygen Species

Since we observed a significant decrease in systemic LDH levels and iNOS expression, we decided to assess ROS formation *in-vitro*. For this purpose, we used Raw246.7, JAWSII and MS1 murine cell lines as they recapitulate the most frequently targeted cell types during sepsis (i.e., monocytes/macrophages, immature dendritic cells and endothelial cells, respectively). For these *in-vitro* experiments, we employed the same timeline used for the *in-vivo* experiments. Of note, these cells were exposed to PFA-inactivated bacteria to mimic sepsis (**Figure 5**, Material and Methods section).

ROS production, measured as integrated density with ImageJ software, was significantly upregulated in all three cell lines treated with fixed bacteria (B) but was not reduced by ampicillin treatment (BA). By contrast, ROS levels were significantly reduced in all three cell lines following treatment with Gas6 or Gas6 and ampicillin (BG and BAG), with both JAWSII and MS1 cells displaying ROS levels similar to those of control P cells (dotted line). Furthermore, a statistically significant reduction was observed in all three BAG- vs. BA-treated cell lines. Instead, in normal medium without infection-like stimuli, neither ampicillin (A) nor Gas6 (G) and their combination (AG) showed to induce or reduce ROS production in all three cell line used (**Figure 21** and **22**).

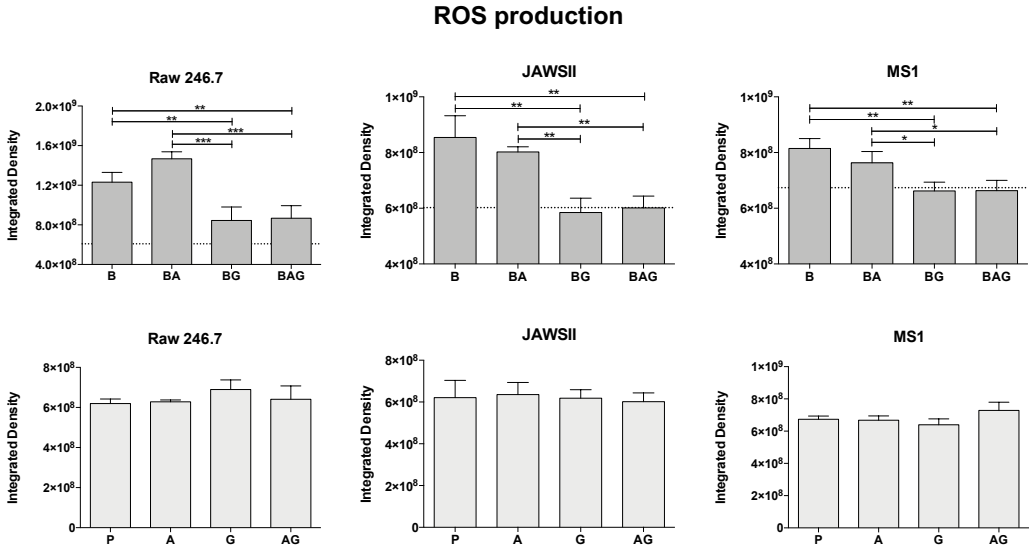

Figure 21. Reactive oxygen species (ROS) production. ROS production, measured by integrated density, in Raw246.7, JAWSII and MS1 cell lines. Cells were cultured with infection-like stimuli (PFA-fixed bacteria) or PBS (control cells) and treated with ampicillin, Gas6 and both. The histograms represent mean values ± SD. The dotted lines represent the mean values of control cells (P). * $p < 0.05$, ** $p < 0.01$, *** $p < 0.001$.

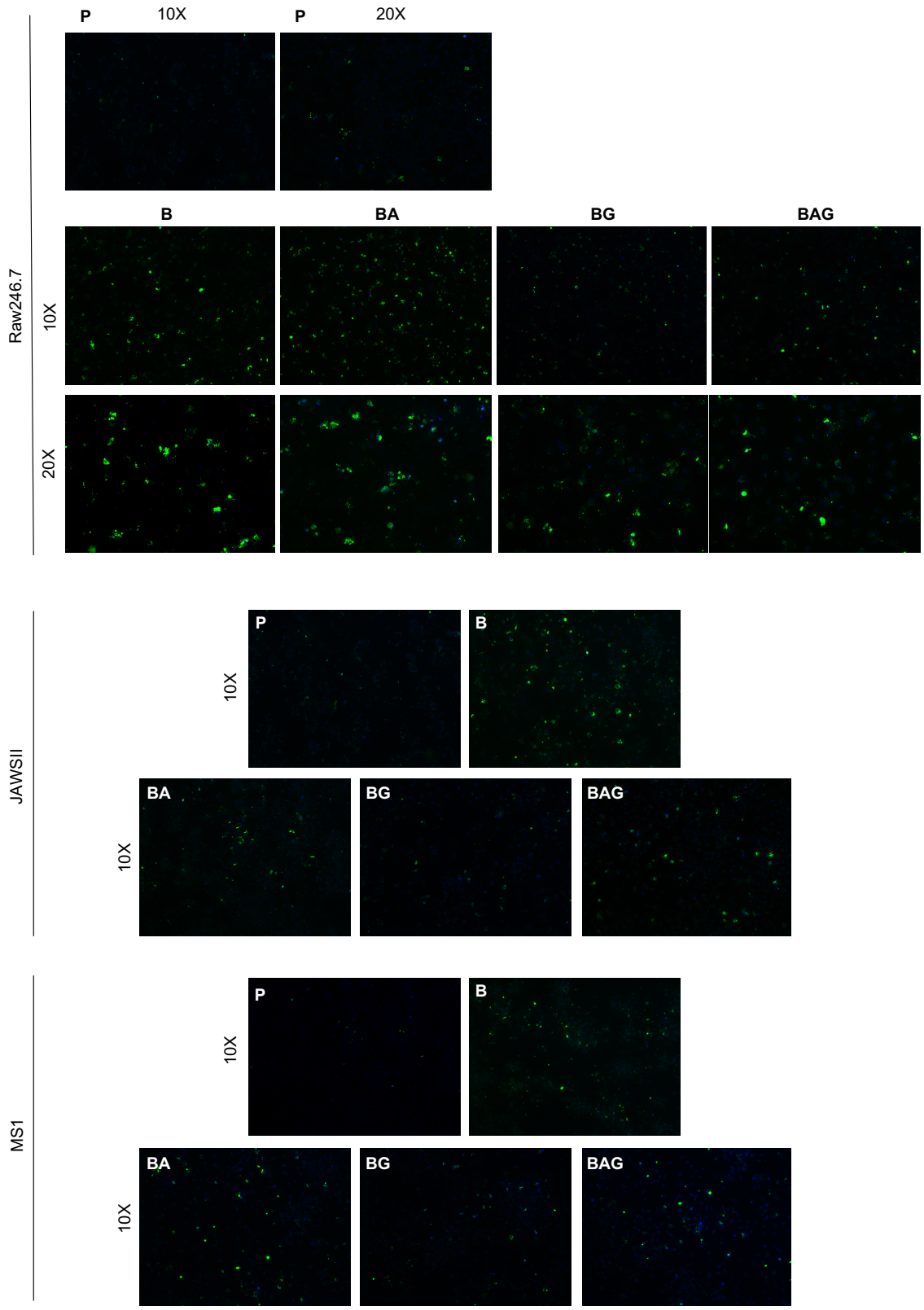

Figure 22. Representative fluorescent images of reactive oxygen species (ROS). ROS were investigated in Raw246.7, JAWSII and MS1 cell lines treated. Green color = ROS, blue color = nuclei.

Lipid Staining

Since lipid metabolism has an important role in inflammation/infection and it is linked to ROS formation, lipid production was investigated in the monocyte/macrophages cell line, Raw 246.7. Only as observational data, we noticed that Raw 246.7 cultured with PFA-fixed bacteria (B) and cells to which Gas6 (BG) or ampicillin + Gas6 have been added (BAG), Gas6 displayed evidence of lipid production with slight amount of lipid droplets (red spot). Instead, cells cultured with PFA-bacteria with the administration of antibiotic (BA) and cells maintained in normal media (P) showed a global lower level of lipids and absence of lipid droplets (**Figure 23**).

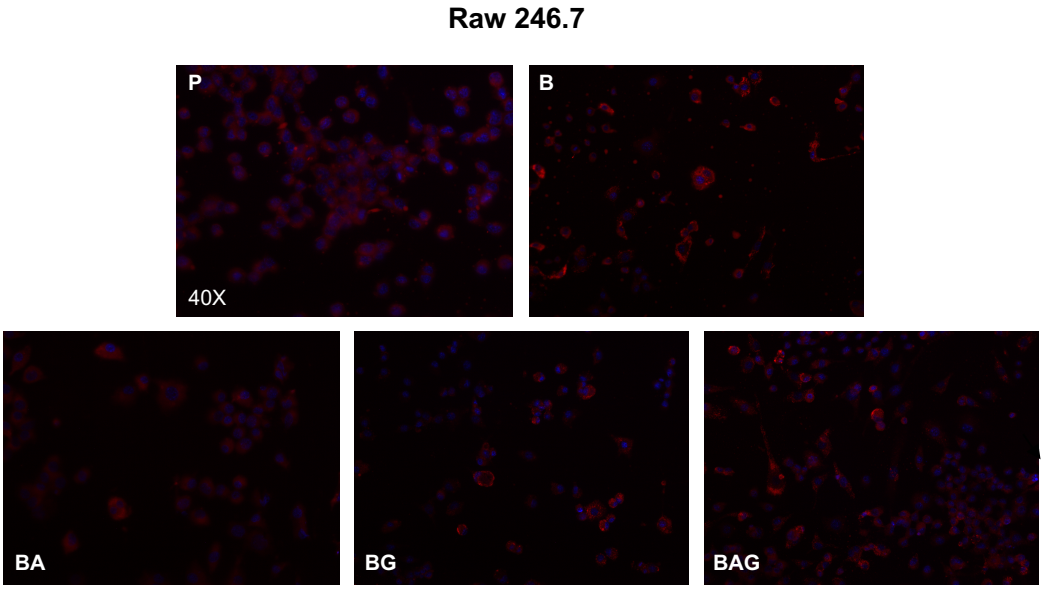

Figure 23. Lipid fluorescence staining on Raw264.7 cell line. Lipids were label with BODIPY™ 493/503 in Raw246.7 cell line treated. Cells were cultured with infection-like stimuli (PFA-fixed bacteria) or PBS (control cells) and treated with ampicillin, Gas6 and both. Red color = lipids, blue color = nuclei.

Cell Vitality

Additionally, despite the nuclear Hoechst dye is not included among the viability assay, we used Hoechst to discriminate healthy cells from necrotic and apoptotic cells as previously described (Crowley et al., 2016). We used this technique to evaluate in the same samples and at the same time ROS production and nuclear integrity, the latter evaluated using the Hoechst staining, thus (broadly) reflecting the status of cells following treatment. **Figure 24** shows the presence of higher number of dead cells when cultured with inactivated bacteria, with or without ampicillin (BA and B, respectively). Conversely, when ampicillin followed by Gas6 were added in the media of cells with PFA-fixed bacteria (BAG) the number of alive cells was

significantly increased and similar to control P cells. Lastly, no significant changes were found among cells that have not been cultured with PFA-fixed bacteria (light grey columns).

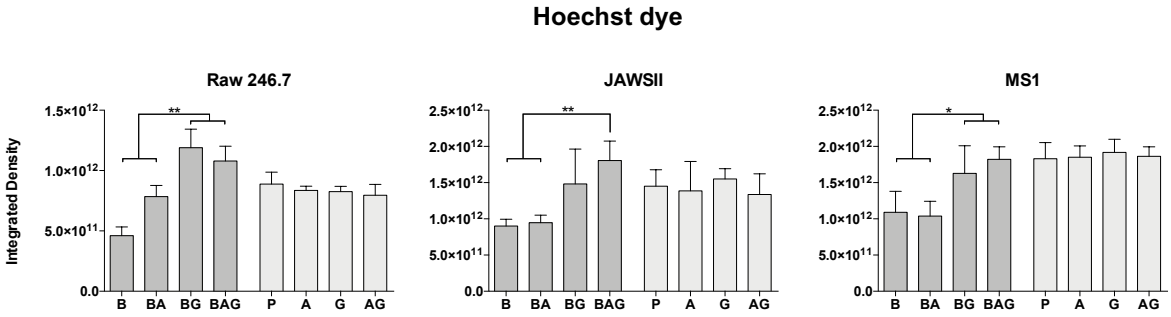

Figure 24. Nuclear integrity measurement by Hoechst dye. Nuclear integrity, measured by integrated density, in Raw246.7, JAWSII and MS1 cell lines. Cells were cultured with infection-like stimuli (PFA-fixed bacteria) or PBS (control cells) and treated with ampicillin, Gas6 and both. The histograms represent mean values ± SD. * $p < 0.05$, ** $p < 0.01$.

Cell Metabolism

Finally, we assessed whether Gas6-treated cells displayed an increased metabolism during infection. Focusing on standard therapy (BA treated cells) vs standard therapy with Gas6 addition (BAG-treated cells), we noticed a significant increase in mitochondrial activity of BAG-treated cells compared to that of BA-treated cells in all three cell lines. This phenomenon was not observed in the same cells cultured in media without infection-like stimuli (**Figure 25**).

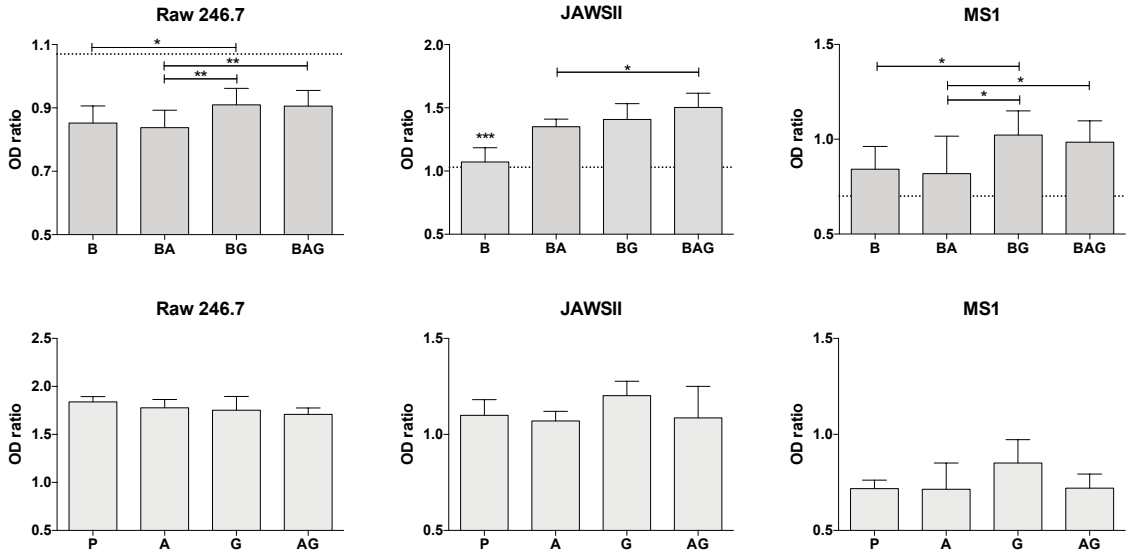

Figure 25. Mitochondrial activity *in-vitro*. Mitochondrial activity in Raw246.7, JAWSII and MS1 cells. The histograms represent mean values ± SD. The dotted lines, where present, represent the mean values of control (P) cells.

Observational Data *In-vivo*

Axl and MerTK Receptors Expression

As circulating Gas6 has several target receptors scattered in different tissues and organs, we focused our attention on the two most important receptors expressed outside the central nervous system, namely Axl and MerTK. In particular, we asked whether general improved MOF damage following Gas6 administration was associated to the expression of Axl, MerTK or both. Thus, we decided to evaluate Axl and MerTK mRNA expression in lung, kidney and liver. Differences between septic mice groups and healthy mice groups are not exhibited.

At the mRNA level, we found no significant changes in Axl expression in lung, kidney and liver among all treatment groups (**Figure 26**). Although we did not observe significant differences in MerTK expression between BA and BAG mice, MerTK was significantly upregulated in BA kidney compared to B and BG mice, and in the liver from BG mice compared to B mice (**Figure 26**).

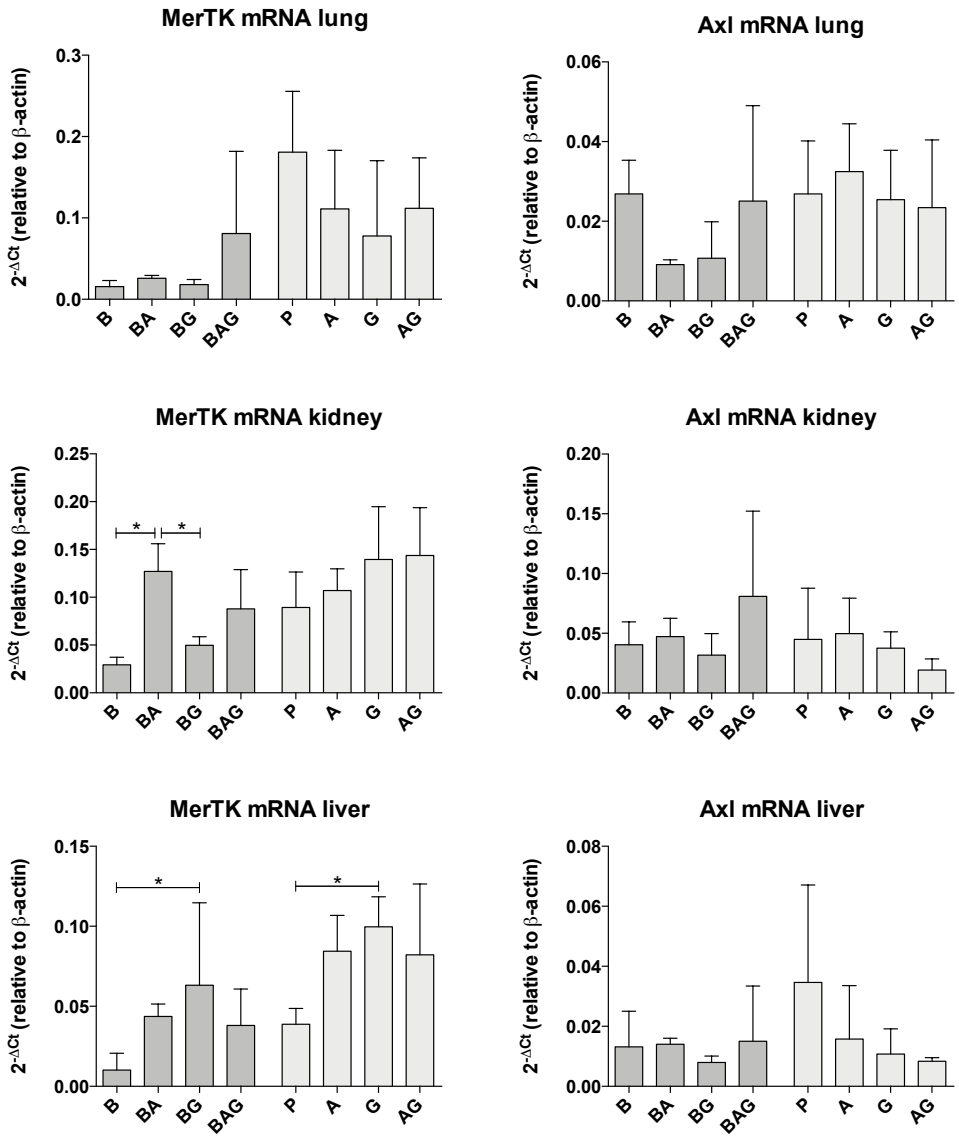

Figure 26. MerTK and Axl expression in mice. MerTK and Axl mRNA expression levels in lung (upper panels), kidney (middle panels) and liver (lower panel) of mice from all mice groups. The histograms represent mean values ± SD. * $p < 0.05$.

Axl and MerTK Receptors Activation

Both Axl and MerTK are tyrosine kinases whose activity depends not only on their expression but also on their activation in response to tyrosine phosphorylation. Thus, we next investigated the phosphorylation status of these two receptors in kidney and liver tissue sections by immunofluorescence using specific anti-phospho Axl (pAxl) and anti-phospho Mer (pMer) antibodies. In addition, these tissue sections were co-stained with an antibody directed against CD45, a marker of hematopoietic cells. We reasoned that co-localization of pMer and pAxl with CD45 would have allowed us to determine whether these receptors exerted their protective

role by immune hematopoietic cells or resident/parenchymal cells. For this purpose, tissue section of B, BA, BG, BAG and P mice were analyzed.

In control kidney cells (P), we could only detect a slight positivity for pAxl, which never co-localized with CD45 staining (**Figure 27a**). Furthermore, we found undetectable pAxl and pMer levels in both B and BA mice. In contrast, BG and BAG mice displayed phosphorylation of both Axl and MerTK receptors in kidney parenchymal cells, but we observed pAxl-CD45 co-localization only in BG-derived tissue (**Figure 27a**).

Unlike the kidney, the liver displayed strong phosphorylation of Axl and MerTK in parenchymal cells from the control group (P) and from BG and BAG mice, with BG mice showing less activation compared to P and BAG mice (white Δ) (**Figure 27b**). In contrast to the kidney, the liver of B and BA mice showed extensive pAxl-CD45 co-localization (white *) (**Figure 27b**). Taken together, these observations suggest that Gas6 administration ameliorates sepsis-driven organ damage and that this effect is likely mediated by parenchymal cells rather than hematopoietic cells.

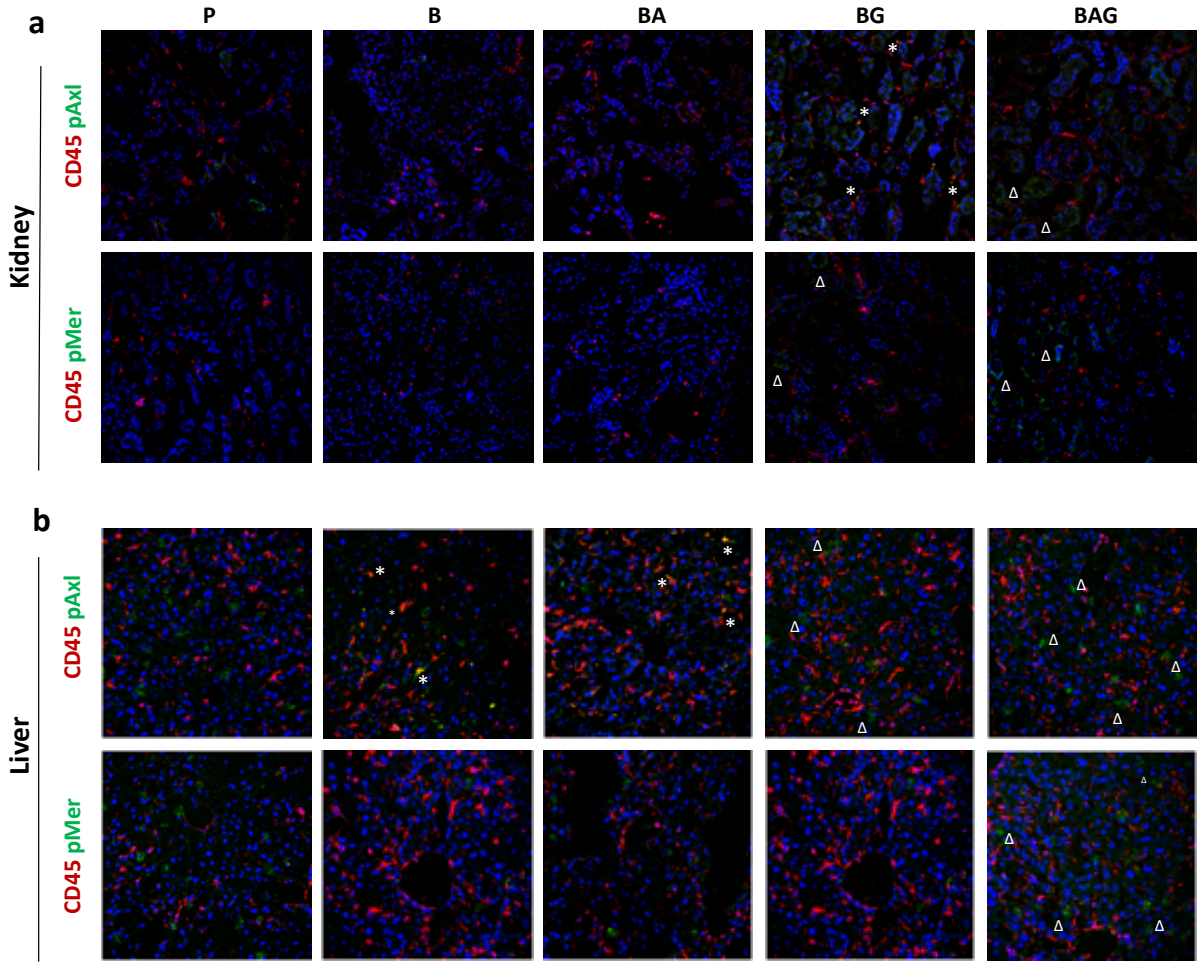

Figure 27. **Mer and Axl activation in mice.** Immunofluorescence on kidney (a) and liver (b) sections showing protein expression of CD45 (red) and 65hosphor-Axl (pAxl) or 65hosphor-MerTK (pMer) (green). The white asterisks (*) indicate pMer/pAxl and CD45 co-staining, whereas the white deltas (Δ) indicates pAxl/pMer localized in CD45-negative cells.

DISCUSSION

In this thesis, we firstly investigated potential biomarkers in different patient's cohorts, including patients with systemic inflammatory response syndrome (SIRS) and septic patients diagnosed with the current available criteria (Singer et al., 2016). Then, we investigated the possible therapeutic efficacy of Gas6 administration following antibiotic therapy in a murine model of sepsis.

Despite the large cohort of SIRS patients (N. 890), we did not find any Gas6 implication at prognostic levels. In fact, when mortality rate has been analyzed at 7 and 30 days only age was strongly associated with mortality at both time points. However, circulating Gas6 levels in SIRS patients averagely reach ~31 ng/mL which is almost double to the median Gas6 levels in healthy subjects, ~16 ng/mL (Jiang et al., 2009). This result is in line with another important study showing more than 10 years ago that circulating Gas6 is increased in sepsis and related syndromes. The authors also observed a correlation between Gas6 concentration, disease severity and organ dysfunction (i.e. kidney failure). However, as our study shows, plasma Gas6 levels did not correlated with patient's death (Ekman et al., 2010a). With our findings we confirmed with a huge population, compared to 232 patients included in the previous study, that Gas6 could be associated with disease severity, but not with prognosis and mortality.
Later, Gas6 plasma levels were also measured in septic patients, enrolled with Sepsis-3 definition, and HMGB1 and OPN were additionally analyzed in the same septic population.
Interestingly, OPN levels progressively increased throughout non-infectious conditions (no sepsis), sepsis and septic shock. This is coherent with the results of a previous study which included SIRS patients (Vaschetto et al., 2008). In addition, this result proves that a pro-inflammatory status is present also in non-septic conditions and that OPN is involved in the pathogenesis of these inflammatory processes, since higher levels correspond to clinical syndromes with a more pronounced inflammatory dysregulation. OPN resulted to be an independent diagnostic predictor of sepsis and showed a good diagnostic performance at the ROC curve analysis, in which the highest sensitivity (88.9%) and specificity (80.4%) were seen when the cut-off was set at 112.8 ng/mL. In particular, the AUC for OPN was very similar to the one for plasmatic lactate levels, a parameter widely and routinely used in the diagnostic workup and prognostic stratification of sepsis. All these results were only mentioned in this thesis, but they are available and published in 2019 by our group (Castello et al., 2019).

In a bit larger cohort of same septic patients, Gas6 and HMGB1 plasma levels were found, like OPN levels, progressively increased throughout no sepsis, sepsis and septic shock. However, when the diagnostic performance was tested through ROC analysis neither Gas6 nor HMGB1 demonstrated strong predictive capability, with an AUC of 0.746 and 0.715 respectively. Nevertheless, contrary to OPN and Gas6, HMGB1 plasma concentration was significantly associated to 7 and 30 days mortality rate. This result is in line with the knowledge of HMGB1 related to sepsis. In fact, elevated plasma HMGB1 was found associated with morbidity and mortality in septic shock patients and HMGB1 blood concentration was related to an exacerbate pro-inflammatory cytokine profile (i.e. IL-1, IL-6 and TNFα) (Stevens et al., 2017). Despite plasma Gas6 being significantly higher in septic shock patients compared to septic ones, it was not a predictor of mortality in our study, demonstrating that not only in SIRS, but also in a septic cohort of patients Gas6 is not correlated to mortality.

These data have several biases: regarding septic cohort, the number of individuals is pretty small, in particular non-septic patients were only ten. Furthermore, long term follow up is missing for both SIRS and septic cohorts. Most important, a single early OPN determination cannot be used as a prognostic tool as well as single HMGB1 determination was not able to discriminate non-septic individuals among the septic patients. However, these results highlight the relevant aspect of a multi-marker approach, in which integrated biomarkers could be more reliable and useful for both diagnosis and prognosis of a pathology where profound circulatory, cellular, and metabolic abnormalities occur.

Eventually, Gas6 shows an increasing trend throughout pathology severity, but is not a death hallmark. This result gave the green light to feasible speculations about the protective role of Gas6 in septic condition which are mentioned in the review published by our group in 2019 (Salmi et al., 2019).

Therefore, we decided to investigate Gas6 role in this tangled disease *in-vivo*.

We decided to induce sepsis using the cecal slurry model instead of cecal ligation and puncture (CLP) since the cecal slurry methodology overcomes CLP-related variability and avoids performing a thoroughly invasive surgery, which can constitute major biases in sepsis models (Ruiz et al., 2016). Thus, approximately 16 hours after sepsis induction, mice were treated with standard broad-spectrum antibiotic or PBS (as control) and ~ 8 hours later Gas6 or PBS were intravenously injected.

Our results indicate that intravenous Gas6 administration, alone or in association with antibiotics, can ameliorate the general health status of septic mice. Indeed, Gas6-treated septic mice showed improved vital signs (BG mice), and the combined treatment with antibiotics and Gas6 (BAG mice) further improved their condition, making them almost indistinguishable from their healthy counterparts (P, A, G and AG mice). With the exception of one mouse, BAG mice were fairly active and characterized by normal respiratory rate and regular vascular blood supply, as judged by the pink color of their ears. Conversely, septic mice treated with antibiotics alone (BA mice) showed a more compromised health status, with signs of disease severity such as tachypnea, closed eyes, white ears and reduced movements.

These clinical findings were confirmed at the histological level. In the first 36 h, we found a substantial reduction of inflammatory activity in both the kidneys and lungs from BAG mice. In our opinion, this is a very promising finding, since sepsis-related lung damage, leading to ARDS, greatly increases the morbidity and mortality rate of septic patients (Hu et al., 2020).

In our study, both BA and BAG mice showed a significant decrease in the number of total cells found in the alveolar space if compared to septic untreated mice, thus suggesting a reduction of infiltrating cells. Conversely, Gas6 and/or ampicillin had not macroscopical effects in physiological condition, thus suggesting that Gas6 injection did not hamper the therapeutic efficacy of antibiotics, which is consistent with the fact that Gas6 administration improves ARDS conditions in CLP-induced sepsis (Giangola et al., 2013).

With regard to the involvement of kidneys during sepsis, a recent study has shown that early reversible AKI within 24 hours is associated with improved survival, whereas long-term survival of patients with sepsis-associated AKI is strongly related to recovery status at hospital discharge (Peerapornratana et al., 2020). Although we did not measure serum creatinine, which is commonly used to monitor renal function, our histological examination showed that the renal structure observed in BAG mice was comparable to control mice. Conversely, BA mice displayed a de-structured kidney, with ischemic areas and tubular damage similar to those observed in septic mice. Moreover, PAS-staining carried out on septic and P mice interestingly showed a general morphology degeneration, tubule cell swelling, with collapsed structure, in ampicillin-treated septic mice (BA). In B and BA mice the glomerular basal membranes and proximal convoluted tubule brush borders were almost totally lost with a strong collagen deposition highlighted by the high PAS intensity. Oppositely, BAG mice showed a PAS-staining that was completely stackable to healthy P mice. Thus, our findings appear to indicate a protective role of Gas6 also in sepsis-induced kidney injury.

Even though we observed an alteration in ALT levels following Gas6 injection, particularly evident in BG mice, such increase was not statistically significant and additional analyses are needed to fully understand the meaning of this response.

Another important effect of Gas6 treatment is a tendency to rebalance the levels of pro- and anti-inflammatory cytokine expression in the different organs, particularly evident in BAG vs. septic mice. This finding is consistent with the role of the Gas6/TAM axis in the regulation of the inflammatory response during sepsis (Salmi et al., 2019; Tutusaus et al., 2020b). In fact, despite single representation of cytokines (CKs) mRNA expression did not clarify the role of Gas6 administration, the CKs differences from a systemic point of view revealed an important aspect of the overall response to Gas6. This aspect seems to be in harmony with the tendency of plasma LDH levels found in septic mice. It was truly surprising to observe a drastic and significant reduction in plasma LDH levels in BAG vs. BA mice, with the latter group showing values comparable to those of septic mice. It is well known that the reduction of lactate and LDH levels are associated with a better disease outcome. Indeed, lactate elevation has been classically attributed to global hypoperfusion in the setting of hemorrhagic shock, but it is well known that in sepsis additional mechanisms, such as accelerated glycolysis, may cause hyperlactatemia (McCarter et al., 2002; Van Wyngene et al., 2018). Additionally, it has been recently observed that high serum LDH levels are independently associated with 28-day mortality in patients with sepsis (Lu et al., 2018). In this regard, accelerated glycolysis can be strictly related to mitochondrial dysfunction and oxidative stress induction (Gwangwa et al., 2018; Pool et al., 2018).

In line with this observation, we also noticed a significant decrease in ROS production in our *in-vitro* experiments, accompanied by increased cell viability. Both ROS production and altered microvascular mechanisms are partially linked to NO and iNOS production. Heemskerk and colleagues reported that the use of selective iNOS inhibitors attenuates sepsis-induced renal dysfunction and improves survival in animals (Heemskerk et al., 2009). More recently, iNOS knockout mice showed improved survival rate against CLP-induced sepsis and were less likely to develop ARDS (Takatani et al., 2018). In our study, BAG mice showed significant iNOS downregulation and, especially in the lungs from BAG mice, iNOS levels were significantly lower compared to mice receiving antibiotics. Likewise, MPO levels in the spleen from BAG mice were comparable to those measured in healthy control mice, while BA mice showed a remarkably higher MPO expression. It is noteworthy that the restoration of MPO expression in the spleen of BAG mice is in line with of the findings by Schrijver et al., showing that plasma MPO levels can be used as a marker to diagnose and predict mortality in septic

patients (Schrijver et al., 2017). Furthermore, Theeß and colleagues observed that malaria-infected MPO-deficient mice did not show increased parasite loads and, unexpectedly, were able to clear the infection more rapidly than wild-type mice (Theeß et al., 2017). It is well known that MPO is a "wake-up call" of inflammation or local tissue damage and, from a systemic point of view, elevated MPO levels in circulation are associated with increased oxidative stress (Ndrepepa, 2019). Furthermore, MPO levels can predict adverse clinical outcomes in critical pathologies, especially in cardiovascular diseases (Kimak et al., 2018; Ramachandra et al., 2020).

In our experiments, we observed a concomitant reduction of both MPO/iNOS levels *in-vivo* and ROS formation *in-vitro* when Gas6 was added. To date, it is consolidated that among Gas6 biological effects, migration, cell growth, and cell survival can be listed (Lemke, 2013; Wu et al., 2017). Thus, from our preliminary data, we propose that Gas6 may play a role in preventing tissue damage exacerbation induced by MPO. However, further analyses are required to verify this hypothesis.

Lastly, we focused our attention on the two Gas6 receptors Axl and MerTK, which are ubiquitously expressed and play an important role in inflammatory responses. In particular, we found MerTK mRNA expression to be modulated in the liver and kidney in response to the various treatments. Whereas, no statistically significant variation was observed in Axl mRNA expression. However, since the activity of these two tyrosine kinase receptors mainly depends on tyrosine phosphorylation, we evaluated their phosphorylation status in our experimental model. Intriguingly, in kidney tissues from B and BA mice, we detected pAxl expression in CD45-positive cells, but such colocalization was never found in tissues from BG and BAG mice as well as control mice, indicating that the Gas6/TAM axis on myeloid cells is not directly involved in the response following Gas6 administration. This finding is in line with the previously reported expression of Mer and Axl in mesangial and endothelial glomerular cells (Li et al., 2017). In the liver, pMer did not colocalize with CD45-positive cells in any mouse group, but it was detected around small-caliber vessels.This aspect is in agreement with previous data by Mukherjee SK and colleagues, showing MerTK expression in liver sinusoidal endothelial cells and hepatic stellate cells, but not hepatocytes (Mukherjee et al., 2016). Thus, systemic administration of Gas6 is able to induce a response against sepsis not only from myeloid cells, either resident or recruited from the bloodstream, as one would expect, but also from parenchymal cells.

Many of these *in-vivo* and *in-vitro* results has been recently published by our group (Salmi et al., 2021). However, this study has several limitations, since further analyses are clearly needed

to better understand and characterize the role of Gas6 and its mechanisms in a complex disease, such as sepsis and sepsis-induced organ damage. Moreover, to better understand the biological role of iNOS in this setting, NO determination would be helpful to link *in-vitro* and *in-vivo* iNOS expression results. Again, the number of mice should be increased to obtain more robust data, evaluate long-term effects and investigate different Gas6 doses in order to understand the minimal effective dose to achieve protection. Furthermore, a more deep investigation on mitochondrial response is required. Notwithstanding, a single dose of Gas6 seems to have a strong beneficial effect in restoring homeostasis and limiting organ damage in septic mice, by reducing systemic LDH levels, decreasing ROS formation and intensifying mitochondrial activity. The fact that Gas6 is an endogenous molecule normally circulating in the body under physiological conditions makes this protein a particularly attractive therapeutic candidate for clinical development. After all, it is the job that is never started as takes longest to finish (Tolkien J.R.R., 1954).

BIBLIOGRAPHY

Agodi, A., Barchitta, M., Auxilia, F., Brusaferro, S., D'Errico, M.M., Montagna, M.T., Pasquarella, C., Tardivo, S., Arrigoni, C., Fabiani, L., et al. (2018). Epidemiology of intensive care unit-acquired sepsis in Italy: results of the SPIN-UTI network. Ann Ig *30*, 15–21.

Akalu, Y.T., Rothlin, C.V., and Ghosh, S. (2017). TAM receptor tyrosine kinases as emerging targets of innate immune checkpoint blockade for cancer therapy. Immunol Rev *276*, 165–177.

Alciato, F., Sainaghi, P.P., Castello, L., Bergamasco, L., Carnieletto, S., and Avanzi, G.C. (2008). Development and validation of an ELISA method for detection of growth arrest specific 6 (GAS6) protein in human plasma. J Immunoassay Immunochem *29*, 167–180.

Alciato, F., Sainaghi, P.P., Sola, D., Castello, L., and Avanzi, G.C. (2010). TNF-alpha, IL-6, and IL-1 expression is inhibited by GAS6 in monocytes/macrophages. J Leukoc Biol *87*, 869–875.

Avanzi, G.C., Gallicchio, M., Cavalloni, G., Gammaitoni, L., Leone, F., Rosina, A., Boldorini, R., Monga, G., Pegoraro, L., Varnum, B., et al. (1997). GAS6, the ligand of Axl and Rse receptors, is expressed in hematopoietic tissue but lacks mitogenic activity. Exp Hematol *25*, 1219–1226.

Balogh, I., Hafizi, S., Stenhoff, J., Hansson, K., and Dahlbäck, B. (2005). Analysis of Gas6 in human platelets and plasma. Arterioscler Thromb Vasc Biol *25*, 1280–1286.

Barreto, M.L., Teixeira, M.G., and Carmo, E.H. (2006). Infectious diseases epidemiology. J Epidemiol Community Health *60*, 192–195.

Behrens, E.M., Gadue, P., Gong, S., Garrett, S., Stein, P.L., and Cohen, P.L. (2003). The mer receptor tyrosine kinase: expression and function suggest a role in innate immunity. Eur J Immunol *33*, 2160–2167.

Bellani, G., Laffey, J.G., Pham, T., Fan, E., Brochard, L., Esteban, A., Gattinoni, L., van Haren, F., Larsson, A., McAuley, D.F., et al. (2016). Epidemiology, Patterns of Care, and Mortality for Patients With Acute Respiratory Distress Syndrome in Intensive Care Units in 50 Countries. JAMA *315*, 788–800.

Bhogal, H.K., and Sanyal, A.J. (2013). The molecular pathogenesis of cholestasis in sepsis. Front Biosci (Elite Ed) *5*, 87–96.

Bloch, A., Berger, D., and Takala, J. (2016). Understanding circulatory failure in sepsis. Intensive Care Med *42*, 2077–2079.

Bone, R.C., Balk, R.A., Cerra, F.B., Dellinger, R.P., Fein, A.M., Knaus, W.A., Schein, R.M., and Sibbald, W.J. (1992). Definitions for sepsis and organ failure and guidelines for the use of innovative therapies in sepsis. The ACCP/SCCM Consensus Conference Committee. American College of Chest Physicians/Society of Critical Care Medicine. Chest *101*, 1644–1655.

Borgel, D., Clauser, S., Bornstain, C., Bièche, I., Bissery, A., Remones, V., Fagon, J.-Y., Aiach, M., and Diehl, J.-L. (2006). Elevated growth-arrest-specific protein 6 plasma levels in patients with severe sepsis. Crit Care Med *34*, 219–222.

Borthwick, L.A., and Mann, D.A. (2016). Liver: Osteopontin and HMGB1: novel regulators of HSC activation. Nat Rev Gastroenterol Hepatol *13*, 320–322.

Boyd, J.H., Forbes, J., Nakada, T., Walley, K.R., and Russell, J.A. (2011). Fluid resuscitation in septic shock: a positive fluid balance and elevated central venous pressure are associated with increased mortality. Crit Care Med *39*, 259–265.

Brealey, D., Brand, M., Hargreaves, I., Heales, S., Land, J., Smolenski, R., Davies, N.A., Cooper, C.E., and Singer, M. (2002). Association between mitochondrial dysfunction and severity and outcome of septic shock. Lancet *360*, 219–223.

Brunt, E.M., Gouw, A.S.H., Hubscher, S.G., Tiniakos, D.G., Bedossa, P., Burt, A.D., Callea, F., Clouston, A.D., Dienes, H.P., Goodman, Z.D., et al. (2014). Pathology of the liver sinusoids. Histopathology *64*, 907–920.

Burgdorff, A.-M., Bucher, M., and Schumann, J. (2018). Vasoplegia in patients with sepsis and septic shock: pathways and mechanisms. J Int Med Res *46*, 1303–1310.

Butovsky, O., Jedrychowski, M.P., Moore, C.S., Cialic, R., Lanser, A.J., Gabriely, G., Koeglsperger, T., Dake, B., Wu, P.M., Doykan, C.E., et al. (2014). Identification of a unique TGF-β-dependent molecular and functional signature in microglia. Nat Neurosci *17*, 131–143.

Caraballo, C., and Jaimes, F. (2019). Organ Dysfunction in Sepsis: An Ominous Trajectory From Infection To Death. Yale J Biol Med *92*, 629–640.

Castello, L.M., Baldrighi, M., Molinari, L., Salmi, L., Cantaluppi, V., Vaschetto, R., Zunino, G., Quaglia, M., Bellan, M., Gavelli, F., et al. (2019). The Role of Osteopontin as a Diagnostic and Prognostic Biomarker in Sepsis and Septic Shock. Cells *8*.

Cecconi, M., Evans, L., Levy, M., and Rhodes, A. (2018). Sepsis and septic shock. Lancet *392*, 75–87.

Crowe, A.R., and Yue, W. (2019). Semi-quantitative Determination of Protein Expression using Immunohistochemistry Staining and Analysis: An Integrated Protocol. Bio Protoc *9*.

Crowley, L.C., Marfell, B.J., and Waterhouse, N.J. (2016). Analyzing Cell Death by Nuclear Staining with Hoechst 33342. Cold Spring Harb Protoc *2016*.

Dahlbäck, B. (2007). The tale of protein S and C4b-binding protein, a story of affection. Thromb Haemost *98*, 90–96.

Dellinger, R.P., Levy, M.M., Rhodes, A., Annane, D., Gerlach, H., Opal, S.M., Sevransky, J.E., Sprung, C.L., Douglas, I.S., Jaeschke, R., et al. (2013). Surviving sepsis campaign: international guidelines for management of severe sepsis and septic shock: 2012. Crit Care Med *41*, 580–637.

Deng, T., Zhang, Y., Chen, Q., Yan, K., and Han, D. (2012). Toll-like receptor-mediated inhibition of Gas6 and ProS expression facilitates inflammatory cytokine production in mouse macrophages. Immunology *135*, 40–50.

Diener, K.R., Al-Dasooqi, N., Lousberg, E.L., and Hayball, J.D. (2013). The multifunctional alarmin HMGB1 with roles in the pathophysiology of sepsis and cancer. Immunol Cell Biol *91*, 443–450.

Ekman, C., Linder, A., Akesson, P., and Dahlbäck, B. (2010a). Plasma concentrations of Gas6 (growth arrest specific protein 6) and its soluble tyrosine kinase receptor sAxl in sepsis and systemic inflammatory response syndromes. Crit Care *14*, R158.

Ekman, C., Stenhoff, J., and Dahlbäck, B. (2010b). Gas6 is complexed to the soluble tyrosine kinase receptor Axl in human blood. J Thromb Haemost *8*, 838–844.

Fuhrmann, V., Kneidinger, N., Herkner, H., Heinz, G., Nikfardjam, M., Bojic, A., Schellongowski, P., Angermayr, B., Kitzberger, R., Warszawska, J., et al. (2009). Hypoxic hepatitis: underlying conditions and risk factors for mortality in critically ill patients. Intensive Care Med *35*, 1397–1405.

Fujimori, T., Grabiec, A.M., Kaur, M., Bell, T.J., Fujino, N., Cook, P.C., Svedberg, F.R., MacDonald, A.S., Maciewicz, R.A., Singh, D., et al. (2015). The Axl receptor tyrosine kinase is a discriminator of macrophage function in the inflamed lung. Mucosal Immunol *8*, 1021–1030.

Giangola, M.D., Yang, W.-L., Rajayer, S.R., Nicastro, J., Coppa, G.F., and Wang, P. (2013). Growth arrest-specific protein 6 attenuates neutrophil migration and acute lung injury in sepsis. Shock *40*, 485–491.

Gibot, S., Massin, F., Cravoisy, A., Dupays, R., Barraud, D., Nace, L., and Bollaert, P.-E. (2007). Growth arrest-specific protein 6 plasma concentrations during septic shock. Crit Care *11*, R8.

Gofton, T.E., and Young, G.B. (2012). Sepsis-associated encephalopathy. Nat Rev Neurol *8*, 557–566.

Gould, W.R., Baxi, S.M., Schroeder, R., Peng, Y.W., Leadley, R.J., Peterson, J.T., and Perrin, L.A. (2005). Gas6 receptors Axl, Sky and Mer enhance platelet activation and regulate thrombotic responses. J Thromb Haemost *3*, 733–741.

Grande, E., Grippo, F., Frova, L., Pantosti, A., Pezzotti, P., and Fedeli, U. (2019). The increase of sepsis-related mortality in Italy: a nationwide study, 2003-2015. Eur J Clin Microbiol Infect Dis *38*, 1701–1708.

Gwangwa, M.V., Joubert, A.M., and Visagie, M.H. (2018). Crosstalk between the Warburg effect, redox regulation and autophagy induction in tumourigenesis. Cell Mol Biol Lett *23*, 20.

Heemskerk, S., Masereeuw, R., Russel, F.G.M., and Pickkers, P. (2009). Selective iNOS inhibition for the treatment of sepsis-induced acute kidney injury. Nat Rev Nephrol *5*, 629–640.

Hirano, Y., Aziz, M., Yang, W.-L., Wang, Z., Zhou, M., Ochani, M., Khader, A., and Wang, P. (2015). Neutralization of osteopontin attenuates neutrophil migration in sepsis-induced acute lung injury. Crit Care *19*, 53.

Hu, Q., Hao, C., and Tang, S. (2020). From sepsis to acute respiratory distress syndrome (ARDS): emerging preventive strategies based on molecular and genetic researches. Biosci Rep *40*.

Hüttemann, M., Lee, I., Grossman, L.I., Doan, J.W., and Sanderson, T.H. (2012). Phosphorylation of mammalian cytochrome c and cytochrome c oxidase in the regulation of cell destiny: respiration, apoptosis, and human disease. Adv Exp Med Biol *748*, 237–264.

Iba, T., Levi, M., and Levy, J.H. (2020). Sepsis-Induced Coagulopathy and Disseminated Intravascular Coagulation. Semin Thromb Hemost *46*, 89–95.

Irion, C.I., Parrish, K., John-Williams, K., Gultekin, S.H., and Shehadeh, L.A. (2018). Osteopontin Expression in Cardiomyocytes Is Increased in Pediatric Patients With Sepsis or Pneumonia. Front Physiol *9*, 1779.

Ji, R., Meng, L., Jiang, X., Cvm, N.K., Ding, J., Li, Q., and Lu, Q. (2014). TAM receptors support neural stem cell survival, proliferation and neuronal differentiation. PLoS One *9*, e115140.

Jiang, L., Liu, C.Y., Yang, Q.F., Wang, P., and Zhang, W. (2009). Plasma level of growth arrest-specific 6 (GAS6) protein and genetic variations in the GAS6 gene in patients with acute coronary syndrome. Am J Clin Pathol *131*, 738–743.

Kazeros, A., Harvey, B.-G., Carolan, B.J., Vanni, H., Krause, A., and Crystal, R.G. (2008). Overexpression of apoptotic cell removal receptor MERTK in alveolar macrophages of cigarette smokers. Am J Respir Cell Mol Biol *39*, 747–757.

Kim, H., Hur, M., Moon, H.-W., Yun, Y.-M., Di Somma, S., and GREAT Network (2017a). Multi-marker approach using procalcitonin, presepsin, galectin-3, and soluble suppression of tumorigenicity 2 for the prediction of mortality in sepsis. Ann Intensive Care *7*, 27.

Kim, J.E., Kim, Y., Li, G., Kim, S.T., Kim, K., Park, S.H., Park, J.O., Park, Y.S., Lim, H.Y., Lee, H., et al. (2017b). MerTK inhibition by RXDX-106 in MerTK activated gastric cancer cell lines. Oncotarget *8*, 105727–105734.

Kimak, E., Zięba, B., Duma, D., and Solski, J. (2018). Myeloperoxidase level and inflammatory markers and lipid and lipoprotein parameters in stable coronary artery disease. Lipids Health Dis *17*, 71.

Kingsley, S.M.K., and Bhat, B.V. (2016). Differential Paradigms in Animal Models of Sepsis. Curr Infect Dis Rep *18*, 26.

Kozlov, A.V., Lancaster, J.R., Meszaros, A.T., and Weidinger, A. (2017). Mitochondria-meditated pathways of organ failure upon inflammation. Redox Biol *13*, 170–181.

Kramer, L., Jordan, B., Druml, W., Bauer, P., Metnitz, P.G.H., and Austrian Epidemiologic Study on Intensive Care, ASDI Study Group (2007). Incidence and prognosis of early hepatic dysfunction in critically ill patients--a prospective multicenter study. Crit Care Med *35*, 1099–1104.

Langley, R.J., Tsalik, E.L., van Velkinburgh, J.C., Glickman, S.W., Rice, B.J., Wang, C., Chen, B., Carin, L., Suarez, A., Mohney, R.P., et al. (2013). An integrated clinico-metabolomic model improves prediction of death in sepsis. Sci Transl Med *5*, 195ra95.

Lee, Y.I., Smith, R.L., Gartshteyn, Y., Kwon, S., Caraher, E.J., and Nolan, A. (2016). Predictors of Acute Hemodynamic Decompensation in Early Sepsis: An Observational Study. J Clin Med Res *8*, 575–581.

Lemke, G. (2013). Biology of the TAM receptors. Cold Spring Harb Perspect Biol *5*, a009076.

Levy, M.M., Evans, L.E., and Rhodes, A. (2018). The Surviving Sepsis Campaign Bundle: 2018 Update. Crit Care Med *46*, 997–1000.

Lew, E.D., Oh, J., Burrola, P.G., Lax, I., Zagórska, A., Través, P.G., Schlessinger, J., and Lemke, G. (2014). Differential TAM receptor-ligand-phospholipid interactions delimit differential TAM bioactivities. Elife *3*.

Lewis, A.J., Seymour, C.W., and Rosengart, M.R. (2016). Current Murine Models of Sepsis. Surg Infect (Larchmt) *17*, 385–393.

Li, S., Guo, Q., Zhu, H., Li, Z., Su, Y., and Dong, B. (2017). Increased Mer and Axl receptor tyrosine kinase expression on glomeruli in lupus nephritis. Clin Rheumatol *36*, 1063–1070.

Loges, S., Schmidt, T., Tjwa, M., van Geyte, K., Lievens, D., Lutgens, E., Vanhoutte, D., Borgel, D., Plaisance, S., Hoylaerts, M., et al. (2010). Malignant cells fuel tumor growth by educating infiltrating leukocytes to produce the mitogen Gas6. Blood *115*, 2264–2273.

Lokhandwala, S., Moskowitz, A., Lawniczak, R., Giberson, T., Cocchi, M.N., and Donnino, M.W. (2015). Disease heterogeneity and risk stratification in sepsis-related occult hypoperfusion: A retrospective cohort study. J Crit Care *30*, 531–536.

Lu, J., Wei, Z., Jiang, H., Cheng, L., Chen, Q., Chen, M., Yan, J., and Sun, Z. (2018). Lactate dehydrogenase is associated with 28-day mortality in patients with sepsis: a retrospective observational study. J Surg Res *228*, 314–321.

Lu, Q., Gore, M., Zhang, Q., Camenisch, T., Boast, S., Casagranda, F., Lai, C., Skinner, M.K., Klein, R., Matsushima, G.K., et al. (1999). Tyro-3 family receptors are essential regulators of mammalian spermatogenesis. Nature *398*, 723–728.

Malawista, A., Wang, X., Trentalange, M., Allore, H.G., and Montgomery, R.R. (2016). Coordinated expression of tyro3, axl, and mer receptors in macrophage ontogeny. Macrophage (Houst) *3*.

Manfioletti, G., Brancolini, C., Avanzi, G., and Schneider, C. (1993). The protein encoded by a growth arrest-specific gene (gas6) is a new member of the vitamin K-dependent proteins related to protein S, a negative coregulator in the blood coagulation cascade. Mol Cell Biol *13*, 4976–4985.

Mantzarlis, K., Tsolaki, V., and Zakynthinos, E. (2017). Role of Oxidative Stress and Mitochondrial Dysfunction in Sepsis and Potential Therapies. Oxid Med Cell Longev *2017*, 5985209.

Matthay, M.A., Zemans, R.L., Zimmerman, G.A., Arabi, Y.M., Beitler, J.R., Mercat, A., Herridge, M., Randolph, A.G., and Calfee, C.S. (2019). Acute respiratory distress syndrome. Nat Rev Dis Primers *5*, 18.

McCarter, F.D., Nierman, S.R., James, J.H., Wang, L., King, J.-K., Friend, L.A., and Fischer, J.E. (2002). Role of skeletal muscle Na+-K+ ATPase activity in increased lactate production in sub-acute sepsis. Life Sci *70*, 1875–1888.

Mearelli, F., Fiotti, N., Giansante, C., Casarsa, C., Orso, D., De Helmersen, M., Altamura, N., Ruscio, M., Castello, L.M., Colonetti, E., et al. (2018). Derivation and Validation of a Biomarker-Based Clinical Algorithm to Rule Out Sepsis From Noninfectious Systemic Inflammatory Response Syndrome at Emergency Department Admission: A Multicenter Prospective Study. Crit Care Med *46*, 1421–1429.

Miller, M.A., Sullivan, R.J., and Lauffenburger, D.A. (2017). Molecular Pathways: Receptor Ectodomain Shedding in Treatment, Resistance, and Monitoring of Cancer. Clin Cancer Res *23*, 623–629.

Mukherjee, S.K., Wilhelm, A., and Antoniades, C.G. (2016). TAM receptor tyrosine kinase function and the immunopathology of liver disease. Am J Physiol Gastrointest Liver Physiol *310*, G899-905.

Nagata, K., Ohashi, K., Nakano, T., Arita, H., Zong, C., Hanafusa, H., and Mizuno, K. (1996). Identification of the product of growth arrest-specific gene 6 as a common ligand for Axl, Sky, and Mer receptor tyrosine kinases. J Biol Chem *271*, 30022–30027.

Najafov, A., Mookhtiar, A.K., Luu, H.S., Ordureau, A., Pan, H., Amin, P.P., Li, Y., Lu, Q., and Yuan, J. (2019). TAM Kinases Promote Necroptosis by Regulating Oligomerization of MLKL. Mol Cell *75*, 457-468.e4.

Nau, G.J., Guilfoile, P., Chupp, G.L., Berman, J.S., Kim, S.J., Kornfeld, H., and Young, R.A. (1997). A chemoattractant cytokine associated with granulomas in tuberculosis and silicosis. Proc Natl Acad Sci U S A *94*, 6414–6419.

Ndrepepa, G. (2019). Myeloperoxidase - A bridge linking inflammation and oxidative stress with cardiovascular disease. Clin Chim Acta *493*, 36–51.

Nichol, A.D., Egi, M., Pettila, V., Bellomo, R., French, C., Hart, G., Davies, A., Stachowski, E., Reade, M.C., Bailey, M., et al. (2010). Relative hyperlactatemia and hospital mortality in critically ill patients: a retrospective multi-centre study. Crit Care *14*, R25.

Paoli, C.J., Reynolds, M.A., Sinha, M., Gitlin, M., and Crouser, E. (2018). Epidemiology and Costs of Sepsis in the United States-An Analysis Based on Timing of Diagnosis and Severity Level. Crit Care Med *46*, 1889–1897.

Paolino, M., Choidas, A., Wallner, S., Pranjic, B., Uribesalgo, I., Loeser, S., Jamieson, A.M., Langdon, W.Y., Ikeda, F., Fededa, J.P., et al. (2014). The E3 ligase Cbl-b and TAM receptors regulate cancer metastasis via natural killer cells. Nature *507*, 508–512.

Peerapornratana, S., Manrique-Caballero, C.L., Gómez, H., and Kellum, J.A. (2019). Acute kidney injury from sepsis: current concepts, epidemiology, pathophysiology, prevention and treatment. Kidney Int *96*, 1083–1099.

Peerapornratana, S., Priyanka, P., Wang, S., Smith, A., Singbartl, K., Palevsky, P.M., Chawla, L.S., Yealy, D.M., Angus, D.C., Kellum, J.A., et al. (2020). Sepsis-Associated Acute Kidney Disease. Kidney International Reports *5*, 839–850.

Peeters, M.J.W., Dulkeviciute, D., Draghi, A., Ritter, C., Rahbech, A., Skadborg, S.K., Seremet, T., Carnaz Simões, A.M., Martinenaite, E., Halldórsdóttir, H.R., et al. (2019). MERTK Acts as a Costimulatory Receptor on Human CD8+ T Cells. Cancer Immunol Res *7*, 1472–1484.

Perner, A., Gordon, A.C., De Backer, D., Dimopoulos, G., Russell, J.A., Lipman, J., Jensen, J.-U., Myburgh, J., Singer, M., Bellomo, R., et al. (2016). Sepsis: frontiers in diagnosis, resuscitation and antibiotic therapy. Intensive Care Med *42*, 1958–1969.

Pierce, A.M., and Keating, A.K. (2014). TAM receptor tyrosine kinases: expression, disease and oncogenesis in the central nervous system. Brain Res *1542*, 206–220.

Pool, R., Gomez, H., and Kellum, J.A. (2018). Mechanisms of Organ Dysfunction in Sepsis. Crit Care Clin *34*, 63–80.

Poston, J.T., and Koyner, J.L. (2019). Sepsis associated acute kidney injury. BMJ *364*, k4891.

Prauchner, C.A. (2017). Oxidative stress in sepsis: Pathophysiological implications justifying antioxidant co-therapy. Burns *43*, 471–485.

Ramachandra, C.J.A., Ja, K.P.M.M., Chua, J., Cong, S., Shim, W., and Hausenloy, D.J. (2020). Myeloperoxidase As a Multifaceted Target for Cardiovascular Protection. Antioxid Redox Signal *32*, 1135–1149.

Reinhart, K., Daniels, R., Kissoon, N., Machado, F.R., Schachter, R.D., and Finfer, S. (2017). Recognizing Sepsis as a Global Health Priority - A WHO Resolution. N Engl J Med *377*, 414–417.

Rhee, C., Kadri, S.S., Dekker, J.P., Danner, R.L., Chen, H.-C., Fram, D., Zhang, F., Wang, R., Klompas, M., and CDC Prevention Epicenters Program (2020). Prevalence of Antibiotic-Resistant Pathogens in Culture-Proven Sepsis and Outcomes Associated With Inadequate and Broad-Spectrum Empiric Antibiotic Use. JAMA Netw Open *3*, e202899.

Rishu, A.H., Khan, R., Al-Dorzi, H.M., Tamim, H.M., Al-Qahtani, S., Al-Ghamdi, G., and Arabi, Y.M. (2013). Even mild hyperlactatemia is associated with increased mortality in critically ill patients. Crit Care *17*, R197.

Rothlin, C.V., Ghosh, S., Zuniga, E.I., Oldstone, M.B.A., and Lemke, G. (2007). TAM receptors are pleiotropic inhibitors of the innate immune response. Cell *131*, 1124–1136.

Rothlin, C.V., Carrera-Silva, E.A., Bosurgi, L., and Ghosh, S. (2015). TAM receptor signaling in immune homeostasis. Annu Rev Immunol *33*, 355–391.

Rudd, K.E., Kissoon, N., Limmathurotsakul, D., Bory, S., Mutahunga, B., Seymour, C.W., Angus, D.C., and West, T.E. (2018). The global burden of sepsis: barriers and potential solutions. Crit Care *22*, 232.

Rudd, K.E., Johnson, S.C., Agesa, K.M., Shackelford, K.A., Tsoi, D., Kievlan, D.R., Colombara, D.V., Ikuta, K.S., Kissoon, N., Finfer, S., et al. (2020). Global, regional, and national sepsis incidence and mortality, 1990-2017: analysis for the Global Burden of Disease Study. Lancet *395*, 200–211.

Ruiz, S., Vardon-Bounes, F., Merlet-Dupuy, V., Conil, J.-M., Buléon, M., Fourcade, O., Tack, I., and Minville, V. (2016). Sepsis modeling in mice: ligation length is a major severity factor in cecal ligation and puncture. Intensive Care Med Exp *4*, 22.

Salmi, L., Gavelli, F., Patrucco, F., Caputo, M., Avanzi, G.C., and Castello, L.M. (2019). Gas6/TAM Axis in Sepsis: Time to Consider Its Potential Role as a Therapeutic Target. Dis Markers *2019*, 6156493.

Salmi, L., Gavelli, F., Patrucco, F., Bellan, M., Sainaghi, P.P., Avanzi, G.C., and Castello, L.M. (2021). Growth Arrest-Specific Gene 6 Administration Ameliorates Sepsis-Induced Organ Damage in Mice and Reduces ROS Formation In Vitro. Cells *10*.

Sandahl, M., Hunter, D.M., Strunk, K.E., Earp, H.S., and Cook, R.S. (2010). Epithelial cell-directed efferocytosis in the post-partum mammary gland is necessary for tissue homeostasis and future lactation. BMC Dev Biol *10*, 122.

Saposnik, B., Borgel, D., Aiach, M., and Gandrille, S. (2003). Functional properties of the sex-hormone-binding globulin (SHBG)-like domain of the anticoagulant protein S. Eur J Biochem *270*, 545–555.

Sather, S., Kenyon, K.D., Lefkowitz, J.B., Liang, X., Varnum, B.C., Henson, P.M., and Graham, D.K. (2007). A soluble form of the Mer receptor tyrosine kinase inhibits macrophage clearance of apoptotic cells and platelet aggregation. Blood *109*, 1026–1033.

Schrijver, I.T., Kemperman, H., Roest, M., Kesecioglu, J., and de Lange, D.W. (2017). Myeloperoxidase can differentiate between sepsis and non-infectious SIRS and predicts mortality in intensive care patients with SIRS. Intensive Care Med Exp *5*, 43.

Scott, R.S., McMahon, E.J., Pop, S.M., Reap, E.A., Caricchio, R., Cohen, P.L., Earp, H.S., and Matsushima, G.K. (2001). Phagocytosis and clearance of apoptotic cells is mediated by MER. Nature *411*, 207–211.

Seitz, H.M., Camenisch, T.D., Lemke, G., Earp, H.S., and Matsushima, G.K. (2007). Macrophages and dendritic cells use different Axl/Mertk/Tyro3 receptors in clearance of apoptotic cells. J Immunol *178*, 5635–5642.

Sevransky, J.E., Martin, G.S., Shanholtz, C., Mendez-Tellez, P.A., Pronovost, P., Brower, R., and Needham, D.M. (2009). Mortality in sepsis versus non-sepsis induced acute lung injury. Crit Care *13*, R150.

Seymour, C.W., Liu, V.X., Iwashyna, T.J., Brunkhorst, F.M., Rea, T.D., Scherag, A., Rubenfeld, G., Kahn, J.M., Shankar-Hari, M., Singer, M., et al. (2016). Assessment of Clinical Criteria for Sepsis: For the Third International Consensus Definitions for Sepsis and Septic Shock (Sepsis-3). JAMA *315*, 762–774.

Seymour, C.W., Gesten, F., Prescott, H.C., Friedrich, M.E., Iwashyna, T.J., Phillips, G.S., Lemeshow, S., Osborn, T., Terry, K.M., and Levy, M.M. (2017). Time to Treatment and Mortality during Mandated Emergency Care for Sepsis. N Engl J Med *376*, 2235–2244.

Shankar-Hari, M., Saha, R., Wilson, J., Prescott, H.C., Harrison, D., Rowan, K., Rubenfeld, G.D., and Adhikari, N.K.J. (2020). Rate and risk factors for rehospitalisation in sepsis survivors: systematic review and meta-analysis. Intensive Care Med *46*, 619–636.

Shao, W.-H., Zhen, Y., Eisenberg, R.A., and Cohen, P.L. (2009). The Mer receptor tyrosine kinase is expressed on discrete macrophage subpopulations and mainly uses Gas6 as its ligand for uptake of apoptotic cells. Clin Immunol *133*, 138–144.

Sheu, C.-C., Gong, M.N., Zhai, R., Chen, F., Bajwa, E.K., Clardy, P.F., Gallagher, D.C., Thompson, B.T., and Christiani, D.C. (2010). Clinical characteristics and outcomes of sepsis-related vs non-sepsis-related ARDS. Chest *138*, 559–567.

Singer, M., Deutschman, C.S., Seymour, C.W., Shankar-Hari, M., Annane, D., Bauer, M., Bellomo, R., Bernard, G.R., Chiche, J.-D., Coopersmith, C.M., et al. (2016). The Third International Consensus Definitions for Sepsis and Septic Shock (Sepsis-3). JAMA *315*, 801–810.

Stevens, N.E., Chapman, M.J., Fraser, C.K., Kuchel, T.R., Hayball, J.D., and Diener, K.R. (2017). Therapeutic targeting of HMGB1 during experimental sepsis modulates the inflammatory cytokine profile to one associated with improved clinical outcomes. Sci Rep *7*, 5850.

Strnad, P., Tacke, F., Koch, A., and Trautwein, C. (2017). Liver - guardian, modifier and target of sepsis. Nat Rev Gastroenterol Hepatol *14*, 55–66.

Subramanian, M., Hayes, C.D., Thome, J.J., Thorp, E., Matsushima, G.K., Herz, J., Farber, D.L., Liu, K., Lakshmana, M., and Tabas, I. (2014). An AXL/LRP-1/RANBP9 complex mediates DC efferocytosis and antigen cross-presentation in vivo. J Clin Invest *124*, 1296–1308.

Sweis, R., Ortiz, J., and Biller, J. (2016). Neurology of Sepsis. Curr Neurol Neurosci Rep *16*, 21.

Takatani, Y., Ono, K., Suzuki, H., Inaba, M., Sawada, M., and Matsuda, N. (2018). Inducible nitric oxide synthase during the late phase of sepsis is associated with hypothermia and immune cell migration. Lab Invest *98*, 629–639.

Theeß, W., Sellau, J., Steeg, C., Klinke, A., Baldus, S., Cramer, J.P., and Jacobs, T. (2017). Myeloperoxidase Attenuates Pathogen Clearance during Plasmodium yoelii Nonlethal Infection. Infect Immun *85*.

Thorp, E., Vaisar, T., Subramanian, M., Mautner, L., Blobel, C., and Tabas, I. (2011). Shedding of the Mer tyrosine kinase receptor is mediated by ADAM17 protein through a pathway involving reactive oxygen species, protein kinase Cδ, and p38 mitogen-activated protein kinase (MAPK). J Biol Chem *286*, 33335–33344.

Tolkien J.R.R., S.G. (1954). The Fellowship of the Ring (George Allen & Unwin).

Tutusaus, A., de Gregorio, E., Cucarull, B., Cristóbal, H., Aresté, C., Graupera, I., Coll, M., Colell, A., Gausdal, G., Lorens, J.B., et al. (2020a). A Functional Role of GAS6/TAM in Nonalcoholic Steatohepatitis Progression Implicates AXL as Therapeutic Target. Cell Mol Gastroenterol Hepatol *9*, 349–368.

Tutusaus, A., Marí, M., Ortiz-Pérez, J.T., Nicolaes, G.A.F., Morales, A., and García de Frutos, P. (2020b). Role of Vitamin K-Dependent Factors Protein S and GAS6 and TAM Receptors in SARS-CoV-2 Infection and COVID-19-Associated Immunothrombosis. Cells *9*.

Van Wyngene, L., Vandewalle, J., and Libert, C. (2018). Reprogramming of basic metabolic pathways in microbial sepsis: therapeutic targets at last? EMBO Mol Med *10*.

Vaschetto, R., Nicola, S., Olivieri, C., Boggio, E., Piccolella, F., Mesturini, R., Damnotti, F., Colombo, D., Navalesi, P., Della Corte, F., et al. (2008). Serum levels of osteopontin are increased in SIRS and sepsis. Intensive Care Med *34*, 2176–2184.

Wallet, M.A., Sen, P., Flores, R.R., Wang, Y., Yi, Z., Huang, Y., Mathews, C.E., Earp, H.S., Matsushima, G., Wang, B., et al. (2008). MerTK is required for apoptotic cell-induced T cell tolerance. J Exp Med *205*, 219–232.

Wan, E., Yeap, X.Y., Dehn, S., Terry, R., Novak, M., Zhang, S., Iwata, S., Han, X., Homma, S., Drosatos, K., et al. (2013). Enhanced efferocytosis of apoptotic cardiomyocytes through myeloid-epithelial-reproductive tyrosine kinase links acute inflammation resolution to cardiac repair after infarction. Circ Res *113*, 1004–1012.

Wang, H., Chen, Y., Ge, Y., Ma, P., Ma, Q., Ma, J., Wang, H., Xue, S., and Han, D. (2005). Immunoexpression of Tyro 3 family receptors--Tyro 3, Axl, and Mer--and their ligand Gas6 in postnatal developing mouse testis. J Histochem Cytochem *53*, 1355–1364.

Wium, M., Paccez, J.D., and Zerbini, L.F. (2018). The Dual Role of TAM Receptors in Autoimmune Diseases and Cancer: An Overview. Cells *7*.

Wu, G., Ma, Z., Hu, W., Wang, D., Gong, B., Fan, C., Jiang, S., Li, T., Gao, J., and Yang, Y. (2017). Molecular insights of Gas6/TAM in cancer development and therapy. Cell Death Dis *8*, e2700.

Wu, G., Ma, Z., Cheng, Y., Hu, W., Deng, C., Jiang, S., Li, T., Chen, F., and Yang, Y. (2018). Targeting Gas6/TAM in cancer cells and tumor microenvironment. Mol Cancer *17*, 20.

Yeh, L.-C., Huang, P.-W., Hsieh, K.-H., Wang, C.-H., Kao, Y.-K., Lin, T.-H., and Lee, X.-L. (2017). Elevated Plasma Levels of Gas6 Are Associated with Acute Lung Injury in Patients with Severe Sepsis. Tohoku J Exp Med *243*, 187–193.

Yende, S., Kellum, J.A., Talisa, V.B., Peck Palmer, O.M., Chang, C.-C.H., Filbin, M.R., Shapiro, N.I., Hou, P.C., Venkat, A., LoVecchio, F., et al. (2019). Long-term Host Immune Response Trajectories Among Hospitalized Patients With Sepsis. JAMA Netw Open *2*, e198686.

Zagórska, A., Través, P.G., Lew, E.D., Dransfield, I., and Lemke, G. (2014). Diversification of TAM receptor tyrosine kinase function. Nat Immunol *15*, 920–928.

Zahuczky, G., Kristóf, E., Majai, G., and Fésüs, L. (2011). Differentiation and glucocorticoid regulated apopto-phagocytic gene expression patterns in human macrophages. Role of Mertk in enhanced phagocytosis. PLoS One *6*, e21349.

Zhong, F., Chen, Z., Zhang, L., Xie, Y., Nair, V., Ju, W., Kretzler, M., Nelson, R.G., Li, Z., Chen, H., et al. (2018). Tyro3 is a podocyte protective factor in glomerular disease. JCI Insight *3*.